Development of a Low-cost Jute Fibre Reinforced Cementitious Composites Using Locally Available Ingredients

by

Md. Atiqur Rahman

MASTER OF SCIENCE IN CIVIL ENGINEERING

July, 2025

Recommendation of the Board of Examiners

The thesis titled "**Development of a Low-cost Jute Fibre Reinforced Cementitious Composites Using Locally Available Ingredients**" submitted by Md. Atiqur Rahman, Student ID 191051012 of Academic Year 2019-2020 has been found as satisfactory and accepted as partial fulfilment of the requirement for the degree of Master of Science in Civil Engineering.

1. Chairman

Dr. Md. Imran Kabir
Assistant Professor
Department of Civil and Environmental Engineering (CEE)
Islamic University of Technology (IUT)

2. Member (Ex-Officio)

Dr. Shakil Mohammad Rifat
Professor and Head
Department of Civil and Environmental Engineering (CEE)
Islamic University of Technology (IUT)

3. Member

Dr. Tanvir Ahmed
Assistant Professor
Department of Civil and Environmental Engineering (CEE)
Islamic University of Technology (IUT)

4. Member (External)

Prof. Dr. Md. Nazrul Islam
Professor
Department of Civil Engineering (CE)
Dhaka University of Engineering and Technology (DUET)

Declaration of Candidate

It is hereby declared that this thesis has not been submitted elsewhere for the award of any Degree or Diploma.

Signature of Candidate:	
Name of Candidate:	Md. Atiqur Rahman
Student ID :	191051012
Academic Year :	2019-2020
Date :	

Dedication

I would like to dedicate this thesis to my family, teachers, and all the individuals who have supported and inspired me throughout this journey.

Table of Content

List of Tables

List of Figures

List of Abbreviations

ACI	American Concrete Institute	JFRCCs	Jute Fibre Reinforced Cementitious Composites
ANOVA	Analysis of Variance	LCA	Life cycle assessment
ASTM	American Society for Testing and Materials	NFRC	Natural Fibre Reinforced Composites
BSEI	Backscattered Electron Imaging	NFRCCs	Natural Fibre Reinforced Cementitious Composites
Coef	Coefficient	OPC	Ordinary Portland Cement
C-S-H	Calcium Silicate Hydrate	PPFs	Polypropylene Fibres
DF	Degrees of freedom	PUNDIT	Portable Ultrasonic Non-destructive Digital Indicating Tester
DOE	Design of Experiment	P-value	Probability value
ECCs	Engineered Cementitious Composites	PVA	Polyvinyl Alcohol
EDS	Energy Dispersive Spectroscopy	RSM	Response Surface Methodology
FA	Fly Ash	RTSF	Recycled Tire Steel Fibre
FA/C	Fly Ash-to-Cement Proportion	S/B	Sand-to-Binder Proportion
FRC	Fibre-Reinforced Concrete	SCBA	Sugarcane Bagasse Ash
FRCCs	Fibre-Reinforced Cementitious Composites	SCMs	Supplementary Cementitious Materials
F-value	Randomization test	SEM	Scanning Electron Microscopy
GI	Galvanized Iron	SFWT	Steel Fibre from Waste Tires
GGBFS	Ground Granulated Blast-Furnace Slag	SSD	Saturated Surface Dry
GWP	Global Warming Potential	T-value	Test statistic for hypothesis testing
IUT	Islamic University of Technology	UPV	Ultrasonic Pulse Velocity
ITZ	Interfacial Transition Zone	UTM	Universal Testing Machine
JF	Jute Fibres	W/B	Water-to-Binder Proportion

List of Symbols

a^k	Number of experiments in full factorial design	MS_{Adj}	Adjusted Mean Square
a	Level of experiments	r	Pearson correlation coefficient
k	Number of factor	R^2	Coefficient of determination
ci	CO_2 intensity	R^2_{adj}	Adjusted coefficient of determination
f_{st}	Splitting tensile strength	SS_{Adj}	Adjusted Sum of Squares
D	Overall desirability	ϵ	Strain at peak compressive strength
f'_c	Compressive strength		

Acknowledgements

First and foremost, I extend my sincere gratitude to the Almighty for granting me the perseverance and resilience required to complete this research endeavour. I am profoundly thankful to my thesis supervisor, Dr. Md. Imran Kabir, for his exceptional mentorship, constructive critiques, and steadfast encouragement, which were pivotal in shaping the academic rigor and direction of this study.

I would like to express my sincere thankfulness to Prof. Dr. Shakil Mohammad Rifaat, Prof. Dr. Md. Nazrul Islam, and Dr. Tanvir Ahmed for their thorough review of this thesis and their invaluable feedback. Their expertise significantly enhanced the quality of this work.

This research was made possible through the generous financial support of the IUT Seed Grant, for which I am sincerely thankful. I also acknowledge the technical and logistical assistance provided by the staff of the Concrete Laboratory at the Department of Civil and Environmental Engineering, IUT, whose contributions were indispensable to the experimental phase of this study.

Above all, I owe an immeasurable debt of gratitude to my family for their unconditional love, emotional backing, and unwavering trust in my academic pursuits. Their encouragement served as a constant source of motivation throughout this challenging yet rewarding journey.

Abstract

The objective of this research is to develop a cost-efficient, optimized Jute Fibre-Reinforced Cementitious Composites (JFRCCs) by incorporating locally available constituents and industrial by-products. This study utilized OPC, fly ash, processed sand, jute fibre, and superplasticizer as constituent materials. The experimental program was conducted in three sequential phases. Phase I investigation focused on identifying the influence of mixing components like water-to-binder proportion (W/B), sand-to-binder proportion (S/B), fly ash-to-cement proportion (FA/C), and jute fibre length on compressive strength and determining their suitable range for Phase II investigation. In Phase II investigation, a Full Factorial statistical design of experiments was employed, focusing on four key mixing parameters: W/B, S/B, FA/C, and jute fibre content. From the Phase I investigation, these mixing parameters were set within their specific lower and upper limits as W/B (0.26 and 0.29), FA/C (1.2 and 2.0), S/B (0.3 and 0.5), and jute content (0.5 % and 1.0 %). A total of 16 mixes were designed and for each mixes, compressive strength, peak strain, splitting tensile strength, and ultrasonic pulse velocity (UPV) were investigated at 28 days of casting. The findings indicated that the developed JFRCCs satisfied the minimum standards for residential concrete as per ACI 318. Life cycle assessment (LCA) was also conducted for all mixes which revealed that emitted CO_2 from material, transport, and mixture varies from 458 kg/m^3 to 668 kg/m^3. Following statistical analysis of the experimental data and material costs for 16 mixes, optimized mix proportion for proposed composites was established via a multi-objective desirability approach implemented in Minitab software. The regression and ANOVA analyses revealed high model accuracy and significance for compressive strength, tensile strength, UPV, and material cost, though not for peak strain. The effect of individual mix proportions on mechanical characteristics and cost-effectiveness of cementitious composites was evaluated before the implementation of the multi-objective desirability approach. With a desirability score of 0.9614, the optimized mix ratio consisted of a W/B of 0.26, FA/C of 1.68, S/B of 0.50, and a jute content of 0.63%, achieving a compressive strength of 35 MPa and a splitting tensile strength of 4 MPa, while simultaneously maximizing peak strain and UPV, and minimizing material cost. Following mix optimization, the Phase III investigation on optimized JFRCCs revealed that both water curing and wet curing methods demonstrated greater compressive behaviour compared with natural curing, indicating critical role of adequate moisture in enhancing hydration and overall performance. Furthermore, during the flexural behaviour assessment, the predominantly brittle failure mode highlighted the necessity for further optimization of the composite mix design and fibre content in order to achieve the desired ductility. Under thermal exposure, JFRCCs exhibited superior resistance compared to conventional concrete, with compressive strength maximizing at 400 °C before declining significantly due to thermal degradation of fibre and matrix dehydration. Microstructural analysis supported these findings by revealing changes in internal structure across different thermal conditions. The study concludes that optimized JFRCCs offer promising potential as a sustainable and cost-effective construction material, exhibiting adequate mechanical and thermal performances.

CHAPTER 1: INTRODUCTION

1.1 General

The construction industry is undergoing constant evolution, with a focus on identifying novel materials that provide improved functionality and a reduced environmental burden. Traditional concrete, although widely used, poses several sustainability challenges such as high carbon emissions, resource depletion, and environmental degradation. In response to these challenges, researchers and industry professionals are exploring eco-friendly alternatives that incorporate locally available and sustainable materials. The expanding need for ecologically conscious and sustainable construction ingredients has motivated widespread study into substitute composite ingredients that balance strength, durability, and environmental impact. Incorporating supplementary materials and natural fibres into cementitious composites provides a promising approach to addressing these environmental concerns. Jute fibre, a natural and renewable resource, has gained attention as a reinforcing material in cementitious composites due to its high tensile strength, low cost, and biodegradability (Kubissa et al., 2017). Furthermore, using fly ash, a by-product of coal power plants, can improve the sustainability of these composites by reducing the amount of cement needed (Sapkal et al., 2021; Tian et al., 2016).

In developing countries like Bangladesh, where jute is locally available and widely cultivated, its use in construction materials not only promotes sustainability but also supports local industries. By using locally available ingredients such as ordinary Portland cement (OPC), fine sand, fly ash, and jute fibre, eco-friendly composites can be developed to reduce costs and environmental footprints while enhancing material performance. Therefore, this study intended to develop an economical Jute Fibre-Reinforced Cementitious Composites (JFRCCs) by combining locally available ingredients (i.e., OPC, fine sand, jute fibre, and superplasticizer) and industrial by-products (i.e., fly ash). In this study, a full factorial design, as established in prior research (Ahmad & Alghamdi, 2014; Antony, 2023; Colette et al., 2023), was utilized to statistically optimize the mixing parameters for developing JFRCCs. Overall, this chapter presents a comprehensive overview of the current study by presenting its background, outlining the specific objectives, and detailing the methodology adopted to achieve these objectives. Furthermore, the structure of this thesis is outlined at the end of chapter.

1.2 Background

Being one of the primary construction materials, the annual consumption of concrete is rapidly rising with economic growth, with an estimated production of over 20 billion tons globally (Huda & Alam, 2014). Consequently, global aggregate production and consumption nearly doubled from 21 billion tons in 2007 to 40 billion tons in 2014 and was projected to expand further to 66.3 billion tons by 2022 (Tam et al., 2018). Cement industries alone are responsible for nearly 8 percent of worldwide CO_2 emissions due to the combustion of limestone into clinker (Shen et al., 2015; Cantero et al., 2020). Thus, a critical and timely imperative is to decrease the environmental consequences related with concrete production. As a result, the usage of recycled materials, industrial by-products, natural, and unconventional construction materials in concrete technology have gained widespread attention among industry professionals and researchers in recent decades (Cantero et al., 2019; Cantero et al., 2019; Revilla-Cuesta et al., 2023). Fly ash, an environmentally hazardous by-product of coal-fired power plants, significantly enhances the mechanical properties and ductility of fibre-reinforced cementitious composites when used in high volumes (Yang et al., 2007; Mehta, 2004). Bangladesh, expected to produce approximately 2.0 million metric tons of fly ash by 2025 (Sultana et al., 2021), faces numerous environmental threats from this abundant material. Therefore, the partial replacement of cement with fly ash represents a significant opportunity to lessen CO_2 emissions from cement production, leading to a considerable environmental gains.

While Fibre-Reinforced Concrete (FRC) formed by adding steel and/or synthetic fibres offers many advantages over conventional concrete (Ahmad et al., 2021), its production cost is high due to the inclusion of these fibres. Motivated by the worldwide energy crisis and the increasing demand for sustainable materials, Natural Fibre-Reinforced Cementitious Composites (NFRCCs) have recently gathered significant attention. Studies have shown that natural fibres such as banana, bagasse, coir, jute, and sisal fibre are effective in reinforcing concrete (Savastano et al., 2000; Coutts, 1990). The incorporation of environmentally sustainable and economically advantageous agricultural by-products could make fibre-reinforced composites more sustainable. Although early research on natural fibre-reinforced composites was limited due to the fibres fragility and susceptibility to degradation in alkaline environments (Gassan & Bledzki, 1999; de Andrade Silva et al., 2010), specific modifications have proven that natural fibres can improve the mechanical properties of composites, even after long-term weathering (Aggarwal, 1995; Jr Savastano et al., 2006; Tonoli et al., 2007; John & Anandjiwala, 2008). Ramaswamy et al. (1983), tested the tensile strength and elongation of jute fibres in both air-dry conditions and after immersion in an alkaline solution (p^H-11) for 28 days. Studies have demonstrated the high tensile strength of jute fibres; however, alkaline exposure leads to a reduction in strength, ranging from 5% to 32%. In addition, fibres embedded in cement concrete showed only marginal strength loss (Mansur & Aziz, 1982). Deb et al. (2020) also revealed that jute fibre-reinforced samples exhibit higher tensile and flexural strength compared to polypropylene (PP) fibre-reinforced samples. Towards this end, several studies in recent years have focused on enhancing the mechanical properties of conventional concrete by incorporating jute fibres (Zakaria et al., 2015; Islam & Ahmed, 2018; Liu et al., 2013; Bheel et al., 2021; Mansur et al., 2022). Although the effects of fly ash and jute fibres have been studied separately in cementitious composites, further investigation is necessary to completely understand the interaction effects of these combined materials within the composites.

Bangladesh, one of the largest jute producers globally, produces approximately 1.6 million metric tons of jute annually (Siraj-UD-Doulah et al., 2020). Hence, this study aimed to develop a cost-efficient JFRCCs using locally available materials such as OPC, jute fibre, fine sand, and superplasticizer, along with industrial by-products like fly ash. Recent studies have shown that the optimization of concrete properties is frequently achieved through the application of statistical techniques, notably Response Surface Methodology (RSM) and Full Factorial Design, which are employed to refine mixing parameters. These approaches allow researchers to systematically evaluate the relationship between multiple input variables and the resulting concrete responses (Hamada et al., 2023; Kursuncu et al., 2022; Ahmad & Alghamdi, 2014; Antony, 2023; Colette et al., 2023). In this study, a full factorial design, as established in prior research

(Ahmad & Alghamdi, 2014; Antony, 2023; Colette et al., 2023), was utilized to statistically optimize the mixing parameters for developing JFRCCs. To optimize the composite's performance, a full factorial design methodology was employed. Within this framework, four key mixing constituents were selected as independent variables for the investigations: the water-to-binder proportion (W/B), sand-to-binder proportion (S/B), fly ash-to-cement proportion (FA/C), and the jute fibre content. This experimental approach was designed to reveal the individual and synergistic effects of these parameters on the resulting properties of the cementitious composite, with the ultimate objective of determining the optimal mix proportion. Preliminary investigations were conducted to identify four key mixing parameters, along with their respective lower and upper limits. Then, ninety-six standard cylindrical specimens (100 mm × 200 mm) were produced and tested to determine different mechanical behaviours of the composites, including compressive strength, ultrasonic pulse velocity (UPV), strain at peak compressive strength, and splitting tensile strength. Subsequently, the experimental results and material costs associated with each mix design were subjected to statistical analysis utilizing Minitab software to determine the optimized mixture proportion for JFRCCs via a multi-objective desirability approach.

This study is innovative in its combined uses of fly ash and jute fibre to develop JFRCCs excluding coarse aggregate. Besides, the study effectively reduces CO_2 releases by significantly replacing cement with fly ash and addresses environmental challenges related to fly ash dumping. In addition, the application of a full factorial methodology for optimizing the mixing parameters ensures the development of sustainable and cost-effective construction materials. This integrated approach not only utilizes resources that are available locally but also presents a viable option for environmentally conscious construction materials in regions like Bangladesh, where both fly ash and jute are abundant. Moreover, the outcomes of this research are expected to significantly advance the development of environmentally sustainable as well as cost-effective construction materials, thereby mitigating both ecological and economic concerns prevalent in the industry.

1.3 Application of Natural Fibre Reinforced Cementitious Composites (NFRCCs)

Natural fibres, recognized for their eco-friendliness and cost-effectiveness, are increasingly regarded as promising alternative materials. Extensive research has been conducted on structural components made from NFRCCs for engineering applications, with a focus on two primary applications: wall panels and roofing tiles. Earlier studies explored the use of natural fibre-reinforced cement as an affordable roofing material. Cook et al. (1978) utilized coir fibre-reinforced cement to construct a roof and conducted various mechanical tests to evaluate its performance, including bending and impact resistance, permeability, water absorption, combustibility, and dimensional stability. Subsequently, Berhane (1994) investigated the incorporation of natural pozzolanic materials, such as silica fume, scoria powder, and pumice powder, as partial replacements for cement. Roofing components reinforced with sisal fibre were produced, and their durability was assessed over 730 days of exposure to environmental conditions. The findings indicated that natural pozzolanic materials could mitigate fibre degradation and enhance composite durability. Furthermore, the application of NFRCs as roofing tiles was advanced by Savastano et al. (1999a), who employed blast furnace slag (BFS)-based composites reinforced with sisal, eucalyptus, and coir fibres.

NFRCCs have been utilized in wall components for decades. Agopyan and John (1992) investigated the use of BFS-based composites reinforced with coir fibres to produce hollow load-bearing wall panels measuring 2.4 meters in height, 0.395 meters in width, and 0.09 meters in thickness in 1989. To assess their performance, carbonated aging conditions were employed to study the short-term effects of accelerated aging, while long-term natural weathering over 2.5 years was evaluated using a prototype. After 12 years of service, the chemical composition of the low-alkaline cement matrix and coir fibres in the wall panels was reanalyzed to assess durability and material performance (John et al., 2005). However, as eco-friendly and cost-effective materials, NFRCCs have primarily been utilized in low-cost roofing and wall components. Further research is essential to advance NFRCCs and develop more sustainable construction materials to expand their applications in engineering.

1.4 Objectives of the Study

The objectives of this study are as follows:

i. To perform statistical analysis to determine a cost-effective optimum mix ratio of JFRCCs using a full factorial statistical approach.
ii. To investigate the compressive strength, strain properties, splitting tensile strength, and microstructure of JFRCCs.
iii. To investigate the effect of different curing conditions and elevated temperature on the compressive strength of JFRCCs.

1.5 Methodology

The methodology adopted in this research is structured to systematically investigate the development of eco-friendly JFRCCs using locally available ingredients. The research is divided into multiple phases, including literature review, material selection, preliminary testing, factorial experimental design, and final experimental validation under various conditions. The research methodology employed for this study is presented in Fig. 1.1. Firstly, a comprehensive literature review was conducted at step-1 to understand the limitations of conventional concrete, synthetic fibre-reinforced concrete, and natural fibre-reinforced composites. This helped in identifying the research gaps and formulating the objectives for developing an optimized JFRCCs mix. Based on these insights, a research scheme was developed to guide the experimental program.

Then, Step-2 focused on material collection and preparation, encompassing Ordinary Portland Cement (OPC) as the primary binder, fly ash as a supplementary cementitious material, fine sand with 150 μm retaining 300 μm passing, treated jute fibres to enhance adhesion with the cement matrix, and a polycarboxylic-based superplasticizer to improve the workability and mechanical properties. A preliminary investigation (Phase I Experiment) was conducted, involving compressive strength tests on 33 cylindrical specimens. Based on the preliminary results, key mix parameters with suitable ranges were identified for further factorial analysis.

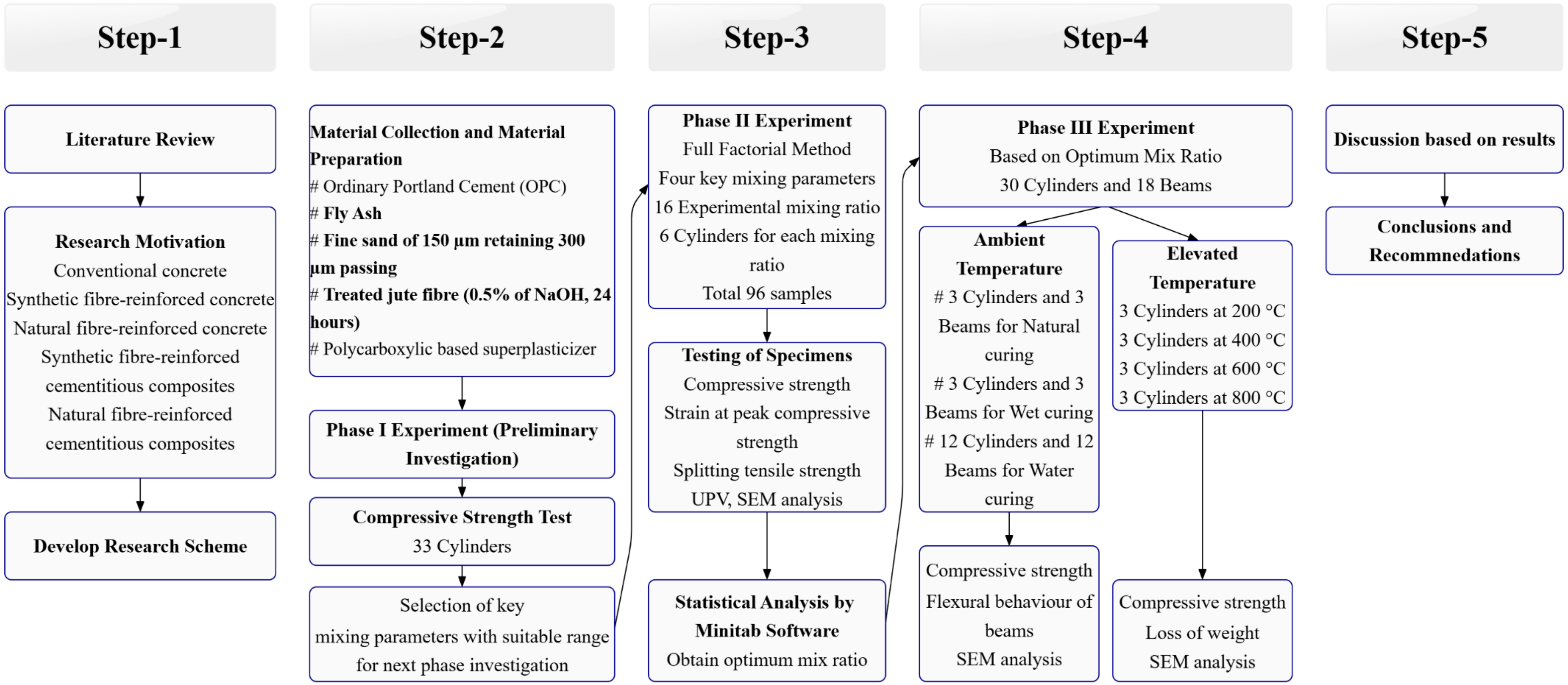

Fig. 1.1: Research flow diagram

Afterwards, Step-3 comprised the Phase II Experiment, utilizing a full factorial design methodology. This phase aimed to optimize the JFRCCs mix ratio by systematically varying four key parameters: W/B ratio, S/B ratio, FA/C ratio, and jute fibre content. For full factorial analysis with four variables, 16 (2^4) experiment were performed and for each case, 6 cylinders was casted, resulting in a total of 96 cylindrical specimens. The specimens were subjected to a range of tests including compressive strength, UPV, strain at peak compressive strength, splitting tensile strength, and SEM analysis. Then, to determine the optimum mixture proportion, statistical analysis was performed utilizing Minitab software.

Thereafter, Step-4, the Phase III Experimental Testing, focused on evaluating the performance and durability of JFRCCs prepared using the optimized mix ratio obtained from Step-3. Thirty cylindrical and 18 beam specimens were prepared. These specimens were subjected to a range of tests under both ambient and elevated temperature conditions (200 °C, 400 °C, 600 °C, and 800 °C). At ambient conditions, specimens were subjected to natural curing, wet curing, and water curing. The tests conducted comprised compressive strength, flexural behaviour of beams, and weight loss due to elevated temperatures.

Finally, Step-5 involved a comprehensive discussion of the results, leading to the formulation of conclusions and recommendations. This systematic approach allowed for a thorough investigation of JFRCCs, from initial material selection to final performance evaluation, ensuring a robust and comprehensive understanding of the material's behaviour.

1.6 Layout of the Thesis

Chapter 1 provides a comprehensive discussion of the study's background and objectives, establishing the foundational framework for the research.

Chapter 2 presents an extensive overview of contemporary research and advancements in the experimental investigation of cementitious composites reinforced with natural fibres. This review highlights the potential of JFRCCs as a sustainable construction material. By addressing challenges and leveraging material science advancements, these composites can enhance durability, cost-effectiveness, and eco-friendliness. The chapter reviews advancements in NFRCCs, covering their chemical composition, physical and mechanical properties, and fibre modification techniques to improve performance.

Chapter 3 outlines the experimental methodology, including material collection and preparation, material properties, sample fabrication, and curing procedures. It also details the testing methods used, like compressive strength, splitting tensile strength, peak compressive strain, flexural strength, UPV, and microstructural analysis of the composites.

Chapter 4 presents a thorough analysis of the Phase I and Phase II experimental investigation on JFRCCs. The study was conducted in three phases: Phase I explored the influence of key mixing parameters on the compressive strength of JFRCCs to establish suitable parameter ranges. Phase II expanded the investigation using a broader range of mix proportions and detailed material characterization to determine the optimum mix ratio. The results from each phase are thoroughly discussed.

Chapter 5 presents a detailed statistical analysis of Phase II experimental results and Phase III investigation. Statistical analysis was conducted to optimize JFRCCs mix ratios. Furthermore, Phase III investigation examined the performance of the optimized composites under diverse curing methods and elevated temperatures. The results from each phase are thoroughly discussed.

Chapter 6 consolidates the research findings, presenting the conclusions derived from the study's results and proposing recommendations to direct future investigations into sustainable JFRCCs.

CHAPTER 2: LITERATURE REVIEW

2.1 Introduction

The construction industry is increasingly focused on developing innovative materials that enhance performance while minimizing environmental impact. Conventional concrete, despite its extensive usage, is a significant contributor to carbon emissions and the depletion of natural resources. In response, research has concentrated toward sustainable alternatives, including cementitious composites including supplementary materials and natural fibres. This motivates research into more sustainable, cost-effective, and eco-friendly construction materials. Therefore, this study explores for development of innovative construction materials utilizing locally available resources. Thereby, this chapter provides a comprehensive overview of concrete technology in general and the chronological development of conventional concrete to fibre-reinforced concrete. The recent advancements in Natural Fibre Reinforced Cementitious Composites (NFRCCs) incorporating various types of natural fibres and supplementary materials are also discussed in this chapter.

2.2 History of Concrete Technology

The origins of concrete date back to ancient civilizations, where early builders used natural materials to create durable structures. Around 6500 BC, the Nabataea traders, also known as Bedouins, discovered an elementary form of concrete to construct floors, housing structures, and underground water storage facilities in regions of southern Syria and northern Jordan (Moropoulou et al., 2005). They understood the benefits of hydraulic lime, which hardens when exposed to water, paving the way for future innovations in concrete technology.

In 3000 BC, the Egyptians made significant strides in using materials that resembled concrete. They combined mud with straw to create bricks and employed gypsum and lime mortars in the construction of monumental structures like the Great Pyramids at Giza. Simultaneously, ancient builders in China utilized a type of cement to build the Great Wall, demonstrating early knowledge of composite materials.

The Romans are credited with refining concrete technology and making it a cornerstone of their construction practices. By 200 BC, Roman engineers developed a blend of volcanic ash, lime, and seawater to create a durable mix known as Roman concrete (Brandon et al., 2008). This material was used extensively in constructing enduring structures such as aqueducts, amphitheaters, and bridges. The Pantheon in Rome, with its massive unreinforced concrete dome, stands as a testament to the Romans ingenuity and mastery of concrete. After the fall of the Roman Empire in 476 AD, concrete technology experienced a decline until the discovery of ancient manuscripts in 1414 revived interest in the material (Oleson et al., 2004). During the Renaissance, builders began experimenting with new methods to produce hydraulic lime. John Smeaton’s discovery in 1793 of a more effective method for creating hydraulic lime by firing limestone containing clay marked a significant milestone. This innovation was instrumental in the reconstruction of the Eddystone Lighthouse in Cornwall, England.

The discovery of Portland cement by Joseph Aspdin in 1824 revolutionized concrete technology. Aspdin created Portland cement by burning finely ground chalk and clay till carbon dioxide was removed, resulting in a material that set more quickly and uniformly than previous versions. Portland cement, which derives its name from the high-grade building stones quarried in Portland, England, has become an essential component in contemporary concrete construction.

The 20th century witnessed rapid advancements in concrete technology. The development of reinforced concrete, pioneered by Francois Hennebique and Joseph Monier, allowed for the construction of stronger and more resilient structures (Van Damme, 2018). The introduction of pre-stressed concrete by Eugene Freyssinet further expanded the materials applications, enabling the creation of longer spans and more intricate designs. Advancements in material science led to the development of high-performance concrete, which provides enhanced strength, durability, and workability. Innovations such as fibre-reinforced concrete and the usage of supplementary cementitious materials like fly ash and slag, have enhanced both the ecological sustainability and versatility of concrete as a construction material. Concrete technology is evolving constantly to meet the demand for sustainable construction and innovative solutions.

The history of concrete technology reflects humanity's ongoing quest for stronger, more viable, and sustainable construction materials. From the early discoveries of ancient civilizations to the sophisticated technologies of today, concrete has played a crucial role in shaping the built environment. As researchers and industry professionals continue to push the boundaries of what is possible, the future of concrete technology promises even greater innovations and advancements, contributing to a more sustainable and resilient world.

2.3 Evolution of Fibre-Reinforced Concrete

Concrete has been a fundamental building material for centuries, with its widespread usage in various construction applications. Conventional concrete, also known as plain or unreinforced concrete, has been the predominant construction material for centuries. Conventional concrete, also known as traditional concrete, is a construction material made from cementing material, water, fine aggregate, course aggregate, and sometimes admixtures (Tipraj et al., 2018). Concretes compressive strength is its primary advantage, making it suitable for various building applications. As a durable and versatile building material, concrete has undergone significant advancements throughout history. However, conventional cement concrete, despite its widespread application, presents fundamental deficiencies, including low tensile strength, low ductility, and cracking susceptibility (Rudnov et al., 2016). The production of cement and coarse aggregates for conventional concrete significantly contributes to greenhouse gas emissions (Shen et al., 2015; Ilg et al., 2016). The cement industry alone is responsible for approximately 8% of global CO_2 emissions. (Ram et al., 2022) This environmental concern has driven the need for more sustainable concrete solutions. Over the previous several decades, researchers have investigated ways to improve the performance and sustainability of concrete. This includes the incorporation of different types of fibres, such as steel, glass, and natural fibres, into the concrete mix (Anandamurthy et al., 2017). The addition of different types of fibres such as steel, glass, polypropylene and basalt has emerged as an important innovation in the field of concrete technology (Rudnov et al., 2016). The primary benefit of using of fibre-reinforced concrete is its greater resistance to cracking and propagation of cracks compared to conventional concrete, an important factor in structures exposed to seismic forces or impact loads (Arivalagan, 2012). The addition of fibres, such as polypropylene, has been shown to impart ductility to structural members, making them more suitable for earthquake-resistant design (Arivalagan, 2012). Fibre-reinforced concrete has the ability to bridge cracks and distribute stresses more evenly, leading to enhanced durability and service life of concrete structures (Ilg et al., 2016; Balea et al., 2021). Furthermore, adding fibres to concrete enhances its mechanical performance, improving tensile strength, ductility, and crack resistance (Bhat & Khan, 2018). Recent research has focused on using renewable, sustainable natural fibres those extracted from agriculture, as a replacement for traditional non-renewable synthetic fibres (Anandamurthy et al., 2017). These eco-friendly fibres have the potential to further lessen the environmental effect of concrete while maintaining or improving its performance. Therefore, Fibre Reinforced Concrete (FRC) represents one of the most noteworthy developments in the evolution of concrete due to its increased strength, durability, and performance in various structural applications.

2.3.1 Types of Fibres Used in Concrete Composites

The fibres used in concrete composites can be broadly categorized into synthetic, metallic, and natural fibres.

- **Synthetic Fibres**: Polypropylene, polyvinyl alcohol, polyethylene, polyolefin, glass fibre and carbon fibres are commonly used due to their high tensile strength, chemical resistance, and low density. These fibres are effective in reducing plastic shrinkage and cracking.

Steel fibres, widely used in Fibre-Reinforced Cementitious Composites (FRCCs), provide superior load-bearing capacity and crack control. But, their susceptibility to corrosion in aggressive environments is a notable limitation.

- **Natural Fibres**: Various types of natural fibres, such as jute, hemp, bagasse, basalt, coir, and sisal have gained attention for their sustainability and low environmental impact. In Bangladesh, jute fibres are distinguished by their abundant supply, affordability, and impressive mechanical properties.

2.3.2 Advantage and Disadvantage of Different Fibres Types Used in Concrete Composites

Concrete composites can be reinforced with either synthetic or natural fibres, each presents some distinct advantages and limitations. A summarized comparison of the advantages and disadvantages of various fibre types is presented in Table 2.1.

Table 2.1: Advantage and disadvantage of different fibres in concrete composites

Fibre Type	Advantages	Disadvantages
Synthetic	• Tensile strength • Chemical resistance • Reduce plastic shrinkage • Excellent load-bearing capacity • Control crack	• Non-biodegradable • Contributes to environmental pollution • Expensive • Steel fibres prone to corrosion and heavy
Natural	• Tensile strength • Sustainable, biodegradable • Lightweight • Cost-effective • Crack resistance of concrete by bridging micro-cracks	• Susceptible to moisture absorption, microbial degradation, and alkali attack

As presented in the table, synthetic fibres provide excellent tensile strength, chemical resistance, and crack control but are non-biodegradable, costly, and may contribute to environmental pollution. In contrast, natural fibres are sustainable, lightweight, and cost-effective, offering good tensile strength and micro-crack bridging. However, they are vulnerable to moisture absorption, microbial degradation, and alkali attack, which can affect long-term durability.

2.3.3 Effect of Different Types of Fibres on Concrete Composites

Fibre-reinforced concrete (FRC) was developed as an innovative construction material in the late 20th century, enhancing conventional concretes mechanical properties. Concrete made with synthetic fibre i.e., polypropylene fibres (PPFs) significantly improved ductility, first crack load, maximum crack width, and load-deflection interrelations. Also, it was revealed that compressive, split tensile, and flexural strengths increased up to 2.0 % PPF addition and subsequently decreased (Ahmad et al., 2021). Zakaria et al. (2016) explored the effects of varying fibre length and content (volume fraction) of natural jute fibre on the mechanical properties of jute fibre-reinforced concrete composites and they found that shorter jute fibres and lower fibre content led to improved mechanical properties compared to plain concrete. Conversely, longer fibres and higher content resulted in balling formation and increased porosity, negatively impacting the composites performance. By incorporating natural jute fibres (JF) into concrete, plastic shrinkage cracks of JF concrete would be decreased by 75–99% in contrast to non-fibre reinforced concrete and, the compressive and tensile strengths were improved by 12.4% and 58%, respectively, depending on the fibre length and content (Gupta et al., 2020).

Alberti et al. (2017) studied the synergistic effects of polyolefin and steel-hooked fibres in self-compacting fibre-reinforced concrete, finding that while fibre inclusion enhanced fracture toughness, ductility, and residual strength, it did not significantly influence compressive strength, indirect tensile strength, or modulus of elasticity. Afterwards, Bheel et al. (2021) examined the combined effects of nylon and jute fibres on cement concrete and found that a 1% volume fraction of both fibres optimally enhanced compressive, split tensile, and flexural strengths at 90 days compared to the control mix, while their inclusion reduced drying shrinkage but also decreased workability.

Yang et al. (2017) investigated the incorporation polyvinyl alcohol (PVA) fibre and high-volume Class F fly ash in engineered cementitious composites (ECCs) to enhance both mechanical properties and environmental sustainability and found that increasing the fly ash content led to improved tensile ductility and robustness, as well as reduced drying shrinkage. Furthermore, the usage of high-volume fly ash contributed to a reduction in cement content which lowering carbon dioxide emissions, promoting the utilization of industrial waste materials and enhancing the overall greenness of the ECCs. In another study, two different type polypropylene fibre (fibrillated and monofilament) were incorporated intro cementitious composites and it was observed that fibrillated based composites shows better tensile strength and flexural capacity in comparison to monofilament, conversely, monofilament fibres were found to improve tensile and flexural ductility (Deb et. al., 2018).

Tian et al. (2015) developed a green hybrid fibre-reinforced cementitious incorporating bagasse fibre and steel fibre combinedly with high volume of fly ash and this study explored that increasing use of the fly ash increases the ductility of the composites but decreases the compressive strength. Additionally, this study explored the effects of treating the bagasse fibres with NaOH and silane, aiming to enhance the bond between fibres and cementitious matrix, which is essential for effective load transfer and overall composite performance.

2.4 Evolution of NFRCCs

The development of NFRCCs has evolved significantly over the past few decades in response to growing environmental concerns and the demand for sustainable construction materials. Early research focused on enhancing cement-based composites with synthetic fibres like polypropylene, glass, steel, etc., which offered improvements in strength and crack resistance. But concerns over cost, non-biodegradability, and environmental impact of synthetic fibres led to the investigation of natural fibres. Over time, natural fibres including jute, sisal, coir, and flax have been investigated due to their renewability, biodegradability, and availability in developing regions. Initially, applications of natural fibres into cementitious composited faced challenges including poor compatibility among natural fibres and the alkaline cement medium, high moisture absorption, and microbial degradation. Despite challenges related to alkali sensitivity, water absorption, and fibre degradation, advancements in fibre treatment and mix design optimization have improved durability and mechanical performance of NFRCCs. As a result, NFRCCs are now being considered as a promising eco-friendly solution for low-cost and sustainable construction applications.

2.4.1 Sources of Natural Fibres

Natural fibres are raw materials obtained from plants, animals, or minerals. Fig. 2.1 highlights that natural fibres come from 3 primary sources: animals, minerals, and plants.

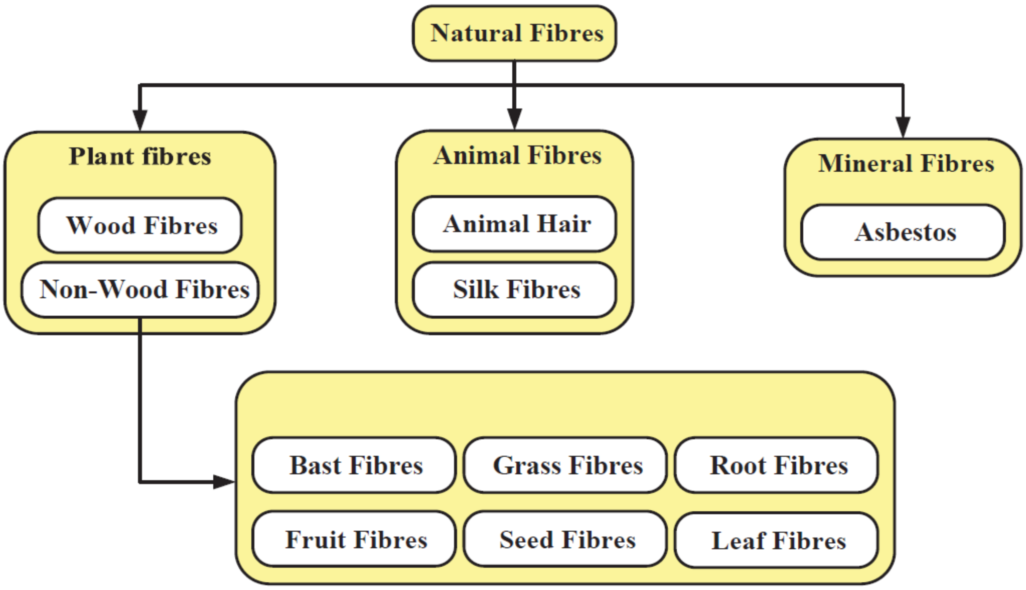

Fig. 2.1: Classification of natural fibres (Sadrmanesh & Chen, 2019)

Animal fibres consist of animal hair and silk, while mineral fibres, such as asbestos and basalt, are associated with major health risks. Plant fibres are classified into 2 primary groups: wood and non-wood. Non-wood fibres, also recognized as lignocellulosic fibres, are further subdivided into bast, seed, straw, leaf, and grass fibres. Notable examples of bast fibre plants include hemp, ramie, flax, kenaf, and jute. As far back as 3,500 years ago, materials such as hay and branches were utilized in building to enhance durability (Brandt, 2008). However, with industrial advancement, newly developed fibres like steel and synthetic fibres have gradually replaced natural fibres.

These modern fibres are now increasingly used to reinforce cement-based materials because of their superior ability to improve the mechanical properties of the composites (Chen and Chung, 1993; Marikunte et al., 1997; Luo et al., 2001; Li et al., 2007). As a result, the progress of natural fibre reinforced building materials was relatively slow, and this trend persisted until 1970. The idea of environmental sustainability was initiated in 1970 and at that time natural fibres get more attention due to its unique properties as recyclable and eco-friendly construction materials, along with the increasing demand for green and sustainable construction and building materials. NFRCCs has gained growing global attention for research in recent decades. The majority of natural fibres used are easily accessible natural waste materials found globally, including wood and vegetable fibres with low elastic modulus. In the mid-1940s, researchers started using cellulose fibre as a cost-effective alternative to asbestos. But due to the health risks associated with asbestos began to be questioned and it was subsequently banned by legislation in many countries in the 1970s (Coutts, 2005). Since then, numerous studies have been carried out to enhance the mechanical properties of natural fibre reinforced cement-based composites (Davis et al., 1981; Coutts and Kightly, 1982; Coutts and Ridikas, 1982a; Rainey, 2009).

The inclusion of natural fibres in concrete offers significant advantages. Firstly, producing NFRCCs generates far less environmental pollution compared to conventional concrete as it involves natural substitutes which makes NFRCCs a key element in advancing sustainability within the construction sector. Moreover, the widespread availability of natural fibres worldwide makes them a more affordable option than steel or synthetic fibres, while also supporting environmentally sustainable development and a reduced carbon footprint. (Savastano and Agopyan, 1999;

Savastano et al., 2000; 2003). Table 2.2 presents the general prices of various types of fibres which clearly shows that using natural fibres can lead to a significant cost reduction compared to other fibre options.

Table 2.2: Price of different fibres

Fibre	Price (USD/ton)	Fibre	Price (USD/ton)
Steel Fibre	740	Bagasse Fibre	200
Polyvinyl Alcohol Fibre (PVA)	2800	Sisal Fibre	280-350
Glass Fibre	2820	Banana Fibre	650
Polypropylene Fibre (PP)	1520	Coir Fibre	255-295
Polyethylene Fibre (PE)	1890	Jute Fibre	500-600

(Source: http://www.alibaba.com)

Furthermore, the mechanical properties of NFRCCs have been experimentally studied and recorded in the literatures, showing that that natural fibres can enhance the mechanical properties of the cementitious matrix, including flexural toughness, flexural strength, compressive strength, impact resistance, tensile strength, and tensile ductility (Al-Oraimi and Seibi, 1995; Savastano and Agopyan, 1999; Savastano et al., 2000; 2003; Ramakrishna and Sundararajan, 2005).

Aziz et al. (1981) reviewed the research and development of NFRCCs made with materials such as coconut husk, sisal, bagasse, bamboo, jute, and wood fibres prior to 1980 and they also provided an overview of the potential applications of NFRCCs in construction. A literature review was carried out by John and Anandjiwala (2008) on the use of vegetable fibres in construction materials, encompassing almost all research conducted up until that year. Pacheco and Jalali (2011) recently carried out a comprehensive review on the properties of fibres, the mechanical characteristics of fibre-reinforced composites, and their durability. However, a comprehensive review of the recent developments in NFRCCs has yet to be showcased.

Following sections provide a review focused on recent progress in experimental studies concerning the mechanical behaviour of NFRCCs. Section 2.4.2 provides information on the mechanical properties and chemical composition of natural fibres. Section 2.4.3 discusses fibre modification, while Sections 2.4.4 review studies on characteristics of NFRCCs.

2.4.2 Mechanical Properties and Chemical Composition of Natural Fibres

Natural fibres can break down over time when exposed to the alkaline conditions in cement-based materials. To ensure the long-term durability of NFRCCs, understanding the composition of these fibres is crucial. This understanding helps explain how they perform in NFRCCs and why they degrade in alkaline environments. This knowledge is key to developing NFRCCs with enhanced durability.

Natural fibres are cellular composites characterized by a distinct structure and composition. Typically, they are made up of cellulose, hemicellulose, lignin, and, in certain cases, pectin as their primary components (John et al, 2005; Arsene et al, 2007; John et al., 2008). Fig. 2.2 shows the structure of a typical natural fibre.

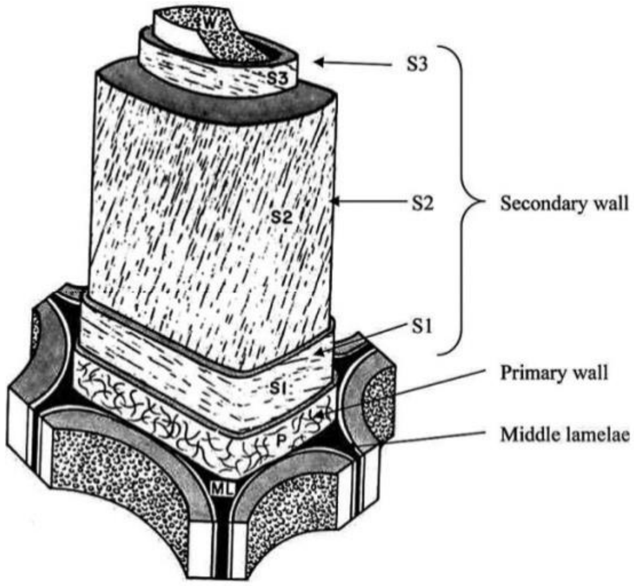

Fig. 2.2: Schematic diagram of natural fibre structure (Sjostrom, 1981; Arsene et al, 2007).

Note: S1, S2 and S3 are the outer layer, middle layer and inner layer of the secondary wall, respectively.

It consists of cellulose fibrils embedded in a matrix of hemicelluloses, lignin, and proteins, forming various layers within the fibre (Le Le Troëdec et al., 2011; Pacheco-Torgal and Jalali, 2011). Cellulose is a linear polymer made up of glucose units, and it serves as the key structural component that gives natural fibres their strength and stability (Reddy and Yang, 2005). Cellulose can withstand strong alkalis, but when exposed to acids, it breaks down easily into water-soluble sugars (John et al., 2008). Hemicellulose is a branched polymer composed of different types of polysaccharides. Hemicellulose doesn't provide as much stiffness or strength to fibres as cellulose does and it is highly hydrophilic, dissolves in alkalis, and is easily broken down by acids (Reddy and Yang, 2005; John et al., 2008). Lignin is an unstructured, diverse mixture made up of aromatic polymers and phenyl propane monomers (John et al., 2005). It contributes to the compressive strength and stiffness of natural fibres (Reddy and

Yang, 2005). Table 2.3 provides a summary of the detailed chemical composition of natural fibres, including jute fibre. Because of variations in their chemical composition, natural fibres often exhibit differences in their properties (Kulkarni et al., 1983), which can result in unpredictable behaviour in concrete (Swamy, 1990; Li et al., 2006; Pacheto-Torgal and Jalali, 2011).

Furthermore, various researchers have investigated the physical and mechanical characteristics of different natural fibres, including jute fibre, with a summary of their results presented in Table 2.4.

Table 2.3: Composition of natural fibres (Tian, 2015)

Chemical Constituent	Abaca	Bagasse	Bamboo	Banana	Coir	Cotton	Eucalyptus	Flax	Henequen	Jute	Sisal
Cellulose (wt. %)	45.4	41.7–55.2	26–43	25.65	33.2–43	85–90	41.57	64.1–71	60–77.6	33.4–71.5	33.4–78
Hemicellulose (wt. %)	38.5	16.8–28	30	17.04	31.1	5.7	32.56	16.7–20.6	4–28.0	13.6–22.7	10.0–24
Lignin (wt. %)	14.9	21.8–25.3	21–31	24.84	20.5	–	25.4	2.0–2.2	8–13.1	11.8–28.0	9.9–22.7
Wax (wt. %)	2	–	–	–	–	0.6	–	1.5	0.5	0.5	0.3–2
References	(John et al, 2008)	(Arsene et al., 2003; 2007; John et al, 2008)	(John et al, 2008)	(Arsene et al., 2003; 2007)	(John et al, 2008)	(John et al, 2008)	(Arsene et al., 2003; 2007)	(Bledzki and Gassan, 1999; John et al, 2008)	(Li et al, 2007; John et al, 2008)	(Ramakrishna and Sundararajan, 2005; Li et al, 2007)	(Li et al, 2007; John et al, 2008)

Table 2.4: Material properties of natural fibres (Tian, 2015)

Property	Abaca	Bagasse	Bamboo	Banana	Coir	Cotton	Flax	Hemp	Henequen	Jute	Sisal
Density (g/cm^3)	1.5	1.25	0.6–1.1	1.35	1.2	1.5–1.6	1.4–1.5	1.5	1.2	1.3–1.46	1.33–1.5
Elongation (%)	3–10	–	–	5.9	15–30	3–10	1.2–3.2	1.6	3.7–5.9	1.5–1.8	2.0–2.5
Tensile Strength (MPa)	400	290	140–230	384–500	175–220	287–597	345–1500	550–900	430–570	393–800	400–700
Young's Modulus (GPa)	12	17	11–17	12–50	4–6	5.5–12.6	27.6–80	34–70	10.1–16.3	10–30	9–22
References	(John et al., 2008)	(John et al., 2008)	(John et al., 2008)	(Arsene et al., 2003; John et al., 2008)	(Bledzki and Gassan , 1999)	(Bledzki and Gassan , 1999; Li et al., 2007)	(Bledzki and Gassan , 1999; Li et al., 2007)	(Arsene et al., 2003; Li et al., 2007)	(John et al., 2008)	(Bledzki and Gassan , 1999; Li et al., 2007)	(Bledzki and Gassan , 1999; Li et al., 2007; John et al., 2008)

2.4.3 Treatment of Natural Fibres

In alkaline cement-based environments, the lignin in natural fibres breaks down, leading to a notable reduction in the strength of the NFRCCs (Bergstrom and Gram, 1984; Arsene et al, 2007). According to some studies, natural fibres could preserve just about 20% of their initial tensile strength after being exposed to NaOH or $Ca(OH)_2$ solutions (Ramakrishna and Sundararajan, 2005a; Kriker et al., 2008). Numerous investigations have been conducted with the aim of improving the mechanical characteristics of natural fibres. The subsequent section provides a detailed overview of various techniques and their impact on the properties of natural fibres or NFRCCs.

Two methods were proposed to mitigate the alkaline attack on fibres. The first involves using pozzolanic materials, such as fly ash (McCarthy and Dhir, 2005; Sakai et al., 2005), rice husk ash (Nehdi et al., 2003), flax particles (Aamr-Daya et al., 2008), slag (Savastano et al., 1999a; 2001), rattan hash particles (Olorunisola, 2008), fine powdered brick residues (Souza and Molin, 2005), and sugar cane bagasse ash (Singh et al., 2000), to partially replace cement and lessen the alkali impact on natural fibres. The second approach involves applying chemical or thermal treatments to the natural fibres. Using pozzolanic materials to partially replace cement can lower the alkali concentration in the matrix, thereby reducing the alkaline attack on natural fibres and helping to preserve the composites mechanical properties. Chemical or thermal treatment of natural fibres could enhance their physical and mechanical properties. As a result, treated natural fibres may show improved durability, even after prolonged exposure to alkali, making them suitable for enhancing the long-term mechanical properties of cement-based composites.

Pulping, a chemical treatment involving a strong alkaline solution, helps remove lignin from natural fibres, improving their bond with the cement matrix and increasing their resistance to alkaline degradation (John et al., 2005, Pacheco-Torgal and Jalali, 2011). Pulping could be carried out either mechanically or chemically, depending on the approach used (Savastano et al., 2003; 2004; Arsene et al., 2013). Compared to kraft pulping, organosolv-pulped fibres could enhance the water absorption, apparent voids, and mechanical properties of composites to a greater extent (Joaquim et al, 2009).

Furthermore, when compared to banana pulp and coir pulp, composites reinforced with sisal pulp and eucalyptus pulp demonstrated superior modulus of rupture, approximately 20 MPa, and fracture toughness ranging from 1.0 to 1.5 kJ/m^2, at fibre concentrations of 8 wt% and 12 wt%, respectively (Coutts and Warden, 1992; Savastano et al., 2000; 2003; Tonoli et al., 2010). Other treatments, like alkali, acid, and pyrolysis treatments, have also been used on vegetable fibres (Arsene et al., 2007).

Alkaline treatment is a widely used technique as it helps to eliminate the amorphous components in the fibres, such as waxes, hemicelluloses, and pectins and following the treatment, the fibres become rougher, allowing them to bond more effectively with the matrix (Valadez-Gonzalez et al., 1999; Le Troëdec et al., 2011; Sawsen et al., 2014). As per Le Troëdec et al. (2011), treating hemp fibres with NaOH could increase the maximum stress by up to 60% compared to composites made from untreated hemp fibres. Additionally, the composites with NaOH-treated fibres exhibited ductile behaviour and stronger bonding between the fibres and the matrix (Sawsen et al., 2014).

Acid treatment boosts the cellulose content while significantly reducing the hemicellulose content (Arsene et al., 2013). Compared to alkali treatment, acid treatment could strengthen the rupture stress of the composites, but it tends to weaken the bond between the natural fibres and the matrix (Le Troëdec et al., 2009). Arsene et al. (2007) reported that pyrolysis treatments could cause the thermal breakdown of hemicellulose and even lignin in natural fibres, which enhances the fibres resistance to alkali when exposed to cement-based environments. When thermal treatment was used, the fibre-reinforced composites showed improvements of 36-46% in splitting tensile strength and 31-45% in compressive strength (Wei and Meyer, 2014).

In addition to the treatments previously outlined, several modification techniques have been explored for specialized applications, such as reducing water absorption in hydrophilic natural fibres and improving fibre-matrix adhesion. For instance, Tonoli et al. (2012) developed a bleaching method, while Claramunt et al. (2011) proposed hornification as an alternative approach.

Additionally, some researchers revealed that coating fibres with certain materials can reduce water absorption and enhance the bonding between the fibres and the matrix (Tonoli et al., 2013). Using a latex-based adhesive enhance the workability of the mixture and improve the fibre-matrix adhesion (Sawsen et al., 2014).

2.4.4 Characteristics of NFRCCs

NFRCCs exhibit distinct mechanical properties compared to conventional fibre-reinforced concrete due to the inherent characteristics of natural fibres. Extensive research has been conducted to investigate their performance, encompassing physical and mechanical properties, fracture mechanics, shrinkage characteristics, impact resistance, and microstructural behaviour. The studies on physical, mechanical properties and shrinkage behaviour of NFRCCs are presented in this section. This section also reviews studies on the fracture surface and the interfacial behaviour between the fibre and the matrix.

2.4.4.1 Physical Properties of NFRCCs

The incorporation of natural fibres into cementitious composites can modify their physical properties, including setting and water absorption characteristics, due to the inherent characteristics of the fibres. Thus, it is essential to investigate how natural fibres impact the physical performance of NFRCCs. Mansur and Aziz (1982) found that as the length and content of jute fibres increased, the workability of the cement paste and mortar decreased. When eucalyptus pulp, coir, or a mix of eucalyptus pulp and sisal fibres were used, cement composites exhibited lower workability compared to the reference mixture without fibres (Savastano et al., 1999a). The observed decrease in workability is primarily due to the hygroscopic nature of natural fibres, which absorb moisture. The fibre aspect ratio and volume fraction are key factors influencing the reduction in workability of NFRCCs. To mitigate the reduced workability, fibre pre-treatment can be used to minimize the water-absorbing chemical components in the fibres (Onuaguluchi & Banthia, 2016).

Alkali treatment is effective method in improving the mechanical, physical, and thermal properties of both fibres and composites, which could also enhance the bond between natural fibres and the composite matrices (Jo et al., 2016).

2.4.4.2 Mechanical Properties of NFRCCs

Numerous investigations have explored the mechanical characteristics of NFRCCs. These investigations extensively have assessed mechanical performance, focusing on parameters such as fibre type, length, content, casting pressure, and distribution to examine properties including compressive strength, tensile strength, flexural strength, fracture toughness, and impact resistance. While the majority of research focuses on fundamental material properties under static loading (compressive, tensile, and bending behaviour), some studies have also investigated aspects such as impact resistance and shrinkage. Blankenhorn et al. (2001) compared key mechanical properties, such as compressive strength, modulus of rupture, and fracture toughness, of cementitious composites containing wood fibres to those of conventional plain concrete specimens. This study aimed to assess the impact of chemically modified fibres on mechanical performance. It was suggested that chemical agents could act as coupling agents to enhance natural fibre properties and improve composite performance (Coutts & Campbell, 1979). Similarly, physical treatments have also been found effective in improving the mechanical properties of NFRCCs. Coutts (1984) demonstrated these improvements in studies involving the modulus of rupture and fracture toughness of concrete reinforced with autoclaved beaten wood fibres or fibres processed under high-temperature thermomechanical conditions (Campbell & Coutts, 1980). Ramaswamy et al. (1983) investigated the tensile strength, fracture toughness, shrinkage, and impact strength of cementitious composites reinforced with jute, coir, and bamboo fibres and they concluded that vegetable fibres offer significant advantages as reinforcing materials for concrete. Similarly, Coutts and Wardent (1987) examined the flexural strength and fracture toughness of air-cured abaca fibre-reinforced composites, comparing them with other NFRCCs to assess whether a high fibre aspect ratio enhances mechanical performance, and found that optimal mechanical properties were achieved with a fibre content of 8% by mass of cement.

Coutts conducted extensive studies on the mechanical properties of cementitious composites reinforced with various natural fibres, including flax (Coutts, 1983), wood fibre (Coutts & Warden, 1990), and sisal fibres (Coutts & Warden, 1992). The research on flax fibre-reinforced concrete investigated the effects of fibre content, ranging from 2% to 12%, and fibre refining on the modulus of rupture (Coutts, 1983). Similar experiments were performed on sisal pulp-reinforced cement mortar (Coutts and Warden, 1992) and the results showed that increasing fibre content from 2% to 12% led to a continuous decrease in the elastic modulus, while the flexural strength reached a peak of approximately 18 MPa at 8% fibre content by weight. In parallel, Savastano et al. (2004) reported that the optimal performance was achieved with 8% sisal fibre and 12% eucalyptus fibre, yielding flexural strength values of approximately 20 MPa, which underscore the critical influence of fibre type and content on the mechanical behaviour of NFRCCs. The superior mechanical properties of eucalyptus fibre-reinforced cementitious composites may be attributed to the rough surface texture of eucalyptus fibres, which enhances their adhesion to the cementitious matrix (Tonli et al., 2010; 2010a). Conversely, studies on pinus radiata fibre-reinforced concrete focused on the influence of casting pressure on the composites mechanical performance (Coutts & Warden, 1990). Zhu et al. (1994) investigated the mechanical properties of banana fibre-reinforced concrete, where banana pulps were derived from fibre strands and processed using a Valley Beater and chemical pulping techniques, and the specimens were air-cured for 28 days before undergoing compressive and flexural strength testing.

Bantie (2010) conducted a study on the modulus of rupture and compressive strength of jute fibre-reinforced concrete, emphasizing toughness indices and residual strength factors. Similarly, Mansur and Aziz (1982) investigated the mechanical behaviour of jute fibre-reinforced mortar through a series of tests, including direct tension, bending, axial compression, and impact tests—examining the effects of fibre length and content on the mechanical performance of the composites.

Impact resistance is a critical mechanical property, particularly for materials intended for use in commercial construction. Several studies have examined the impact resistance of NFRCCs (Mansur & Aziz, 1982; Al-Oraimi & Seibi, 1995; Ramakrishna & Sundararajan, 2005). Ramakrishna and Sundararajan (2005) compared the impact behaviour of concrete reinforced with various natural fibres, including coir, sisal, jute, and hibiscus—under different fibre lengths (20 mm, 30 mm, and 40 mm) and mass ratios (0.5%, 1%, 1.5%, and 2.5%), revealing that coir fibre-reinforced concrete exhibited the highest impact resistance. In another study, the impact resistance of high-strength concrete reinforced with palm tree fibres was investigated and compared to that of glass fibre-reinforced composites, revealing that palm fibre-reinforced concrete demonstrated comparable performance with glass fibre (Al-Oraimi & Seibi, 1995).

2.4.4.3 Fracture Surface and Fibre-Matrix Interfacial Behaviour of NFRCCs

Research on the fibre-matrix interfacial behaviour and fracture surfaces has been conducted to explore the micromechanics of NFRCCs, with early investigations focusing on evaluating the interfacial bond strength of natural fibre-cement composites through tensile testing (Tian, 2015). Bessell and Mutuli (1982) pioneered a method for quantifying the interfacial bond strength in sisal fibre-reinforced cementitious composites. Although the findings showed discrepancies when compared to experimental data, this research laid a foundational understanding of bonding behaviour in NFRCCs. Further studies on the interfacial bond behaviour were conducted by Coutts and Kightly (1984), who used scanning electron microscopy (SEM) to investigate the fibre-to-fibre and fibre-to-matrix bonding at the fracture surfaces of wood fibre-reinforced composites that had undergone pretreatment with high temperatures, water, or relatively high humidity. Coutts (1987) detailed a sequential process, including concrete hydration, fibre refining, interlocking between the two phases, and the complete fracture of the composites. The SEM images offered a comprehensive understanding of the role natural fibres play in reinforcing brittle matrices.

Savastano and Agopyan (1999) investigated the transition zone in NFRCCs, characterized by a water film at the interface between the matrix and natural fibre, which exhibited unique properties compared to the rest of the matrix. Fibre-matrix interface was investigated at 7, 28, 90, and 180 days by using Backscattered electron imaging (BSEI) and energy dispersive spectroscopy (EDS) and the findings were compared with those of composites reinforced with polypropylene fibres and vegetable fibres (Savastano & Agopyan, 1999).

2.5 Effect of Fly Ash in Cementitious Composites

The incorporation of fly ash in cementitious composites has been a subject of significant research interest, as it can contribute to the sustainability and environmental friendliness of these materials. Fly ash is a waste product generated from coal-fired power plants, and its utilization in concrete can reduce the need for cement, which is a major contributor to greenhouse gas emissions (Kubissa et al., 2017). Researchers have reported that the use of high volumes of fly ash in concrete, referred to as "high volume fly ash concrete," not only has a positive ecological effect but also enhances the durability of the material (Kubissa et al., 2017). This is because the pozzolanic reaction between fly ash and calcium hydroxide, a by-product of cement hydration, can lead to the formation of additional calcium silicate hydrate gel (C-S-H), which improves the overall strength and durability of the concrete (Li et al., 2020).

Kumar et al. (2023) investigated the effect of galvanized iron (GI) reinforcement on the tensile strength and ductility of fly ash-based composites, observing that the inclusion of GI within the fly ash layers significantly increased both the peak stress and axial strain at failure. Furthermore, increasing the number of GI reinforcements reduced the influence of fly ash on the composite's behaviour, while decreasing the moisture content in the fly ash led to increased strength, suggesting promising applications for fly ash as a construction material when reinforced with GI (Kumar et al., 2023).

Shaikh et al. (2018) studied the effects of incorporating fly ash into ultra-high performance steel fibre-reinforced cementitious composites by replacing 20%, 30%, 40%, and 50% of cement with fly ash and adding 2 wt. % nano-silica, finding that a fly ash content of 30–40% yielded the best results. These mixtures exhibited improved compressive strength, tensile strain-hardening behaviour, and energy absorption compared to other fly ash contents and the control mix; however, it is important to note that exceeding 40% fly ash content led to a decline in performance (Shaikh et al., 2018). This is likely due to the dilution effect, where the reduced cement content outweighs the benefits of fly ash addition. Also, beyond a certain point, fly ash acts more as a fine aggregate than a reactive pozzolanic material. This study highlights the potential of using fly ash in UHP-FRCC to enhance mechanical properties while reducing environmental impact. Incorporating low-calcium fly ash (replacing cement by volume) at levels of 10-15% alongside recycled tire steel fibre (RTSF) improved compressive strength, splitting tensile strength, modulus of rupture, and electrical resistivity while reducing water absorption (Akhtar et al., 2022). Besides, higher fly ash replacements (25-35%) decreased mechanical properties but still offered some benefits compared to plain concrete. The study suggests that combining RTSF and moderate levels of FA (10-15%) is an effective strategy for enhancing concrete performance and promoting sustainable construction by utilizing waste materials.

Hossain et al. (2023) explored the combined effects of fly ash and jute fibre on concrete properties, finding that fly ash enhances both fresh and hardened characteristics, specifically improving workability, as evidenced by increased slump and compacting factor values. Furthermore, the inclusion of fly ash led to notable improvements in mechanical properties, including such as compressive, splitting tensile, and flexural strengths—highlighting the synergistic benefits of combining fly ash and jute fibres for developing sustainable and high-performance concrete (Hossain et al., 2023). The optimal combination, according to their research, was 10 % fly ash and 0.2 % jute fibre by volume, which yielded the best balance of workability and strength enhancement. This combination resulted in a compressive strength improvement of up to 25.9 % compared to the control mix. These improvements are attributed to the filler effect of fly ash, resulting in a denser microstructure, and the pozzolanic reaction, which enhances the formation of additional C-S-H gel. This study provides valuable insights for utilizing industrial by-product like fly ash in conjunction with natural fibres to create more sustainable and durable concrete materials.

Merta et al. (2024) studied the impact of freeze-thaw cycles and deicing salts on cementitious composites containing natural fibres such as hemp and flax, and found that the incorporation of fly ash significantly improved the composites resistance to freeze-thaw damage. The fly ash's contribution to a denser matrix and its pozzolanic activity, which reduces calcium hydroxide content, are cited as key factors in enhancing durability under these harsh conditions. Specifically, the study observed that composites with fly ash exhibited less scaling and retained higher compressive strength after exposure to freeze-thaw cycles and deicing salts compared to control mixes without fly ash. Mechanical behaviour of green hybrid fibre-reinforced cementitious composites containing bagasse fibre, steel fibre and high volumes of fly ash was investigated which showed that increasing fly ash content (while keeping fibre content constant) decreased compressive strength, Young's modulus, and modulus of rupture (Tian et al., 2015). However, the inclusion of fly ash increased the ductility of the composites. This is attributed to the filling effect of fly ash, which creates a more compact matrix even in the absence of coarse aggregates.

Ali et al. (2021) studied the synergistic effects of fly ash and hooked steel fibres on the strength and durability of high-strength recycled aggregate concrete, observing that the incorporation of fly ash effectively mitigated the negative impacts of recycled aggregates and steel fibres on durability, particularly in terms of water and chloride-ion permeability. Furthermore, the combination of fly ash and steel fibres significantly enhanced the concrete's resistance to acid attack, and a synergistic effect between 15% fly ash and 1% steel fibre was observed to improve flexural, splitting tensile, and compressive strengths compared to recycled concrete without these additions (Ali et al., 2021).

Fauzan et al. (2019) investigated the effects of steel fibre from waste tires (SFWT) on high-strength concrete containing fly ash and found that incorporating 2% SFWT and 30% fly ash as partial cement replacement yielded the best performance, enhancing compressive strength by approximately 10%, tensile strength by 64%, and flexural strength by 18%. Moreover, the fly ash itself enhanced both the strength and workability of the concrete mix, highlighting the potential of using waste materials like SFWT and fly ash to improve concrete properties and promote sustainable construction practices (Fauzan et al., 2019). In another study, Pappu and Thakur (2017) demonstrated that incorporating natural cellulosic sisal fibres with fly ash enhanced the tensile properties and surface finish of composites.

Yaseen et al. (2023) investigated the use of fly ash (FA) and sugarcane bagasse ash (SCBA) as supplementary cementitious materials in polyvinyl alcohol (PVA) fibre-reinforced engineered cementitious composites (ECCs), finding that substituting FA with SCBA reduced compressive strength while enhancing flexural strength and ductility. Notably, while ECCs with 100% FA exhibited the highest compressive strength, a 50/50 FA-SCBA blend achieved superior flexural strength. The improved flexural performance was attributed to the finer particle size and elevated silica content of SCBA, which facilitated better fibre dispersion and interfacial bonding, underscoring the potential of utilizing industrial by-products to enhance the mechanical properties and sustainability of ECCs (Yaseen et al., 2023).

Moreover, the incorporation of fly ash in cementitious composites can lead to cost savings, as it is generally a less expensive material than cement. This economic benefit, combined with the environmental advantages, makes the use of fly ash an attractive option for the development of eco-friendly cementitious composites.

2.6 Research Gaps

Based on the literature review, FRC developed by synthetic fibres demonstrated many advantages like enhance tensile strength, resistance to chemical attacks, reduce shrinkage, improve load bearing capacity, control crack propagation but synthetic fibres are costly, derived from non-renewable fossil fuels and are non-biodegradable, contributing significantly to environmental pollution. The production and disposal of synthetic fibres are associated with high greenhouse gas emissions and the release of micro-plastics into ecosystems. In contrast, natural fibres are sustainable, biodegradable, and generally require fewer chemicals during manufacturing, resulting in a lower environmental footprint. Additionally, natural fibres are lightweight and cost-effective, making them a more environmentally friendly and economical choice for various applications. For this reason, FRC made with natural fibre have gained concentration to develop sustainable construction material. Natural fibre e.g. jute fibre is abundant in Bangladesh and Bangladesh, one of the largest jute producers globally, produces approximately 1.6 million metric tons of jute annually (Siraj-UD-Doulah et al., 2020). Numerous studies, as summarized in Table 2.5, have investigated the integration of jute fibres into traditional concrete preparations that incorporate coarse aggregates.

Table 2.5: Previous researches on jute fibre reinforced cement material.

Composites Materials	Material Composition[a]	Evaluated Properties[b]	References
Jute fibre reinforced mortar	JF, S, C, W	CS, FS, MOR, FS	Mansur and Aziz, 1982
Jute fibre reinforced concrete	JF, CA, S, C, W	CS, FS, SSB, IS	Ramaswamy et al., 1983
Jute fibre reinforced mortar	JF, S, C, W	IS, CR	Ramakrishna and Sundararajan, 2005
Jute fibre-reinforced concrete	JF, CA, S, C, W	CS, FS, TB	Bantie, 2010
Jute fibre reinforced concrete	JF, CA, S, C, W	CS, FS, CR	Liu et al, 2013
Jute fibre reinforced concrete	JF, CA, S, C, W	CS, FS, TS	Zakaria et al., 2015
Jute fibre reinforced mortar	JF, S, C, W	CS, FS	Jo et al., 2016
Jute fibre reinforced concrete	JF, CA, S, C, W	CS, FS, TS	Zakaria et al., 2016
Jute fibre reinforced concrete	JF, CA, S, C, W	CS, STS, FS, W	Islam and Ahmed, 2018
Jute fibre reinforced concrete	JF, CA, S, C, W	CS, STS, DS	Gupta et al., 2020
Jute fibre-reinforced comentitious composites	JF, C, FA, SF, UFS	UDT, FPBT	Deb et. al., 2020
Hybrid fibre reinforced concrete	JF, NF, CA, FA, C, W	CS, FS, DS, W, MOE	Bheel et. al., 2021
Jute fibre reinforced concrete	JF, CA, FA, C, W	CS, W	Mansur et al. 2022
Jute fibre-reinforced concrete	JF, CA, S, C, FA, W	CS, STS, FS, MOR, W	Hossain et al., 2023

[a] C: Cement, CA: Coarse aggregate, FA: Fly ash, JF:Jute fibre, NF: Nylon fibre, S: Sand, SF: Silica fume, UFS: Ultra-fine sand, W: Water.

[b] CS: Compressive strength, CR: Crack resistance, DS: Drying shrinkage, FPBT: Four point bending test, FS: Flexural strength, FT: Flexural toughness, IS: Impact strength, MOR: Modulus of rupture, MOE: Modulus of elasticity, SSB: Stress-strain behaviour, STS: Splitting tensile strength, TS: Tensile strength, TB: Toughness behaviour, UDT: Uniaxial direct tensile test, W: Workability.

From literature review, it is observed that several studies in recent years have focused on enhancing the mechanical properties of conventional concrete by incorporating jute fibres (Zakaria et al., 2015; Islam & Ahmed, 2018; Liu et al., 2013; Bheel et al., 2021; Mansur et al., 2022). The integration of jute fibres into natural fibre-reinforced composites is observed to improve setting properties and enhance mechanical performance, encompassing compressive strength, tensile strength, modulus of rupture, impact resistance, and shrinkage behaviour.

The extraction and processing of these coarse aggregates are known to contribute to CO_2 emissions. However, the application of jute fibres in cementitious composites, particularly those that eliminate coarse aggregates, remains underexplored. Further research is warranted to develop composite systems without coarse aggregates, aiming to reduce the environmental footprint of construction materials. Tian et al. (2015) explored that the inclusion of high volume fly ash increased the ductility of the bagasse fibre reinforced composites, which was attributed to the filler effect of fly ash, leading to a more compact matrix even in the absence of coarse aggregates.

On the other hand, cement production is a major contributor to greenhouse gas emissions. Although several studies have explored partial replacement of cement with supplementary materials like fly ash (Kubissa et al., 2017; Shaikh et al., 2018; Akhtar et al., 2022), the optimization of such replacements in jute fibre composites is underexplored. While alkaline nature of the cement matrix can potentially lead to the degradation of the jute fibres over time (Bergstrom and Gram, 1984; Arsene et al, 2007), the incorporation of fly ash in composites can help mitigate this issue, as the pozzolanic reaction of fly ash can reduce the alkalinity of the cement matrix and improve the overall durability of the composite. Therefore, further research is needed to assess the performance of jute fibre reinforced cementitious composites with high fly ash content as the synergistic effects of jute fibres and fly ash can lead to the development of high-performance, durable, and environmentally-friendly construction materials. Also, the optimization of the mix design, including the proportions of jute fibres, cement, fly ash, and other constituents, is crucial to ensure the efficient utilization of these materials and to achieve the desired performance characteristics of the composite.

In the context outlined above, a comprehensive study was conducted to develop a cost-effective, optimized Jute Fibre-Reinforced Cementitious Composites (JFRCCs) using locally available materials such as ordinary Portland cement, fine sand, jute fibre, and superplasticizer, along with industrial by-products like fly ash. To achieve this, the mechanical characteristics of the composites, including compressive strength, peak compressive strain, UPV, and tensile strength, were investigated. Following this, Minitab software was used to analyze the experimental results and manufacturing costs associated with each mix design. A multi-objective desirability function was then applied to determine the optimal mix ratio for JFRCCs.

2.7 Summary

This chapter provides a comprehensive review of the advancements in NFRCCs over recent years. The review encompasses many significant studies on various types of NFRCCs published over the past decades. Additionally, the chapter discusses modification techniques designed to remove degradable components such as hemicellulose and lignin, aiming to enhance the mechanical performance of natural fibres. The influence of these modification techniques on fibre characteristics and composite performance is also discussed.

Furthermore, the incorporation of natural fibres enhances mechanical performance of composites, including compressive strength, modulus of rupture, and impact resistance in NFRCCs. Strategies such as reducing alkali content by partially substituting OPC with low-alkali materials and using pre-treated natural fibres have proven effective in enhancing the long-term durability of composites.

Finally, this literature review highlights the potential of JFRCCs as a sustainable construction material. Based on the literature review on the mechanical properties of NFRCCs, this study utilizes short-cut jute fibre as a reinforcing material. To enhance the mechanical performance of jute fibre, alkali pre-treatments with NaOH solution are employed. Additionally, fly ash has been utilized as filling material into composites as the inclusion of fly ash exhibited improved durability of the composite by reducing the permeability and mitigating the effects of alkali-silica reactions. This makes the material more resistant to environmental degradation. However, the subsequent chapter details the material collection, material preparation, specimen preparation, and experimental methodology used in this study to develop cost-effective JFRCCs.

CHAPTER 3: MATERIAL COLLECTION, CASTING AND TESTING PROCEDURES

3.1 Introduction

Building upon the insights gained from the literature review, which identified a significant gap in the development of sustainable and cost-effective cementitious composites incorporating natural fibres, this chapter outlines the material collection, sample preparation, comprehensive experimental approach adopted in the present study. It includes descriptions of the materials used, material preparation, materials properties, mix design strategy, sample casting, curing procedure, and various testing procedure such as compressive strength, peak compressive strain, splitting tensile strength, flexural strength and UPV. Microstructural analysis was also conducted to understand the fibre-matrix interaction.

3.2 Selection of Materials and Material Preparation

This research develops a novel, low-cost green cementitious composite reinforced with jute fibre and a high volume of fly ash, aimed at creating an eco-friendly and sustainable construction material. The new green composites are a special type of Fibre Reinforced Cementitious Composites (FRCCs), consisting of Ordinary Portland Cement (OPC), fly ash, processed sand, jute fibre, water, and superplasticizer. The following sections provide detailed information on each of these constituent materials, highlighting their properties, and the reasons for their selection.

3.2.1 Cement

In this study CEM Type I OPC which conforms to as per BDS EN 197–1: 2005 was used as binding material and this cement was collected from Crown Cement PLC. CEM I, or Portland cement, is primarily composed of clinker, with up to 5% minor additional constituents, such as gypsum. This composition underscores its predominantly clinker-based nature and the specific gravity of the OPC varied between 3.11 and 3.15 (Ali et al., 2021; Mansur et al., 2022; Deb et al., 2020). The chemical compositions of CEM Type I cement have been previously detailed by various researchers and are shown in Table 3.1.

Table 3.1: Chemical composition of Ordinary Portland Cement (Ali et al., 2008; Hossain et al., 2023; Islam and Islam, 2014; Ali et al., 2021)

Chemical constituents	Cement (%)
SiO_2	18.60-23.50
Al_2O_3	3.89-6.20
Fe_2O_3	3.15-4.30
CaO	61.5-66.02
MgO	1.16-1.92
SO_3	0.95-3.56
Free lime	1.09-1.27
IR	0.35-0.65
LOI	1.23-3.10

3.2.2 Fly Ash

In the current study, fly ash, sourced as a by-product of coal combustion in thermal power plants, is utilized as a supplementary cementitious material and this selection of fly ash was based on its pozzolanic characteristics, which have the potential to improve the long-term strength and durability of cementitious composites (Li et al., 2020).

Using fly ash also promotes sustainability by reducing cement use, lowering CO_2 emissions, and providing a cost-effective option. For this study, low-calcium Class F fly ash was collected from Bashundhara Cement Company. It's a fine, powdery material primarily composed of silicon dioxide, aluminum oxide, calcium oxide, and iron oxide (Tamim et al., 2013) and the fly ash used in this study exhibited a specific gravity of 2.18 (Karim et al., 2017). The chemical composition of the fly ash utilized in this study, as determined by prior research, is presented in Table 3.2.

Table 3.2: Chemical composition of fly ash (Tamim et al., 2013; Hossain et al., 2023; Khan et al., 2013; Islam and Islam, 2014)

Chemical constituents	Fly Ash (%)
SiO_2	50.20-58.60
Al_2O_3	26.30-40.10
Fe_2O_3	2.80-6.40
TiO_2	2.38-3.20
Mn_3O_4	0.05-0.11
CaO	0.56-3.4
K_2O	0.66-1.1
Na_2O	0.06-0.38
MgO	0.18-0.50
P_2O_5	0.46-0.66
SO_3	0.13-0.45

3.2.3 Sand Preparation

Locally sourced fine aggregate, Sylhet sand was utilized in this study. The gradation curve of Sylhet sand is presented in Fig. 3.1, which maintain ASTM C33 specifications.

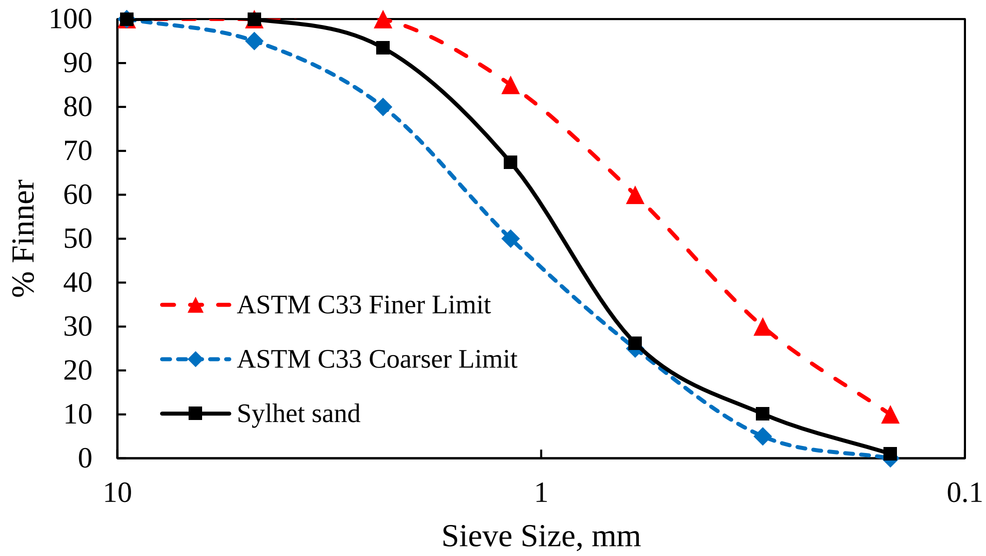

Fig. 3.1: Gradation curve of Sylhet sand (As per ASTM C33)

The physical properties of the fine aggregate, such as its fineness modulus, absorption capacity, unit weight, and specific gravity, were measured. The material properties of the fine aggregate are detailed in Table 3.3.

Table 3.3: Properties of Sylhet sand

Aggregate Type	Fineness Modulus	Absorption Capacity (%)	SSD Unit weight (Kg/m^3)	Bulk (SSD) Specific Gravity
Fine Aggregate	3.02	1.95	1525	2.56

Prior to utilization, fine aggregate was subjected to specific processing procedures. The sand was processed by drying, sieving to obtain the fraction passing through a 300 µm sieve and retained on a 150 µm sieve, and then oven-drying at 150 °C for 24 hours (Rahman & Kabir, 2025). After screening sand, specific gravity and absorption capacity of fine sand were measured with a value of 2.48 and 7.46%, respectively. Fig. 3.2 presents the raw and processed forms of sand.

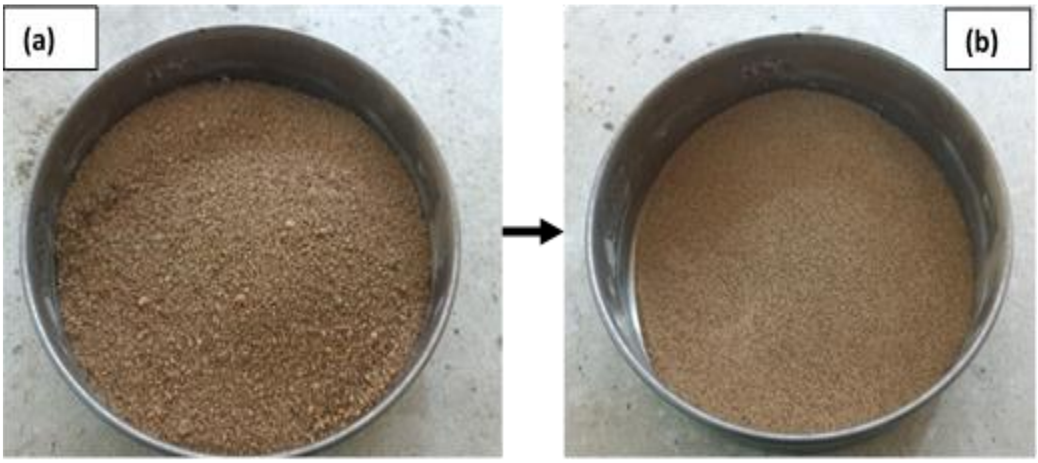

Fig. 3.2: Sand preparation process: (a) raw sand prior to processing; (b) processed sand

3.2.4 Jute Fibre Preparation

Jute, a natural fibre, is sourced from the stem of the Corchorus plant. These plants grow in warm, moist environments, often near water sources. To obtain jute fibres, the stems are processed through a series of steps: they are cut, then soaked in water (retting) to loosen the fibres, followed by separation of the fibres (defibration), and finally dried for further use (Farias et al., 2024). Jute fibres exhibit an irregular shape in cross-section and consist of multiple individual fibrocells connected by a middle lamella, with a vascular lumen present within, as shown in Fig. 3.3.

Untreated jute fibres are highly hydrophilic, leading to significant water absorption and specific gravity of jute fibre ranges from 1.45 to 1.48 (Islam and Ahmed, 2018; Islam and Ali, 2018). It was observed that untreated jute fibre can absorb water approximately 210% of its dry weight (Abdalla et al., 2023).

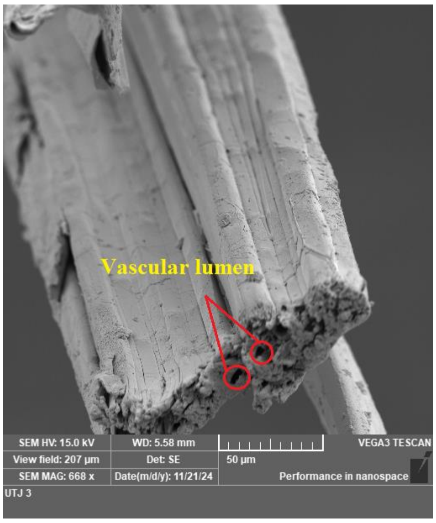

Fig. 3.3: SEM cross-sectional view of jute fibre

To reduce the hydrophilicity of jute fibres and enhance the fibre–matrix interface, an alkaline treatment was applied. This process involved immersing the fibres in a sodium hydroxide (NaOH) solution. Different stages of jute fibre preparation are presented in Fig. 3.4.

Fig. 3.4: Jute fibre treatment and sizing: (a) fibres in NaOH solution; (b) treated fibres; (c) chopped fibre strands; (d) final 10 mm fibre lengths

The jute fibres underwent an alkali treatment using a 0.5% NaOH solution, prepared by dissolving 5 g of NaOH pellets in 1 litre of water. The raw jute was then immersed in this solution for 24 hours, following the method described by Jo et al. (2016). This treatment was employed to remove surface impurities such as pectin and vegetable lipids. Following treatment, the fibres were sun-dried and cut into lengths of 10 mm and 20 mm for using into the cementitious composites. The water absorption of treated jute fibre was measured approximately 145% of its dry weight. Alkali treatment of jute fibres has been shown to reduce their water absorption capacity. This reduction is attributed to the removal of hemicellulose and other impurities, leading to decreased hydrophilicity of the fibres.

Scanning Electron Microscopy (SEM) was conducted to analyse the surface morphology of both untreated (Fig. 3.5a) and treated (Fig. 3.5b) jute fibres. The SEM analysis of the untreated fibres revealed a rough surface with the presence of impurities, including hemicellulose and lignin. In contrast, Fig. 3.5b depicts that treated jute fibre with alkali treatment became comparatively smooth surface due to removal of impurities (Haq et al., 2024).

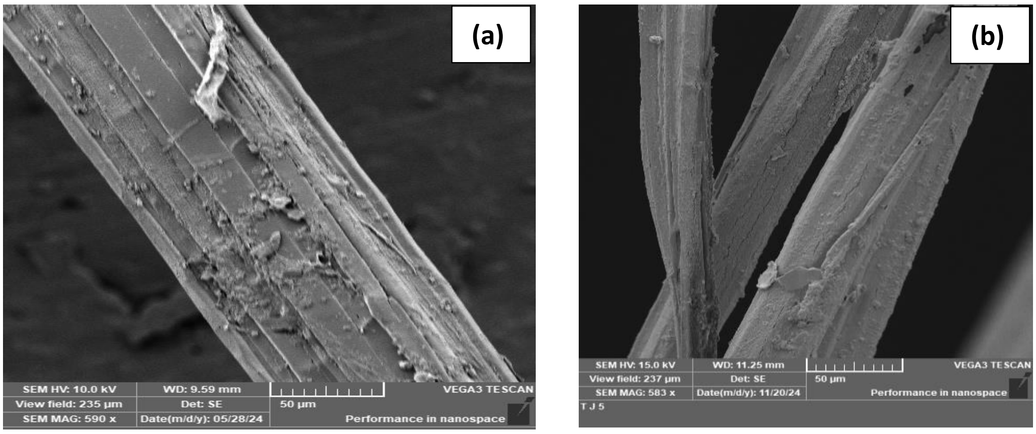

Fig. 3.5: SEM analysis, (a) untreated jute fibre (b) treated jute fibre

3.2.5 Superplasticizer

Superplasticizers, also known as high-range water reducers, are chemical admixtures that enhance concrete performance by significantly improving workability, reducing water content by up to 30%, and increasing both early and ultimate compressive strengths. The polycarboxylic-based superplasticizer was used in this study. The specific admixture used in this study was Armix Emmecrete PC 10, manufactured by MYK Arment Private Limited and procured through a local supplier. Armix Emmecrete PC 10 is a high-performance superplasticizer based on polycarboxylic ether polymer technology. Its chemical composition is detailed in Table 3.4.

Table 3.4: Chemical composition of Armix Emmecrete PC 10.

Properties	Results
Solid content (%)	27.5
Specific gravity at 27 °C temp	1.075
p^H at 27 °C temp	6.45
Colour	Yellow to brown
Appearance	Liquid

In this study, superplasticizer was incorporated into the composites at a dosage of 1.2% by weight of the binder as suggested by technical data sheet of Armix Emmecrete PC 10.

3.3 Overview of the Experimental Program

The experimental program of this study was strategically divided into three sequential phases—Phase I, Phase II, and Phase III—to ensure a systematic and comprehensive investigation into the development and performance evaluation of Jute Fibre-

Reinforced Cementitious Composites (JFRCCs). Each phase was designed to build upon the knowledge acquired from the previous one, progressively refining the mix parameters and deepening the understanding of the material's behaviour under both standard and adverse conditions. The summary of the experimental workflow, including the key activities of each phase, is visually presented in Fig. 3.6, providing a framework of the research process.

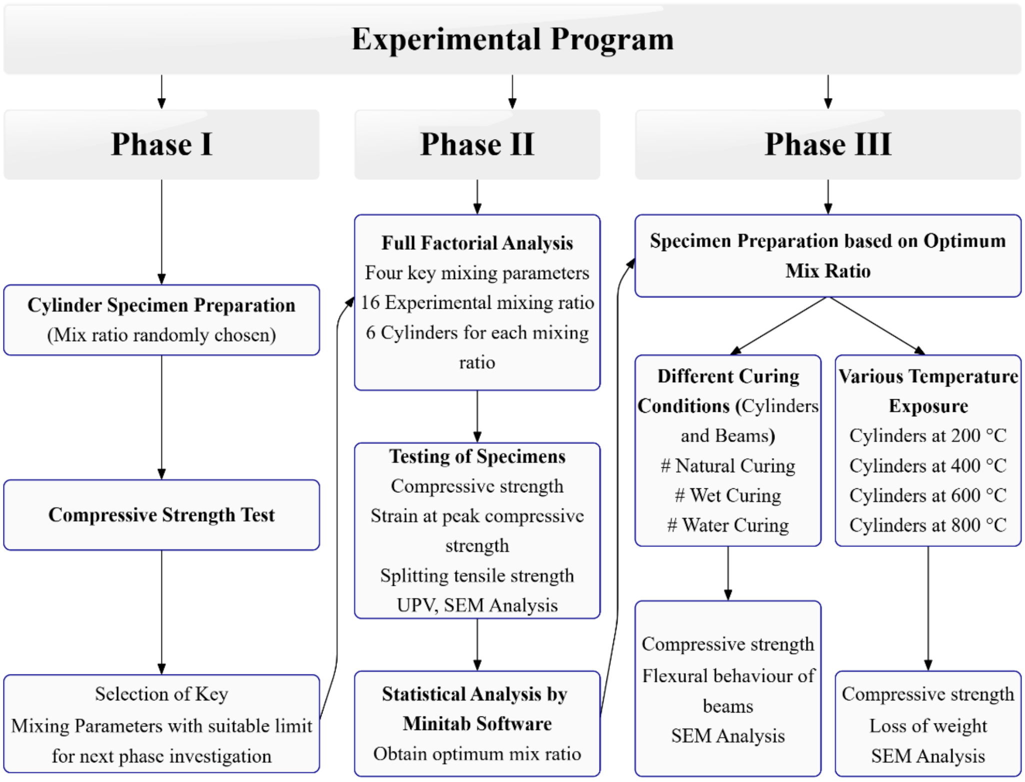

Fig. 3.6: Overview of experimental workflow.

Phase I served as an exploratory stage, focusing on the preliminary identification of key mixing parameters such as the water-to-binder (W/B) ratio, sand-to-binder (S/B) ratio, fly ash-to-cement (FA/C) ratio, and jute fibre length and content. A limited number of mix combinations were tested to evaluate their effect on compressive strength and to develop an initial understanding of how these variables interact. The insights gained from this phase played a pivotal role in setting the bounds and levels of the mix variables for the next phase, ensuring that the experimental design was both meaningful and focused.

Phase II was structured as a full factorial experiment, where sixteen distinct mix combinations were systematically prepared and tested. This phase aimed to explore the individual and combined effects of the four selected parameters on various mechanical properties, including compressive strength, peak compressive strain, splitting tensile strength, and UPV, along with unit weight and material cost. Statistical tools such as regression analysis and analysis of variance (ANOVA) were employed to derive predictive models and to identify the optimal mix design that offers a balance between strength, ductility, and cost-efficiency.

Phase III focused on the extended performance assessment of the optimal mix identified in Phase II. In this phase, the optimized mix was subjected to different environmental and thermal conditions to evaluate its durability, thermal resistance, and short-term performance. These evaluations provided insights into the composite's applicability in real-world construction scenarios, particularly under various environmental and thermal conditions.

3.4 Quantitative Mix Proportioning Approach

The mix proportions used in this study were determined by weight, with the total mass of the composites components corresponding to a volume of 1 cubic meter. This relationship is expressed by the following equation:

$$\frac{C}{G_c\gamma_w}+\frac{FA}{G_{FA}\gamma_w}+\frac{S}{G_s\gamma_w}+\frac{J}{G_J\gamma_w}+\frac{W}{G_w\gamma_w}+Air\ (\%)=1 \qquad (3.1)$$

Where, C = Unit content of cement (kg/m^3 of composites);

FA = Unit content of fly ash (kg/m^3 of composites);

S = Unit content of fine sand (kg/m^3 of composites);

J = Unit content of jute fibre (kg/m^3 of composites);

W = Unit content of water (kg/m^3 of composites);

γ_w = Unit weight of water (kg/m^3);

G_c = Specific gravity of cement;

G_{FA} = Specific gravity of fly ash;

G_s = Specific gravity of fine sand (SSD);

G_J = Specific gravity of jute fibre;

G_w = Specific gravity of water;

Air (%) = Percentage of air in mortar (assumed at 0% without air entraining agent)

3.5 Mold Preparation

Two shapes of specimens were casted for this investigation. 100 mm × 200 mm cylindrical shaped mold and 75 mm × 75 mm × 300 mm beam mold were used to prepare specimens. Molds of all types of specimens were available at the Concrete

Laboratory of the Department of Civil and Environmental Engineering (CEE), Islamic University of Technology (IUT). Proper preparation of molds is essential to ensure the integrity and accuracy of test specimens. Therefore, the mold was thoroughly cleaned to remove residual concrete or debris from previous use. Sandpaper was used to create a smooth interior surface. After smoothing, a thin, even layer of a suitable non-reactive form release agent, such as grease was applied to the interior surfaces according to ASTM C 31–03 to facilitate demolding and prevent adhesion between the composites and the mold. Prior to casting, the molds were secured by tightening the nut-bolts to ensure watertightness, thereby preventing any potential leakage that could compromise the specimen dimensions. Once prepared, the molds were placed on a level, stable surface to maintain uniformity during the casting. Adhering to these preparation steps is vital for producing reliable and consistent specimens for testing. Fig. 3.7 represents the prepared molds used in this study.

(a) (b)

Fig. 3.7: (a) Cylinder mold (100 mm × 200 mm), (b) Beam mold (75 mm × 75 mm × 300 mm).

3.6 Mixing of Fresh Composites and Casting Procedure

The preparation of test specimens followed a systematic three-step process for each batch. The detailed flow diagram illustrating the sequence from ingredient mixing to specimen casting is presented in Fig. 3.8.

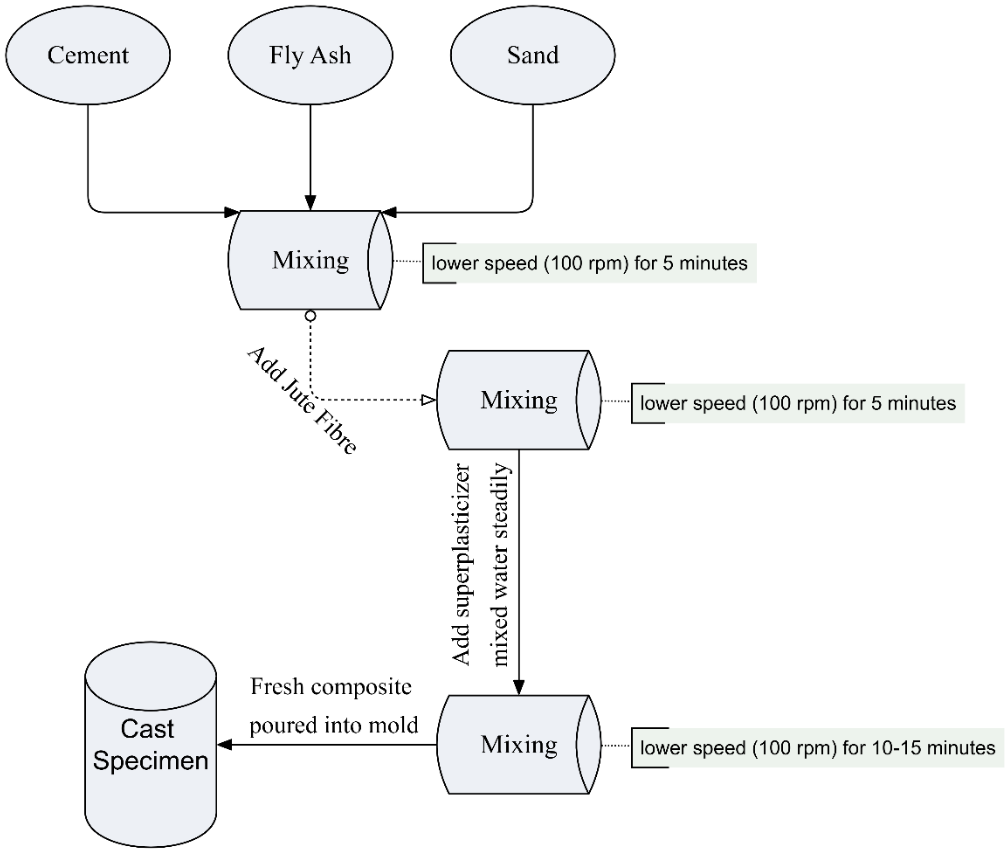

Fig. 3.8: Flow diagram of specimen preparation process from mixing to casting.

The mixing procedure was conducted using a 20-liter capacity mechanical mixer (Fig. 3.9a), following a systematic protocol to ensure homogeneous composite preparation. Initially, the dry constituents—cement, fly ash, and sand were introduced into the mixing chamber and blended at a low rotational speed (100 rpm) for 5 minutes to achieve uniform dispersion. Subsequently, pre-treated jute fibres were incrementally incorporated into the dry mixture over a 5-minute interval to prevent fibre agglomeration. The final stage involved the gradual addition of water premixed with superplasticizer, which was carefully administered until a cohesive, workable paste was attained (Fig. 3.9b). Fig. 3.9 comprehensively shows the sequential stages of the specimen preparation process.

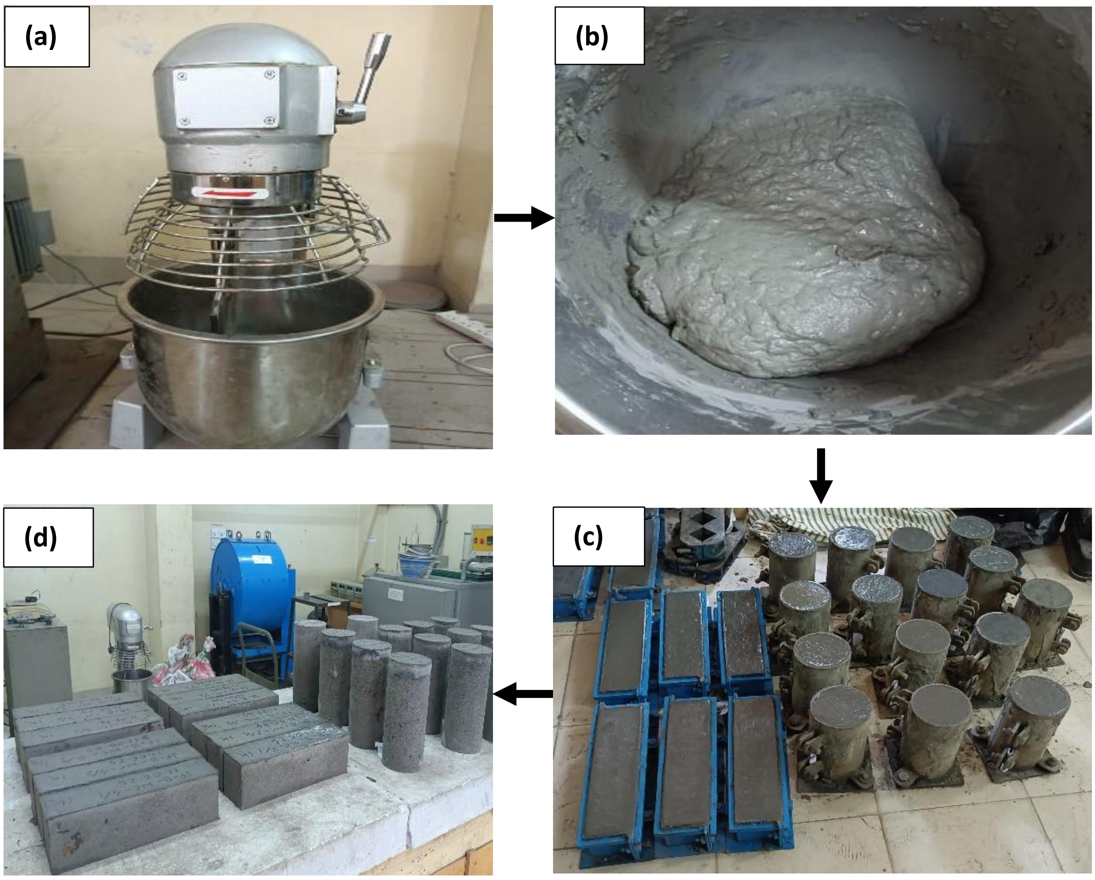

Fig. 3.9: Casting workflow and sample stages: (a) 20 L capacity mixer; (b) freshly mixed composite; (c) fresh mixed composite in steel molds; (d) demolded specimens at 7 days

To ensure optimal homogeneity, the mixture was subjected to a final blending phase at a reduced rotational speed (100 rpm) for a duration of 10-15 minutes. Following completion of the mixing protocol, the freshly prepared cementitious composite was immediately poured to pre-prepared molds, as shown in Fig. 3.9c. This procedure was carefully executed to minimize air entrapment and achieve uniform specimen consolidation. To ensure proper compaction of the JFRCCs, a hand-held mechanical vibrator equipped with a 38 mm diameter nozzle was employed. The use of a tamping rod for consolidating JFRCCs was not effective to eliminate voids due to the tendency of fibres to form clumps or "balling" during mixing. This clumping creates area within the mix that are resistant to compaction by standard rodding techniques, leading to entrapped air voids and a less dense matrix. Additionally, the presence of fibres impede the movement of the tamping rod, preventing adequate consolidation around the fibres and resulting in non-uniform distribution. To address these challenges, alternative consolidation methods, such as mechanical vibration, was used to ensure proper compaction and uniformity in fibre-reinforced composites.

Due to the pronounced interfacial adhesion between the jute fibres and the metallic mold surfaces, demolding was carefully conducted following a 7-day curing period (Fig. 3.9d). Subsequently, the specimens were transferred to a curing chamber, where they remained until reaching the designated testing age, ensuring adequate hydration and strength development.

3.7 Curing of Specimens

Curing is a process in the development of cementitious composites, ensuring adequate hydration and strength gain. In this study, specimens were subjected to different curing methods depending on the experimental phase, which are summarized in Table 3.5.

Table 3.5: Summary of specimen curing methods used in each experimental phase.

Experimental Phase	Curing Type
Phase I Experiment	Water Curing
Phase II Experiment	Water Curing
Phase III Experiment	Natural Curing
	Wet Curing
	Water Curing

Immediately after casting, preventing moisture loss from freshly cast composite specimens is essential. Therefore, molded specimens were immediately covered with wet burlap and then specimens were covered with plastic sheet to prevent moisture loss in accordance with ASTM C192-07.

This early age curing of the specimens to surface moisture protection continued until the samples were demolded. After removing mold, the specimens were transferred to the designated curing conditions outlined in Table 3.5 and kept there until the time of testing. During the first and second phases of the experimental program, all specimens were subjected to water curing in a controlled water chamber. In contrast, during the third phase, various curing regimes, including water curing, natural curing, and wet curing, were employed to investigate the effects of different environmental conditions on the performance of the composites. The following sections describe each curing methods in detail, outlining their procedures in the context of the experimental program.

3.7.1 Water Curing

Water curing method involves completely submerging the concrete samples in water. After demolding, samples were placed in a water tank as shown in Fig. 3.10 and it was ensured the samples are fully submerged throughout the curing period. This curing method provides optimal moisture conditions for hydration. Ambient environmental condition was ideally maintained for the curing temperature. The water used for curing was apparently clean and free from harmful substances.

Fig. 3.10: Water curing

3.7.2 Natural Curing

Natural curing method involves exposing the samples to ambient air and humidity without any additional measures to control moisture loss. After demolding, samples were placed in a shaded area away from direct sunlight and wind as depicted in Fig. 3.11 where adequate ventilation was ensured to prevent excessive temperature build-up. This method relies on environmental humidity and temperature to facilitate the hydration process.

Fig. 3.11: Natural curing

3.7.3 Wet Curing

Specimens were covered with moisture-retaining materials with wet burlap, immediately after demolding and a non-absorptive polythene sheet was placed on top of the wet burlap as displayed in Fig. 3.12.

Fig. 3.12: Wet curing.

These coverings were kept continuously damp throughout the curing period to maintain a moist environment, preventing moisture loss and promoting complete hydration. Burlap was regularly sprinkled with water to keep it saturated throughout the curing period.

3.8 Testing Procedure

3.8.1 Compressive Strength

Compressive strength, representing the peak axial stress capacity of cementitious materials prior to structural failure, serves as a fundamental mechanical property for evaluating composite performance. In accordance with ASTM C39/C39M-18 specifications, standardized cylindrical specimens (dia-100 mm × height-200 mm) were subjected to compression testing at a controlled displacement rate of 100 kN/min. For each composite formulation, three specimens were tested to ensure statistical reliability, with the mean compressive strength value derived from these replicates. Fig. 3.13 demonstrates the experimental configuration employed for the compressive strength evaluation.

Fig. 3.13: Test setup for compressive strength.

According to ASTM C39/C39M-18, a length-to-diameter ratio of less than 1.75 necessitates a correction factor for the measured strength. In this study, since the ratio was 2.0, no correction factor was applied.

3.8.2 Strain at Peak Compressive Strength

Strain at peak compressive strength was also measured using a strain dial gauge placed at two sides of the sample during the compressive test. The test arrangement for strain at peak compressive strength is presented in Fig. 3.14.

Fig. 3.14: Test setup for strain at peak compressive strength.

3.8.3 Splitting Tensile Strength of Cementitious Composites

The splitting tensile strength test of cementitious composites was conducted following ASTM C496/C496M-04. The test arrangement for splitting tensile strength measurement is presented in Fig. 3.15.

Fig. 3.15: Test setup for splitting tensile strength.

Cylindrical specimens were assessed for splitting tensile strength in accordance with ASTM C496 standards, utilizing the Universal Testing Machine (UTM). This technique involves the application of a compressive force along the diameter of cylindrical specimens until structural failure is observed. The loading rate was consistently controlled within the range of 0.7 to 1.4 MPa/min. Under this loading condition, tensile stresses develop along the plane subjected to the applied load, while localized compressive stresses arise in the vicinity of the loading points. Failure occurs due to tensile mechanisms rather than compression, as the areas under load experience triaxial compression, enhancing their capacity to withstand compressive forces beyond uniaxial compressive strength test results. Splitting tensile strength is then derived by dividing the maximum sustained load by related geometrical parameters, as expressed in the corresponding equation (3.2).

$$T = \frac{2P}{\pi l d} \tag{3.2}$$

Where,

T = splitting tensile strength (MPa);

P = the peak load recorded by the testing apparatus (N);

l = length of cylinder (mm);

d = diameter of cylinder (mm).

3.8.4 Ultrasonic Pulse Velocity

Ultrasonic Pulse Velocity (UPV) measurements were conducted to evaluate the internal homogeneity and structural integrity of the cylindrical specimens in accordance with ASTM C597-16. The test arrangement for UPV measurement is displayed in Fig. 3.16.

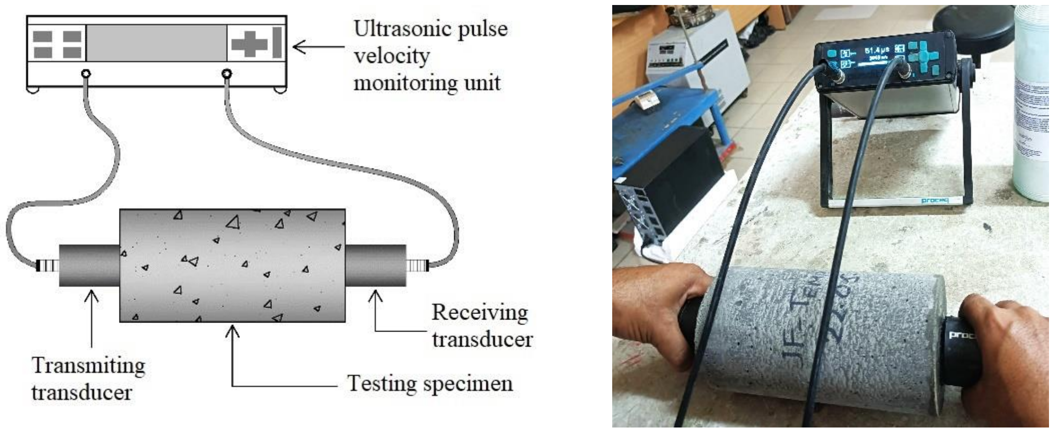

(a) (b)

Fig. 3.16: Test setup for Ultrasonic Pulse Velocity (UPV).

A Portable Ultrasonic Non-destructive Digital Indicating Tester (PUNDIT) was employed for this purpose. This device comprises two transducers: one for transmitting and another for receiving ultrasonic pulses. The direct transmission method was utilized, wherein a coupling agent (Castrol Pyroplex Blue) was applied to the flat surfaces of the cylinders to ensure optimal contact between the transducers and the specimen. An ultrasonic pulse, operating at a frequency of 54 kHz, was emitted by the transmitting transducer, traversed the cylinder, and received by the receiving transducer. The PUNDIT device recorded the pulses travel time and calculated the traveling velocity of the ultrasonic pulse. For each cylinder, three measurements were taken, and their average was considered as the final result. The PUNDIT device underwent calibration prior to each measurement session, utilizing a standard calibration rod supplied by the manufacturer.

3.8.5 Flexural Strength

The flexural strength of cementitous composites was determined following the ASTM C78/C78M-18 standard, which employs a simple beam subjected to third-point loading. This method determines the modulus of rupture, reflecting the materials tensile strength under bending stress. Cementitous composites beams were cast with dimensions of 75 mm × 75 mm × 300 mm, ensuring a span length three times the depth of the specimen. Post-casting, specimens were cured in specified curing condition until the time of testing. The testing setup consisted of a calibrated flexural testing machine equipped with support and loading blocks. The support blocks were positioned to provide a span length of 250 mm, while the loading blocks were placed at the upper third points, dividing the span into three equal segments, which is demonstrated in Fig. 3.17. This configuration ensures the application of force without inducing eccentricity.

Each beam was positioned on the support blocks with the molded surface facing laterally, ensuring the tension face was perpendicular to the applied load.

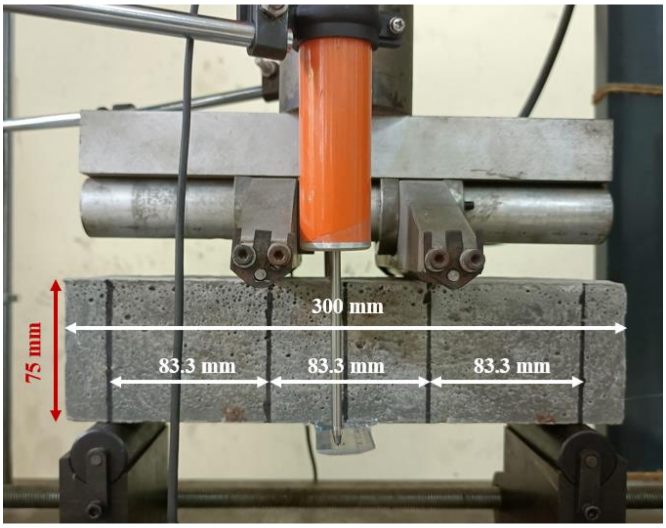

Fig. 3.17: Test setup for Flexural Strength.

The loading blocks were brought into contact with the specimen's surface at the designated third points. Feeler gauges (0.10 mm and 0.40 mm) were used to detect any gaps exceeding permissible limits between the specimen and the blocks. A continuous load was applied without shock, increasing the stress on the tension face at a rate between 0.9 MPa/min and 1.2 MPa/min until failure occurred. This controlled loading rate ensures accurate measurement of the flexural strength.

The modulus of rupture is calculated using the following formula when the fracture starts at the tension surface within the center third of the span.

$$R = \frac{PL}{bd^2} \tag{3.3}$$

Where, R = modulus of rupture (MPa);

P = the peak load recorded by the testing apparatus (N);

L = span length (mm); b = average width of specimen at the fracture (mm); d = average depth of specimen at the fracture (mm)

When the fracture is originated at the tension surface beyond the middle third of the span length, but remains within a range not exceeding 5% of the span length, the modulus of rupture is calculated using the equation below:

$$R = \frac{3Pa}{bd^2} \tag{3.4}$$

Where,

a = arithmetic mean of the distances between the fracture line and the closest support, measured on the tension surface of beam, mm

But when the fracture is originated at the tension surface beyond the middle third of the span length by a margin exceeding 5% of the span length, the test results are to be excluded. Above calculation provides the flexural strength, indicating the composites capacity to resist bending stresses.

3.8.6 Microstructural Investigation

After performing mechanical testing, freshly broken pieces of cementitious composites were collected, and fracture surface of cementitious composites were analysed using Scanning Electron Microscope (SEM) at the age of 9 months. The pictures of the SEM apparatus utilized in this study are presented in Fig. 3.18.

(a)

(b)

(c)

(d)

Fig. 3.18: (a) Scanning Electron Microscope; (b) gold sputter coater; (c) uncoated specimens; (d) coated specimens.

For SEM analysis, the samples were first dried for 2 hours at 60 °C to remove moisture. Subsequently, they were immersed in an acetone solution to eliminate surface dusts. Prior to SEM examination, the samples underwent gold sputter coating to prevent charging effects during SEM investigation under high voltage. The microstructural features of samples were investigated by taking images using a TESCAN VEGA3 SEM.

3.9 Summary

This chapter outlined the materials, preparation methods, and testing procedures used to investigate JFRCCs. The sample preparation process, including mix proportioning, mixing, casting, and curing methods, was described step-by-step with supporting flow diagrams. Various testing procedure, such as compressive strength, splitting tensile strength, peak strain, flexural strength, UPV, and SEM analysis were described in this chapter.

Overall, this chapter established a clear experimental framework to support the analysis and discussion of results in the following chapters.

CHAPTER 4: EVALUATION OF MECHANICAL PROPERTIES OF JFRCCs^

4.1 Introduction

The study was conducted in three distinct phases- Phase I, Phase II, and Phase III, each building upon the knowledge gained from the previous one. This chapter presents a detailed discussion about preliminary or Phase I and Phase II investigations. The Phase I investigation aimed to assess the impact of various mixing parameters on the compressive strength of Jute Fibre-Reinforced Cementitious Composites (JFRCCs). Additionally, the findings from the Phase I investigation intended to establish suitable ranges for the key mixing parameters for conducting the comprehensive Phase II investigation. The Phase II investigation explored a wider range of mix proportions, and investigated the material characteristics in greater depth to determine the optimized mixing proportion of JFRCCs.

---

^The experimental investigations and corresponding findings presented in this chapter have been partially disseminated through the following publications:

1. Rahman, M. A., & Kabir, M. I. (2025). Development of a sustainable and cost-optimized cementitious composites incorporating local resources and jute fibre. *Cleaner Materials*, 17, 100322.
   DOI: https://doi.org/10.1016/j.clema.2025.100322

2. Rahman, M. A., & Kabir, M. I. (2024). PRELIMINARY STUDY ON GREEN CEMENTITIOUS COMPOSITES WITH JUTE FIBRE. In 7th International Conference on Civil Engineering for Sustainable Development, Khulna, Bangladesh.

4.2 Phase I Experimental Procedure

The JFRCCs were developed using ordinary Portland cement, fly ash, fine sand, jute fibre, and a superplasticizer. The mechanical performance of JFRCCs depends significantly on various mixing parameters, which influence the microstructure, bonding, and mechanical properties of the composites. Hence, it is crucial to understand how different mixing parameters affect the compressive strength of proposed composites to ensure effective development of JFRCCs. Therefore, a preliminary investigation was undertaken to evaluate the impact of different mixing parameters on the compressive strength of JFRCCs.

The Phase I investigation focused on determining the effects of several mixing parameters such as fly ash content, jute fibre length, jute fibre percentage, sand-to-binder proportion and water-to-binder proportion on the compressive strength of JFRCCs. In this preliminary investigation, the ranges of mixing parameters were selected arbitrarily. The water-to-binder proportion was adjusted between 0.23 and 0.36, while the fly ash-to-cement proportion ranged from 1.2 to 2.0. A sand-to-binder proportion of 0.3 to 0.5 was employed. Treated jute fibres of 10 mm and 20 mm lengths were incorporated, with a constant fibre content of 0.5% by total volume. Mix proportions for each casting batch are specified in Table 4.1. For each batch, three cylindrical specimens were prepared, and their compressive strength was evaluated using a compression testing machine. Then, testing was conducted on randomly selected samples at various intervals after casting.

Table 4.1: Mix proportion for different batch of cementitious composites.

Water to binder proportion	Fly ash to cement proportion	Sand to binder proportion	Length of the jute fibre, mm
0.23	1.2	0.5	20
0.23	1.2	0.3	20
0.27	1.2	0.5	20
0.27	2	0.5	20
0.27	2	0.3	10
0.27	2	0.3	20
0.30	1.4	0.3	10
0.36	1.2	0.5	20
0.36	1.2	0.5	10
0.36	1.2	0.3	10
0.36	1.2	0.3	20

While some specimens were tested at 28 days of the casting date, others were tested at 42 days, and 170 days, respectively. Testing conducted in different ages of composites allowed to assess the time-dependent compressive behaviour of JFRCCs. However, the following section describes the mix design procedure used to prepare JFRCCs for this phase I investigation.

4.3 Mix Design-Phase I Experiment

In the initial phase of the experimental program, the mix design of JFRCCs was established through a standard mix design practices. The target mix proportions were determined by weight, assuming a total volume of 1.00 cubic meter of the composite material. This volumetric basis allowed for accurate conversion of material weights into batch quantities suitable for laboratory-scale sample casting. Based on the preliminary selection of constituent ratios outlined in Table 4.1, the detailed mix compositions are outlined in Table 4.2.

Table 4.2: Mix design of cementitious composites for phase I experiment

SL No.	Water to binder ratio	Fly ash to cement ratio	Sand to binder ratio	Length of the jute fibre, mm	Water, Kg/m^3	Fly ash, Kg/m^3	Sand, Kg/m^3	Jute fibre, Kg/m^3	Cement, Kg/m^3
1	0.23	1.2	0.5	20	271.4	643.7	590.1	10.3	536.5
2	0.23	1.2	0.3	20	300.3	712.1	391.6	10.1	593.4
3	0.27	1.2	0.5	20	304.2	614.6	563.4	10.1	512.2
4	0.27	2	0.5	20	298.7	737.5	553.1	9.9	368.8
5	0.27	2	0.3	10	328.2	810.4	364.7	9.6	405.2
6	0.27	2	0.3	20	328.2	810.4	364.7	9.6	405.2
7	0.30	1.4	0.3	10	356.6	693.3	356.6	9.6	495.2
8	0.36	1.2	0.5	20	368.2	557.9	511.4	9.6	464.9
9	0.36	1.2	0.5	10	368.2	557.9	511.4	9.6	464.9
10	0.36	1.2	0.3	10	401.6	608.5	334.7	9.3	507.1
11	0.36	1.2	0.3	20	401.6	608.5	334.7	9.3	507.1

In this phase, the jute fibre content was maintained consistently at 0.5% of the total volume across all samples. The consistent application of a 0.5% jute fibre content across all experimental samples suggests a carefully considered experimental design, intended to isolate and analyse specific effects of other mixing parameters on the composite material (Zakaria et al., 2018).

4.4 Preliminary Evaluation on Mechanical Properties of JFRCCs

This section presents the preliminary evaluation on compressive strength of JFRCCs. The investigation aimed to understand the influence of key mixing parameters on mechanical performance. Specifically, the effects of water-to-binder ratio, sand-to-binder ratio, fly ash-to-cement ratio, jute fibre length, and curing duration were examined on compressive strength performance of JFRCCs. In the following subsections, influence of key mixing parameters are discussed to identify trends and select suitable ranges for further investigation.

4.4.1 Effect of Water to Binder Ratio

The influence of water-to-binder ratio on the compressive behaviour of JFRCCs was systematically investigated through an experimental program employing W/B ratios ranging from 0.23 to 0.36. As detailed in Table 4.3, compressive strength measurements were conducted while all other mix design parameters maintained constant to isolate the effect of water content on mechanical performance.

Table 4.3: Variation in compressive strength with different water-to-binder ratios

Water to binder ratio	Fly ash to cement ratio	Sand to binder ratio	Length of the jute fibre, mm	Curing age, Days	Compressive strength, MPa
0.23	1.2	0.5	20	28	15.61
0.36	1.2	0.5	20	28	12.00
0.23	1.2	0.5	20	170	27.08
0.36	1.2	0.5	20	170	17.33

This investigation was conducted to evaluate the influence of W/B ratio on the mechanical performance of the composites. Short term and long term curing effect were also evaluated on compressive strength of JFRCCs. All samples were cured under water curing conditions and tested at designated curing ages (e.g., 28 and 170 days).

The variation in compressive strength of the JFRCCs with the changing of W/B ratios and curing durations are presented in Fig. 4.1. As shown, the compressive strength showed a decreasing trend with increasing W/B ratio. Specifically, specimens prepared with a W/B ratio of 0.23 demonstrated significantly higher strength compared to those with a ratio of 0.36, indicating that lower water content, while potentially challenging for workability, contributed to a denser and stronger microstructure. This finding aligns with well-established cement hydration principles, where reduced water availability minimizes porosity and enhances the degree of hydration in the long term (Bentz, 2006; Zivica, 2009).

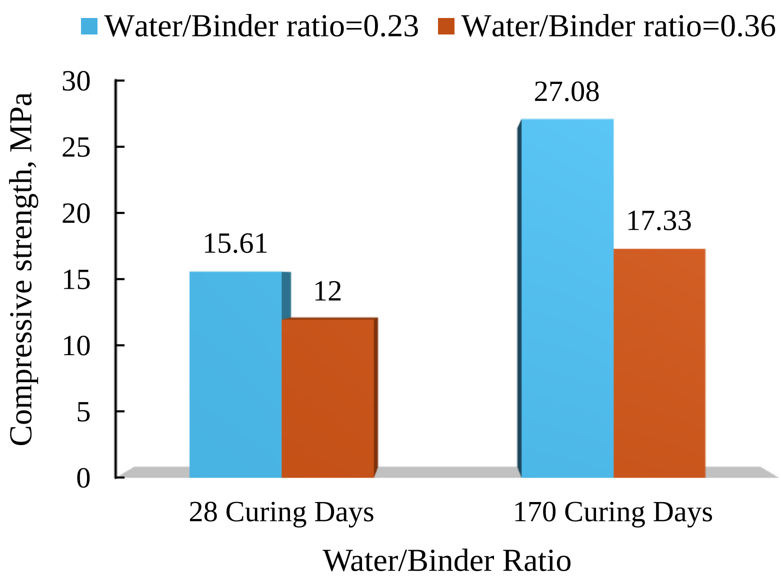

Fig. 4.1: Influence of the water-to-binder ratio on the compressive strength

In addition to the compressive strength results, the failure behaviour of the cementitious composites specimen was also observed after the compression test, as shown in Fig. 4.2.

(a) (b)

Fig. 4.2: Specimen failure pattern, (a) W/B=0.23 and (b) W/B=0.36

The specimen with W/B = 0.23 and 20 mm jute fibre exhibited a shear-type failure under compressive loading shown in Fig. 4.2(a), suggests that the ultimate strength was governed by the internal shear resistance of the composite and the jute fibres provided some resistance to crack propagation. Fig. 4.2(b) represents the columnar or splitting failure of specimen which was prepared with W/B = 0.36 and 20 mm jute fibre, indicating brittle behaviour likely due to inadequate fibre-matrix bonding as higher water-to-binder ratio contributed to a less dense matrix.

Alongside W/B ratio effect, the results also demonstrate that longer curing periods significantly improve the compressive strength of JFRCCs. While early age (28 days) strength is commonly reported in most studies, long-term performance is often a more critical indicator of durability and structural integrity. In this investigation, the experimental results demonstrated a progressive enhancement in compressive strength of the composite specimens with extended curing duration. A noticeable strength development was observed, with specimens achieving approximately 150% greater compressive strength at 170 days compared to 28-days cured samples. This long-term strength enhancement can be principally attributed to two concurrent mechanisms: (1) sustained pozzolanic activity of the fly ash component, and (2) ongoing hydration of cementitious phases. These processes collectively contribute to microstructural densification, resulting in improved load-bearing capacity and mechanical performance over time. These findings highlight the importance of selecting an appropriate W/B ratio and providing sufficient curing duration to achieve optimal performance in fibre-reinforced cementitious composites, especially when incorporating supplementary cementitious materials such as fly ash.

4.4.2 Effect of Sand to Binder Ratio

The compressive strength results of cementitious composites prepared with varying sand-to-binder (S/B) ratios are demonstrated in Table 4.4. Cementitious composites were prepared with varying S/B ratios, ranging from 0.50 to 0.30, while all other mix factors like W/B ratio, fly ash content, and jute fibre volume were kept constant. This part of the investigation aimed to investigate the impact of fine aggregate content on the compressive strength of the composites.

Table 4.4: Influence of sand content on compressive strength (20mm fibres, W/B=0.27, FA/C=2.0)

Water to binder ratio	Fly ash to cement ratio	Sand to binder ratio	Length of the jute fibre, mm	Compressive strength, MPa
0.27	2	0.5	20	21.00
0.27	2	0.3	20	19.48

The influence of varying the sand-to-binder (S/B) ratio from 0.50 to 0.30 on the compressive strength of JFRCCs are also graphically presented in Fig. 4.3.

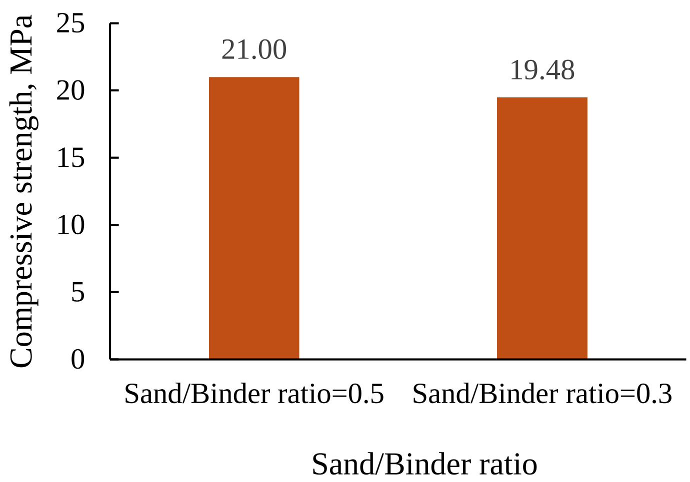

Fig. 4.3: Effect on compressive strength due to sand/binder ratio changes.

The results revealed that the compressive strength remained nearly unchanged across the different S/B ratios. This suggests that within the tested range, reducing sand content did not significantly affect compressive performance. Lower sand content may have improved matrix continuity due to increased binder content, while higher sand content improved particle packing density. The inclusion of jute fibres also likely contributed to crack control and stress distribution, helping maintain strength regardless of sand variation. These findings highlight the mix design's flexibility in adjusting sand content without compromising compressive strength, which is useful for balancing workability, cost, and material availability.

The effect of S/B ratio on the compressive performance of cementitious composites was also examined maintaining a constant FA/C ratio of 1.2. This experimental matrix incorporated 20 mm jute fibre reinforcement and two distinct W/B ratios (0.23 and 0.36) to evaluate the combined effects of mixture proportions on mechanical behaviour. Table 4.5 presents the compressive strength characteristics corresponding to the investigated S/B ratio variations, revealing significant trends in composite performance.

Table 4.5: Effect of S/B ratio on compressive strength at two different W/B ratios (20mm fibres, FA/C=1.2)

Water to binder ratio	Fly ash to cement ratio	Sand to binder ratio	Length of the jute fibre, mm	Compressive strength, MPa
0.23	1.2	0.5	20	27.08
0.23	1.2	0.3	20	10.72
0.36	1.2	0.5	20	20.15
0.36	1.2	0.3	20	13.98

In both cases, increasing S/B ratio from 0.30 to 0.50 led to a noticeable improvement in compressive strength, as shown in Fig. 4.4.

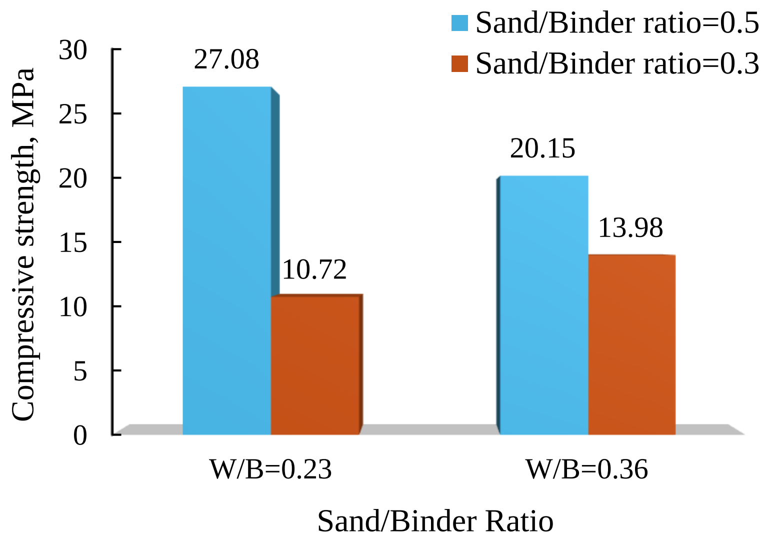

Fig. 4.4: Influence of S/B ratio on the compressive strength at two different W/B ratios (20mm fibres, FA/C=1.2)

While the S/B = 0.30 mixes had a higher binder content, the S/B = 0.50 mixes demonstrated better mechanical performance. This can be attributed to improved particle packing density, reduced internal voids, and more uniform fibre dispersion in the higher sand mixes. Despite containing a higher proportion of cementitious content, composites with S/B = 0.30 exhibited less compressive strength than composites with S/B = 0.50. A higher quantity of cementitious material develops an increased paste volume, leading to microcracking and the use of 20 mm length jute fibre in composites, resulting in poor fibre alignment. This combination of factors compromised the structural integrity of the mixes, thereby reducing the expected strength gains. Furthermore, the FA/C ratio of 1.2 appeared to enhance the matrix reactivity more effectively in well-balanced mixes with S/B = 0.50, contributing to a denser and more cohesive structure. This result reinforces the importance of not only optimizing binder content but also achieving a balanced aggregate-paste ratio for maximizing strength in JFRCCs.

Effect of S/B ratio on compressive strength was then investigated for JFRCCs specimen using 10 mm length jute fibre. The compressive strength results for changing S/B ratios, are presented in Table 4.6.

Table 4.6: Effect of S/B ratio on compressive strength (10mm fibres, W/B=0.36, FA/C=1.2)

Water to binder ratio	Fly ash to cement ratio	Sand to binder ratio	Length of the jute fibre, mm	Compressive strength, MPa
0.36	1.2	0.5	10	30.75
0.36	1.2	0.3	10	39.09

Unlike the composites with 20 mm jute fibres, which showed improved compressive strength at higher sand-to-binder (S/B) ratios, composites with 10 mm fibres followed the opposite trend. This contrasting behaviour indicates that shorter fibres may interact differently with the matrix, potentially benefiting from the increased binder content in mixes with lower sand ratios. It is noted that compressive strength was higher at S/B = 0.30 than at 0.50, as presented in Fig. 4.5. At S/B = 0.30, the increased paste volume may have enhanced fibre-matrix bonding for the shorter fibres, improving crack-bridging efficiency and stress transfer.

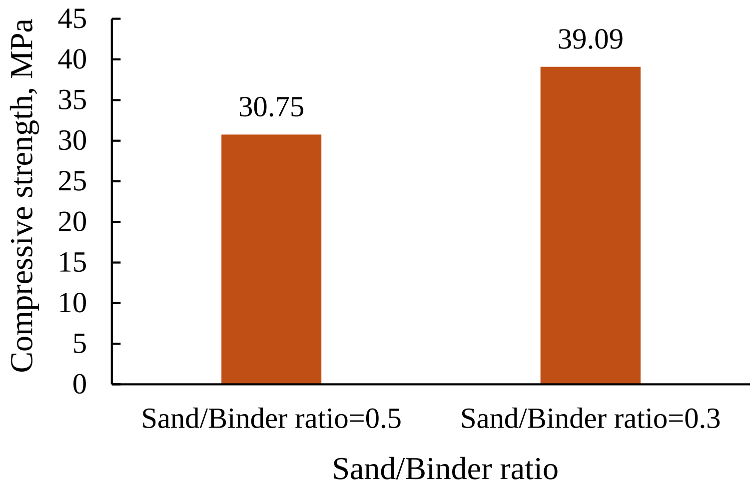

Fig. 4.5: Influence of S/B ratio on the compressive strength (10mm fibres, W/B=0.36, FA/C=1.2)

In contrast, at S/B ratio of 0.50, the lower binder volume did not sufficiently embed and hold the shorter fibres in place, resulting in reduced performance. For shorter fibres, a higher binder matrix appears more favourable for maximizing compressive strength of JFRCCs.

4.4.3 Effect of Fly Ash to Cement Ratio

The relationship between fly ash-to-cement (FA/C) ratio and compressive strength development was evaluated, with results presented in Table 4.7. The experimental investigation examined FA/C ratios ranging from 2.0 to 1.2, keeping other mix parameters constant to isolate the effect of cementitious composition. As shown in Fig. 4.6, reducing the FA/C ratio to 1.2 yielded a statistically significant enhancement in compressive strength, demonstrating the critical influence of binder composition on the mechanical performance of the composites.

Table 4.7: Impact of the fly ash-to-cement ratio on compressive strength

Water to binder ratio	Fly ash to cement ratio	Sand to binder ratio	Length of the jute fibre, mm	Compressive strength, MPa
0.27	2	0.5	20	21.00
0.27	1.2	0.5	20	28.70

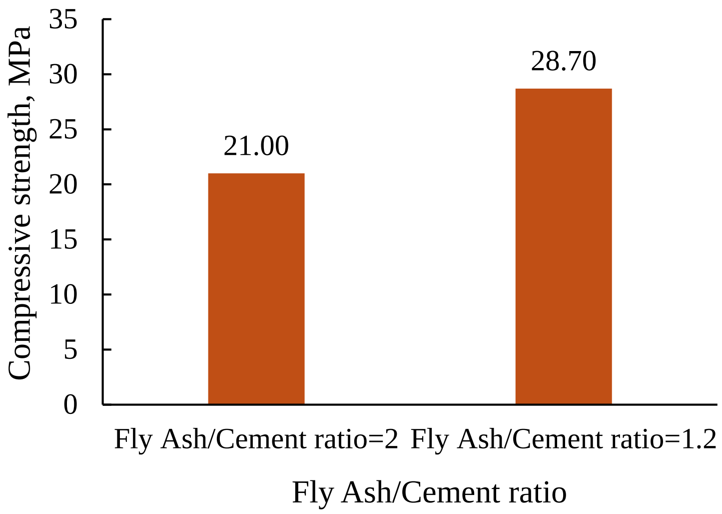

Fig. 4.6: Effect on compressive strength due to fly ash/cement ratio changes at W/B=0.27, S/B=0.5 and fibre length=20mm

Notably, cementitious composites with FA/C=1.2 demonstrated higher strength compared to the FA/C=2.0 mix at all curing periods. This enhancement is likely due to the increased proportion of cement in the binder system, which contributed to higher early-age reactions and improved matrix densification. Although fly ash plays a crucial role in long-term pozzolanic activity, an excessive replacement level (such as FA/C = 2.0) may lead to a dilution of the cement matrix, thereby limiting strength development, especially in early to mid-term curing periods.

Following the investigation of compressive strength, the failure pattern of the cementitious composites specimen containing FA/C ratios of 2.0 and 1.2, was also observed after the compression test, as shown in Fig. 4.7.

(a) (b)

Fig. 4.7: Specimen failure pattern, (a) FA/C=2.0 and (b) FA/C=1.2

The cylindrical specimen with a high fly ash to cement ratio (FA/C = 2.0) and 20 mm jute fibre exhibited a columnar or splitting failure under compressive loading shown in Fig. 4.7(a). The high fly ash content might have contributed to this brittle behaviour likely due to insufficient fibre-matrix bonding as lower cement content contributed to a less dense matrix. 4.7(b) represents the shear failure of specimen which was prepared with FA/C = 1.20 and 20 mm jute fibre. This failure mode suggests that the ultimate strength was governed by the shear capacity of the composite. Reducing fly ash content at FA/C = 1.20, likely contributed to a strong and cohesive matrix capable of resisting direct tensile splitting and jute fibres appears to have played a significant role in the shear failure behaviour.

4.4.4 Effect of Jute Fibre Length Changes

This section discusses the effect of jute fibre length on the compressive strength of cementitious composites. Three distinct sets of mixing parameters were utilized to evaluate the influence of jute fibre length, as outlined in Table 4.8. In this comparison, only the jute fibre length was varied from 10 mm to 20 mm, while all other mix components were kept constant. Composites containing 10 mm jute fibres exhibited higher compressive strength compared to those with 20 mm fibres, as shown in Fig. 4.8.

Table 4.8: Effect of jute fibre length on compressive strength

Water to binder ratio	Fly ash to cement ratio	Sand to binder ratio	Length of the jute fibre, mm	Compressive strength, MPa
0.36	1.2	0.3	10	39.09
0.36	1.2	0.3	20	13.98
0.36	1.2	0.5	10	30.75
0.36	1.2	0.5	20	20.15
0.27	2	0.3	10	29.41
0.27	2	0.3	20	19.48

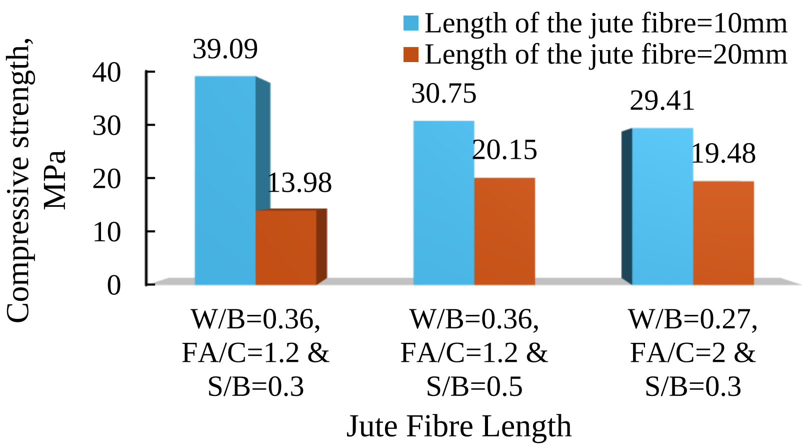

Fig. 4.8: Effect on compressive strength due to jute fibre length changes

The observed trend in compressive strength behaviour associated with shorter jute fibres aligns with findings from previous studies by Islam and Ahmed (2018) and Zakaria et al. (2015). This trend could arise due to the balling effect associated with longer fibres, which creates additional porous spaces within the composite. As a result, composites made with shorter fibres (10 mm) exhibit higher compressive strength than those with longer fibres (20 mm).

Beyond the compressive strength, the failure mode of the cementitious composites specimen containing 10 mm length jute fibres, was also observed after the compression test, as presented in Fig. 4.9. As shown in Fig. 4.9(a), the cylindrical specimen exhibited columnar or splitting failure. However, a magnified view of the fracture surface provides evidence of the significant role played by fibre bridging in this failure process. The jute fibres connect across the crack, effectively bridging the separated matrix components.

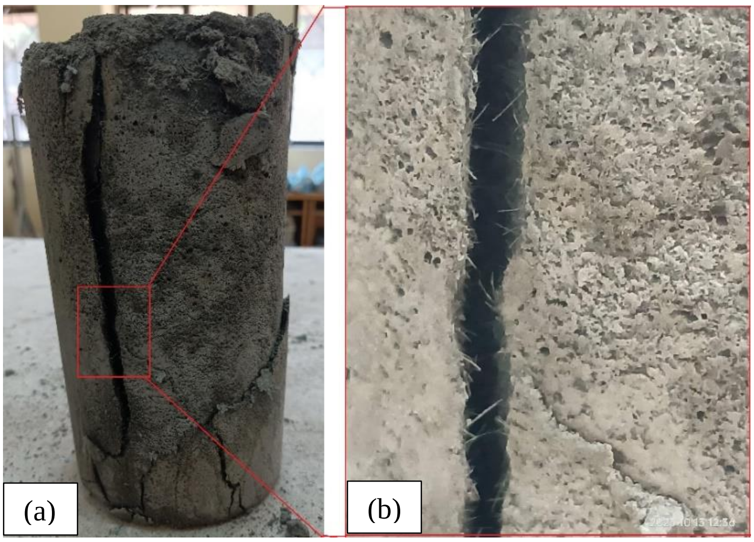

Fig. 4.9: Specimen failure pattern and bridging action of jute fibre

The fibre bridging action generate tensile forces that resist crack opening and propagation. The observed pull-out and breakage of fibres indicate energy dissipation during the loading process, contributing to an increased toughness compared to plain concrete (Merta et al., 2025).

4.4.5 Effect of Curing Days

This section presents the impact of curing duration on the compressive strength development of the cementitious composites. The test results, presented in Table 4.9 and Fig. 4.10, demonstrate a clear correlation between curing period and improved mechanical performance.

Table 4.9: Compressive strength development over varying curing durations

Water to binder ratio	Fly ash to cement ratio	Sand to binder ratio	Length of the jute fibre, mm	Curing age, Days	Compressive strength, MPa
0.30	1.4	0.3	10	28	17.44
0.30	1.4	0.3	10	42	31.78

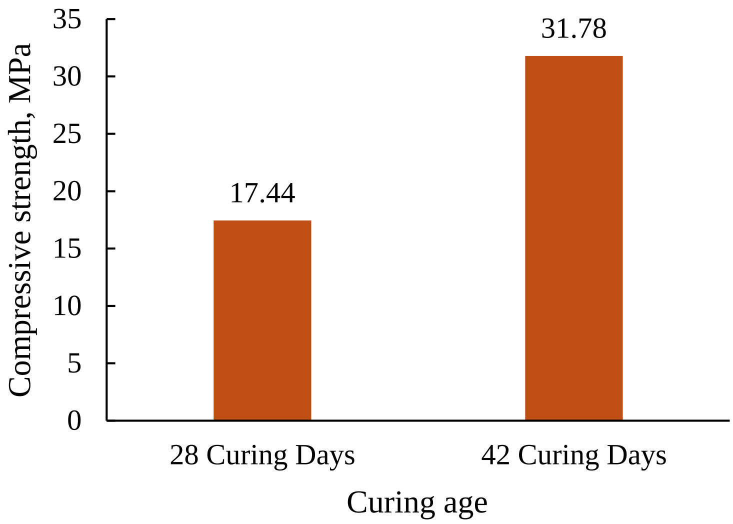

Fig. 4.10: Effect of curing duration on compressive strength

The composites exhibited a significant increase in compressive strength (approximately 180%) when the curing period was extended from 28 to 42 days. This pronounced improvement can be attributed to two synergistic mechanisms: (1) prolonged hydration of the cementitious matrix, and (2) sustained pozzolanic activity of the fly ash component. These processes collectively facilitate the progressive formation of calcium silicate hydrate (C–S–H) gel, which enhances microstructural densification and improves interfacial bonding within the composite system. The resultant microstructure exhibits superior cohesion and reduced porosity, directly correlating with the observed mechanical performance improvement.

This compressive strength enhancement suggests that the proposed cementitious composites continue to gain substantial strength beyond the standard 28 days curing period unlike the conventional concrete.

Thus, the findings highlight the importance of extended curing period, particularly in mixes including fly ash and natural fibres, where early-age strength development may be slower. Therefore, adequate curing beyond the standard 28 days is essential to fully understand the long-term strength potential of JFRCCs.

Based on the above discussions of experimental results, the following key points can be drawn:

- Jute fibre demonstrates significant potential for enhancing the compressive strength of cementitious composites, making it a valuable component in the development of fibre-reinforced cementitious composites.

- Studies have demonstrated that incorporating 10 mm jute fibres into cementitious composites results in higher compressive strength compared to using 20 mm fibres.
- The investigation showed that incorporating industrial by-products, such as fly ash, significantly increases the compressive strength of cementitious composites. This finding suggests that eco-friendly construction materials, like JFRCCs, could be developed by partially substituting cement with fly ash.
- A W/B ratio of 0.23 resulted in superior compressive strength compared to other tested ratios.
- Composites with S/B ratio of 0.5 demonstrated better compressive strength compared to those with a ratio of 0.3, particularly when the FA/C ratio was maintained at 1.2.

These findings underscore the significant impact of mixing parameters including W/B ratio, FA/C ratio, S/B ratio, and jute fibre length—on the compressive strength of cementitious composites. While this preliminary investigation identified notable trends and promising mixing ratios, it did not establish an optimal mix design that balances maximum compressive strength with cost-effectiveness. Hence, further investigation is needed to determine optimum mixing proportions of JFRCCs taking into account both mechanical performance and economic considerations. Building on the trends identified in the Phase I investigation, the upper and lower limits for each mixing parameter were defined and used in the Phase II experimental program. The following sections present a comprehensive analysis on the experimental results obtained in the Phase II investigation to determine the optimum mix ratios of JFRCCs.

4.5 Phase II Experimental Procedure- Design of Experiment

In Phase II of the experimental program, the primary objective was to determine the optimal mixture proportion of JFRCCs. To achieve this, a full factorial analysis, performed using Minitab software, was employed to obtain the optimum mix ratio for JFRCCs. Design of Experiment (DOE) methodologies, particularly full factorial designs, are commonly employed in experimental programs that examine the influence of multiple factors (Ahmad & Alghamdi, 2014; Antony, 2023; Colette et al., 2023). In this context, the effect of factors and their interactions were investigated on different responses in a full factorial design. Notably, in a full factorial design, the number of experiment is a^k in a full factorial design where k is number of factor and a is level of experiments and this approach is particularly effective in maximizing the information obtained from a limited number of trials and is especially efficient for two-level experimental designs (Khan et al., 2016; Montgomery, 2013). Accordingly, in this phase of the investigation, key variables such as the W/B ratio, FA/C ratio, S/B ratio, and jute fibre content were selected as key mixing parameters for the preparation of JFRCCs. Furthermore, full factorial analysis was performed for two level experiment (lower level and higher level).

Based on the experimental results of Phase I investigation, the selection range for key mixing parameters was refined to conduct investigation in this phase. For the W/B ratio, initial tests across a broad range of 0.23 to 0.36 revealed context-specific optimal values. At a FA/C ratio of 1.2, a lower W/B ratio of 0.23 yielded higher compressive strength (Fig. 4.1), whereas at FA/C = 2.0 and 10 mm jute fibre, W/B ratio of 0.27 performed moderate results (Fig. 4.8), indicating that an optimal balance must be maintained between adequate hydration and workability. Consequently, the W/B ratio range was confined within 0.26–0.29 for this Phase II investigation. The S/B ratio was maintained within the range of 0.30 to 0.50, despite mixed performance trends. At a FA/C ratio of 1.2, composites with a S/B ratio of 0.5 yielded superior strength (Fig. 4.4), whereas shorter jute fibres (10 mm) performed better with a lower S/B ratio of 0.3 (Fig. 4.5).

For the FA/C ratio, the initial range of 1.2 to 2.0 was retained. Although higher fly ash content (FA/C = 2.0) generally led to lower strength due to delayed pozzolanic activity, the environmental advantages of fly ash, such as reducing cement demand and associated carbon emissions, justified its continued evaluation for sustainability trade-offs. Additionally, 10 mm jute fibres, which exhibited superior performance compared to 20 mm at a preliminary dosage of 0.5% (Fig. 4.8), were selected for further testing. The fibre content range was expanded to 0.5%–1.0% by weight of binder to examine its influence on both strength and toughness. Therefore, the lower and higher limits of 4 principle mixing parameters were finalized as shown in Table 4.10. It is important to note that, the length of the jute fibre was kept constant at 10 mm in this study, as they provided better compressive strength compared to 20 mm fibres in preliminary investigation.

Table 4.10: Range of key mixing parameters investigated for JFRCCs development

Key mixing parameters	Water to binder ratio (W/B)	Fly ash to cement ratio (FA/C)	Sand to binder ratio (S/B)	Jute fibre content, %
Lower limit	0.26	1.2	0.3	0.5
Upper limit	0.29	2.0	0.5	1.0

Following the 2^4 factorial design (two level experiment with four factors), a total of 16 mix ratios were extracted. The experimental design runs were developed using coded units, where –1 and 1 represent the lower and higher limits of the mixing variables, respectively, as detailed in Table 4.11.

Table 4.11: Summary of factorial mix design parameters (mixing limits shown in parentheses)

Mix no.	W/B	FA/C	S/B	Jute content
1	-1 (0.26)	-1 (1.2)	1 (0.5)	1 (1.0)
2	1 (0.29)	-1 (1.2)	1 (0.5)	-1 (0.5)
3	1 (0.29)	-1 (1.2)	-1 (0.3)	1 (1.0)
4	1 (0.29)	1 (2.0)	1 (0.5)	1 (1.0)
5	-1 (0.26)	1 (2.0)	1 (0.5)	1 (1.0)
6	1 (0.29)	-1 (1.2)	-1 (0.3)	-1 (0.5)
7	1 (0.29)	1 (2.0)	-1 (0.3)	-1 (0.5)
8	-1 (0.26)	-1 (1.2)	1 (0.5)	-1 (0.5)
9	-1 (0.26)	1 (2.0)	-1 (0.3)	-1 (0.5)
10	1 (0.29)	-1 (1.2)	1 (0.5)	1 (1.0)
11	-1 (0.26)	-1 (1.2)	-1 (0.3)	-1 (0.5)
12	1 (0.29)	1 (2.0)	-1 (0.3)	1 (1.0)
13	-1 (0.26)	-1 (1.2)	-1 (0.3)	1 (1.0)
14	-1 (0.26)	1 (2.0)	1 (0.5)	-1 (0.5)
15	1 (0.29)	1 (2.0)	1 (0.5)	-1 (0.5)
16	-1 (0.26)	1 (2.0)	-1 (0.3)	1 (1.0)

Based on the design of experiments outlined in this section, suitable mix ratios were identified for further investigation. These selected mixes serve as the foundation for preparing the composite specimens in this investigation. The following section provides detailed descriptions of the mix design procedures and sample preparation for casting and testing.

4.6 Mix Design- Phase II Experiment

In the Phase II experiment, the mix design was determined according to the proportions specified in Table 4.11. The material quantities for 1.0 m^3 of each cementitious composite mix are detailed in Table 4.12. In this investigation, the jute fibre length was consistently maintained at 10 mm for all mix proportions, as preliminary investigations indicated that this length yielded superior compressive strength compared to 20 mm fibres. The mechanical behaviour of the newly developed composites was assessed across 16 unique formulations. This characterization involved measuring key performances, namely compressive strength, corresponding strain at peak load, splitting tensile strength, and ultrasonic pulse velocity (UPV).

From each mix formulation, six standard 100 mm × 200 mm cylindrical specimens were casted, making a total of 96 cylinders for evaluation after 28 days of curing. The experimental program comprised compressive and splitting tensile strength tests on three specimens each, with strain at peak compressive stress also being recorded. Prior to destructive testing, all specimens were assessed using the non-destructive ultrasonic pulse velocity (UPV) method. In parallel, the economic feasibility of each batch was determined through a manufacturing cost analysis that accounted for material, processing, and labour expenses.

Table 4.12: Mix design of cementitious composites for phase II experiment

Mix No.	Water to Binder ratio	Fly Ash to Cement ratio	Sand to Binder ratio	Jute fibre content (% of total volume)	Water, Kg/m^3	Fly Ash, Kg/m^3	Sand, Kg/m^3	Jute fibre, Kg/m^3	Cement, Kg/m^3
1	0.26	1.2	0.5	1	294.3	617.5	566.0	20.1	514.6
2	0.29	1.2	0.5	0.5	319.6	601.0	551.0	9.9	500.9
3	0.29	1.2	0.3	1	348.7	656.0	360.8	19.3	546.6
4	0.29	2	0.5	1	311.8	716.8	537.6	19.4	358.4
5	0.26	2	0.5	1	288.9	740.9	555.7	19.7	370.4
6	0.29	1.2	0.3	0.5	351.0	660.2	363.1	9.7	550.2
7	0.29	2	0.3	0.5	344.1	791.1	356.0	9.5	395.6
8	0.26	1.2	0.5	0.5	296.3	621.7	569.9	10.1	518.1
9	0.26	2	0.3	0.5	320.0	820.4	369.2	9.7	410.2
10	0.29	1.2	0.5	1	317.5	597.1	547.3	19.8	497.6
11	0.26	1.2	0.3	0.5	326.6	685.2	376.8	9.9	571.0
12	0.29	2	0.3	1	342.0	786.1	353.8	18.9	393.1
13	0.26	1.2	0.3	1	324.5	680.7	374.4	19.7	567.2
14	0.26	2	0.5	0.5	290.9	745.8	559.3	9.9	372.9
15	0.29	2	0.5	0.5	313.8	721.5	541.1	9.8	360.7
16	0.26	2	0.3	1	317.9	815.1	366.8	19.3	407.6

4.7 Comprehensive Performance Evaluation of JFRCCs- Phase II Experiment

In this section, a detailed evaluation is presented on the performance of JFRCCs. Key properties such as specimen dimensions, unit weight, compressive strength, splitting tensile strength, strain at peak compressive strength, and UPV were examined to understand their structural characteristics. Additionally, material cost was calculated to evaluate the economic viability. A summary of the different mixtures, including specimen dimensions, mechanical characteristics, and material costs, is provided in Table 4.13. This table highlights variations in compressive strength, strain at peak compressive strength, tensile strength, unit weight, and UPV for different mixes.

Based on the comparative analysis, it is evident that certain mixes are more suitable for high-stress applications due to their greater compressive and tensile strengths, whereas some mixes are more appropriate for lightweight or cost-sensitive applications due to reduced unit weight or material cost. However, the following subsection verifies the dimensional consistency of the test specimens to support of the reliability of the mechanical performance data.

Table 4.13: Summary of experimental observations (standard deviations reported in parentheses)

Mix no.	Average diameter (mm)	Height (mm)	Compressive strength, MPa	Average compressive strength (MPa)	Strain at peak compressive strength, ϵ	Average strain at peak compressive strength, ϵ	Split tensile load (kN)	Split tensile strength (MPa)	Avg. split tensile strength (MPa)	Unit weight (kg/m^3)	Avg. unit weight (kg/m^3)	UPV (m/s)	Avg. UPV (m/s)	Material cost (Tk/m^3)
	101.70	202.00	44.03		0.0034		201.38	6.41		1966.60		3874		
1	102.40	201.00	46.02	46.45 (2.66)	0.0033	0.0033 (0.00013)	198.23	6.31	6.35 (0.06)	1935.01	1956.58 (18.70)	3893	3893 (18.50)	12,742
	102.50	201.00	49.29		0.0032		198.55	6.32		1968.14		3911		
	102.94	204.00	55.19		0.0030		109.33	3.48		1987.98		3874		
2	102.32	201.00	50.57	55.19 (4.62)	0.0031	0.0031 (0.00005)	108.07	3.44	3.46 (0.02)	2045.40	2019.70 (29.18)	3911	3899 (21.36)	11,565
	102.03	204.00	59.80		0.0031		108.39	3.45		2025.71		3911		
	102.13	200.00	33.60		0.0025		152.05	4.84		1934.98		3791		
3	102.28	203.00	33.26	35.81 (4.12)	0.0040	0.0031 (0.00079)	151.43	4.82	4.85 (0.03)	1931.36	1944.01 (18.86)	3799	3792 (6.56)	13,072
	101.66	201.00	40.56		0.0028		153.31	4.88		1965.68		3786		
	102.74	202.00	23.31		0.0020		126.29	4.02		1853.54		3568		
4	100.80	200.50	20.42	23.31 (2.89)	0.0023	0.0023 (0.00025)	128.81	4.10	4.06 (0.04)	2031.79	1948.11 (89.62)	3537	3558 (17.90)	10,960
	102.75	201.00	26.20		0.0025		127.23	4.05		1959.00		3568		

	102.14	200.00	20.65		0.0026		118.75	3.78		1886.69		3632		
5	102.60	203.00	21.81	21.97 (1.41)	0.0033	0.003 (0.00038)	119.38	3.80	3.81 (0.04)	1816.67	1856.93 (36.17)	3631	3621 (18.77)	11,325
	103.01	202.00	23.45		0.0031		120.95	3.85		1867.42		3599		
	101.30	202.00	54.95		0.0018		113.73	3.62		1974.56		3945		
6	102.36	202.00	39.03	45.19 (8.55)	0.0017	0.0018 (0.00018)	114.35	3.64	3.64 (0.02)	1945.83	1958.47 (14.67)	3948	3904 (73.63)	12,336
	102.28	204.00	41.60		0.0020		114.67	3.65		1955.02		3819		
	101.90	201.00	33.06		0.0024		130.69	4.16		1933.43		3732		
7	99.82	201.00	33.86	33.30 (0.49)	0.0025	0.0024 (0.00003)	126.61	4.03	4.06 (0.09)	2018.15	1951.06 (60.25)	3725	3733 (8.54)	10,830
	102.27	202.00	32.98		0.0025		125.04	3.98		1901.59		3742		
	103.49	202.00	49.54		0.0027		137.60	4.38		2022.88		4044		
8	101.60	201.00	45.76	47.74 (1.90)	0.0021	0.0027 (0.00065)	138.54	4.41	4.42 (0.05)	2063.24	2015.02 (52.60)	3956	4023 (58.97)	11,971
	102.56	202.00	47.93		0.0034		140.74	4.48		1958.93		4068		
	102.35	201.00	31.95		0.0029		103.99	3.31		1942.17		3788		
9	101.62	202.00	36.34	35.12 (2.77)	0.0027	0.0029 (0.00018)	105.87	3.37	3.40 (0.10)	1940.59	1936.91 (7.78)	3766	3785 (17.69)	11,243
	101.89	200.00	37.08		0.0031		110.27	3.51		1927.97		3801		
	101.57	200.85	28.47		0.0026		202.63	6.45		1984.28		3775		
10	102.00	201.00	36.80	35.04 (5.89)	0.0030	0.0028 (0.00018)	204.20	6.50	6.49 (0.04)	1965.58	1962.19 (23.97)	3698	3758 (53.56)	12,324
	102.47	203.00	39.84		0.0028		205.15	6.53		1936.70		3801		

	101.43	201.00	47.78		0.0026		99.59	3.17		2005.33		3937		
11	103.70	203.00	40.78	47.68 (6.85)	0.0021	0.0026 (0.00045)	94.88	3.02	3.10 (0.08)	1921.64	1968.76 (42.83)	3874	3883 (50.56)	12,815
	101.67	202.00	54.47		0.0030		98.02	3.12		1979.30		3837		
	101.85	201.00	21.53		0.0020		119.69	3.81		1878.73		3506		
12	99.96	202.00	24.31	23.52 (1.74)	0.0021	0.0021 (0.00013)	122.52	3.90	3.88 (0.06)	1916.06	1888.32 (24.40)	3506	3506 (0.00)	11,569
	101.66	201.00	24.73		0.0022		123.15	3.92		1870.19		3506		
	102.80	203.00	39.43		0.0025		163.05	5.19		1953.72		3837		
13	101.94	203.00	42.55	39.71 (2.72)	0.0025	0.0025 (0.00005)	165.25	5.26	5.26 (0.08)	1920.55	1938.72 (16.81)	3837	3837 (0.00)	13,563
	101.45	202.00	37.14		0.0024		167.76	5.34		1941.89		3837		
	101.21	202.00	26.03		0.0023		101.16	3.22		1940.22		3698		
14	101.55	201.00	31.80	28.24 (3.11)	0.0023	0.0023 (0.00003)	101.79	3.24	3.25 (0.04)	1943.65	1933.29 (15.07)	3766	3732 (34.00)	10,551
	102.66	202.00	26.89		0.0023		103.36	3.29		1916.00		3732		
	102.06	204.00	30.38		0.0021		90.79	2.89		1956.20		3738		
15	102.09	204.00	30.51	30.88 (0.75)	0.0023	0.0022 (0.00013)	93.31	2.97	2.92 (0.04)	1965.89	1954.77 (11.89)	3747	3742 (4.73)	10,198
	102.32	201.00	31.74		0.0024		91.11	2.90		1942.23		3740		
	102.21	202.00	35.01		0.0022		97.70	3.11		1897.43		3698		
16	102.30	203.00	37.69	33.42 (5.24)	0.0021	0.0021 (0.00010)	103.67	3.30	3.22 (0.10)	1902.99	1896.65 (6.76)	3650	3682 (27.71)	11,995
	102.30	201.00	27.57		0.0020		102.10	3.25		1889.53		3698		

4.7.1 Dimensional Consistency of Test Specimens

Dimensional consistency verification of test specimens is crucial for ensuring the reliability of mechanical performance data. The distribution of diameters and heights of all cylindrical specimens is shown in Fig. 4.11, which reflects a normal distribution for both parameters. Diameters range from 99.5 mm to 104 mm, with a mean of 102.1 mm and a standard deviation of 0.72 mm. Similarly, heights range from 200 mm to 204 mm, with a mean of 202 mm and a standard deviation of 1.12 mm. These uniform dimensions across all test specimens confirm the accuracy of sample preparation, thereby enhancing the credibility of the mechanical and statistical analyses presented in this study.

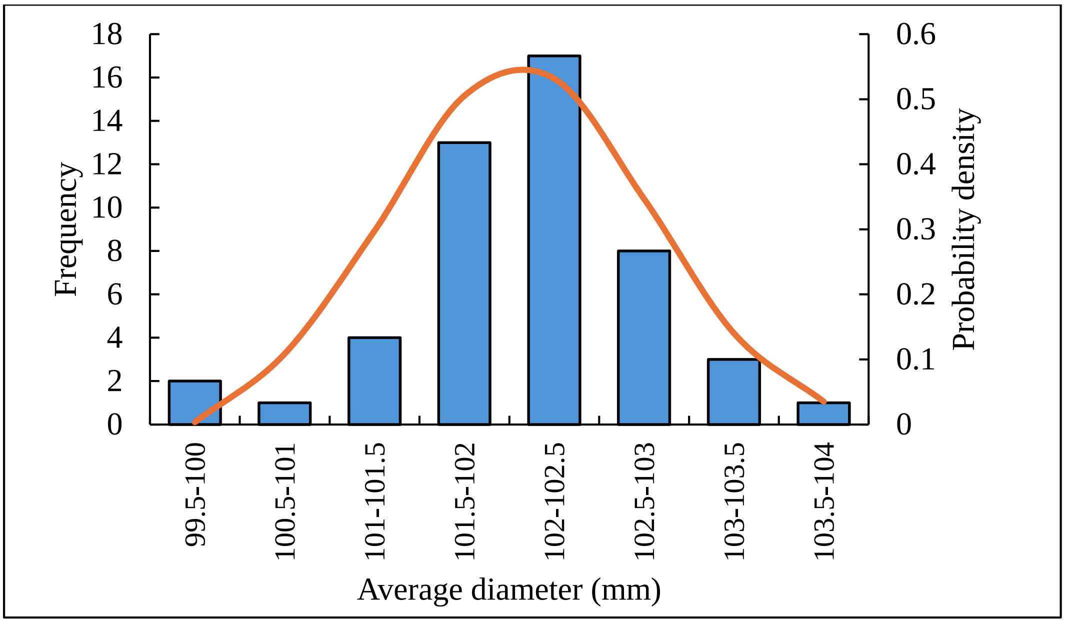

(a)

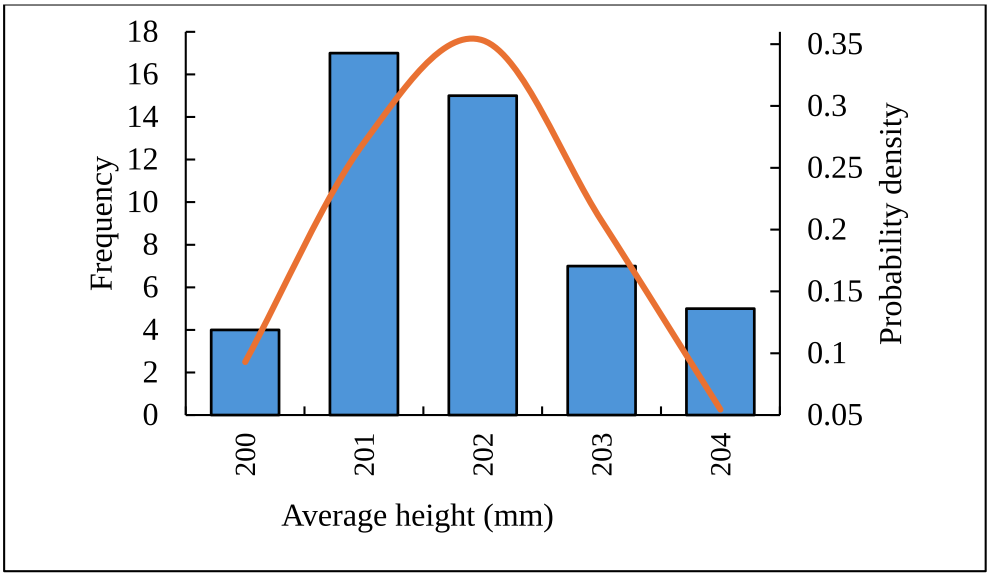

(b)

Fig. 4.11: Variation in cylinder specimen geometry: (a) diameter distribution, (b) height distribution

4.7.2 Compressive Strength

Compressive strength, a key indicator of cementitious composite performance, is the maximum axial load a specimen can bear before failure. A compressive strength test was performed on cylindrical specimen of JFRCCs at 28 days of casting. The comparative compressive strength results of the various cementitious composite mixes are presented in Fig. 4.12. The results highlight significant variations among the different mixes, reflecting the influence of mix design parameters on mechanical performance.

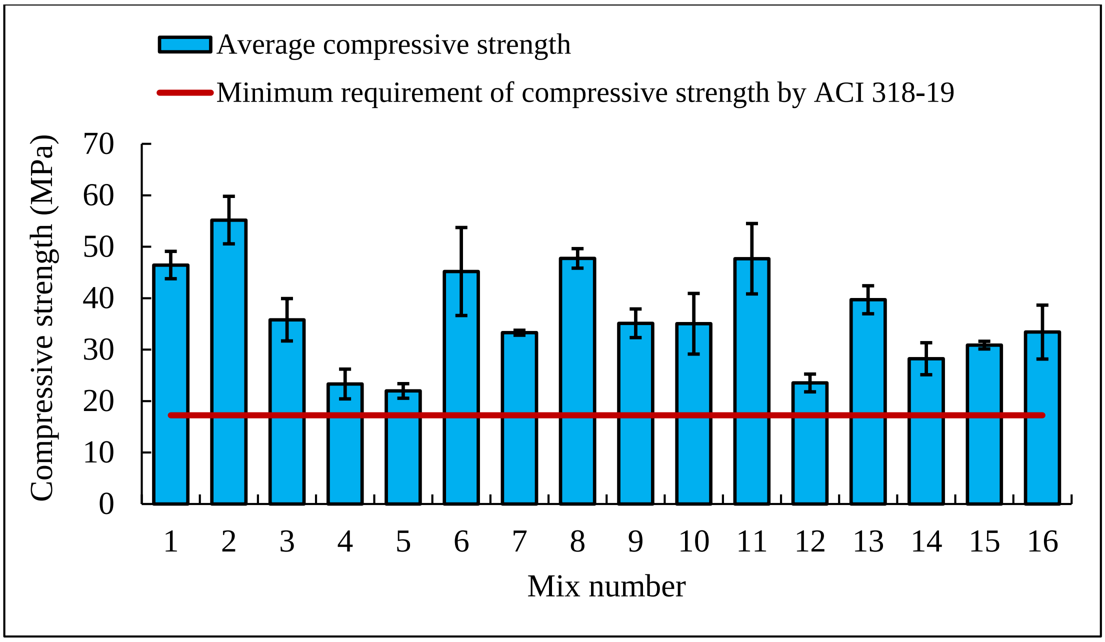

Fig. 4.12: Compressive strength characteristics across all mix designs

Among all tested specimens, Mix-2 exhibited the highest compressive strength of 55.19 MPa, positioning it as a strong candidate for use in structural elements subjected to high loads, such as reinforced concrete columns, beams, and slabs in multi-storey and high-rise buildings. Its superior strength indicates efficient matrix compaction, optimal fibre-matrix interaction, and balanced hydration.

In contrast, Mix-5 recorded the lowest compressive strength of 21.97 MPa, which, although adequate for certain non-structural applications, may limit its use in load-bearing components where higher strength is essential. The lower performance could be attributed to suboptimal proportions of binder and/or fibre content that compromised the matrix integrity.

Despite these variations, it is important to note that all mixes exceeded the minimum compressive strength requirement specified by ACI 318-19, which mandates a minimum of 17.25 MPa (2500 psi) for structural concrete in residential buildings. This confirms the baseline suitability of all developed mixes for general construction use, while also enabling strategic selection based on specific structural demands.

These findings underscore the potential of JFRCCs as sustainable and structurally viable alternatives to conventional materials, particularly when mix designs are optimized for targeted applications.

4.7.3 Strain at Peak Compressive Strength

Strain at peak compressive strength was measured using mechanical strain dial gauges placed on opposite sides of the cylinder samples during compression test of composites. This parameter provides valuable information about the ductility and deformation capacity of the composite material at its maximum load-bearing capacity. Furthermore, the distribution of strain at peak compressive strength for the various cementitious composite mixes is presented in Fig. 4.13.

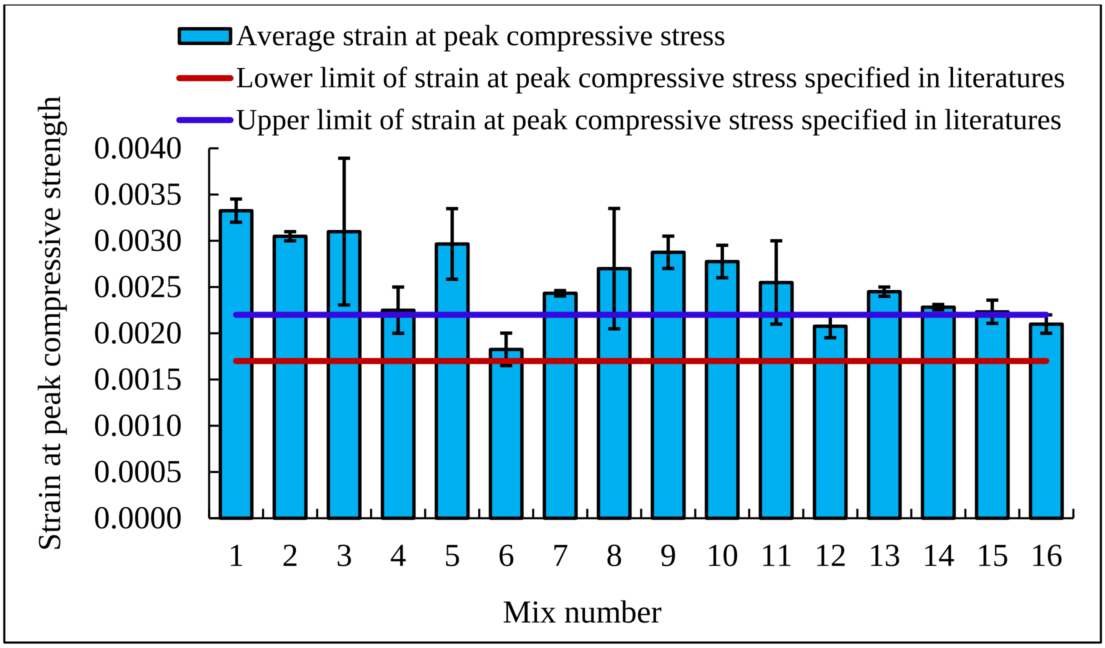

Fig. 4.13: Peak compressive strain across all mix designs

As shown in Fig. 4.13, there is a clear variation among the mixes, reflecting the influence of constituent proportions and fibre interaction on the overall stress-strain response. Mix-1 recorded the highest peak strain of 0.0033, well above the typical strain limits for conventional concrete. This elevated strain level indicates a pronounced ductile behaviour, allowing the material to undergo significant deformation before failure. Such ductility is advantageous in seismic or high-stress applications, where energy dissipation and crack bridging are critical. This performance is attributed to the synergistic effect of jute fibre reinforcement and the fineness of pozzolanic materials such as fly ash, which together improve the interfacial bond, delay crack propagation, and enhance strain capacity.

On the other end of the spectrum, Mix-6 exhibited the lowest peak strain of 0.0018, suggesting a more brittle failure mode. Similar brittle tendencies were also observed in Mix-12 and Mix-16, with strain values falling below the upper threshold. These mixes, although structurally sound, may offer limited deformation capacity and could be more susceptible to sudden failure under dynamic or excessive loading conditions.

Importantly, most of the developed mixes lie within or near the accepted strain limits for normal-strength concrete, as defined by several international design standards: ACI 318 (2019), Norme Tecniche (1992), Eurocode (1991), and C.E.B.-FIP Model Code (1991). These standards typically cite a strain range of 0.0017 to 0.0022 at peak compressive stress. The fact that the majority of mixes exceed the upper limit (except Mix-6, Mix-12, and Mix-16) is indicative of the enhanced ductility achieved through the integration of natural fibres and supplementary cementitious materials. According to Tian et al. (2015), the inclusion of pozzolanic fillers like fly ash contributes to a denser microstructure and stronger fibre-matrix bonding, both of which are key contributors to the ductile performance observed in composites.

Overall, the findings validate the requirement for optimization of mix design in producing composites that not only meet but surpass traditional concrete performance benchmarks in terms of deformability and failure resilience.

4.7.4 Splitting Tensile Strength

Tensile strength is a vital property for cementitious composites, especially in residential applications where resistance to cracking from shrinkage, thermal changes, and loading is essential. Splitting tensile strength tests were conducted to obtain the tensile capacity of the JFRCCs specimens at 28 days of casting. The splitting tensile strength results for different mixes are presented in Fig. 4.14, along with the lower limit specified in ACI 318-19 (0.1f’c). Among the mixes, Mix-10 achieved the highest tensile strength at 6.49 MPa, indicating strong crack resistance and suitability for applications such as slabs and beams where tensile loads are significant.

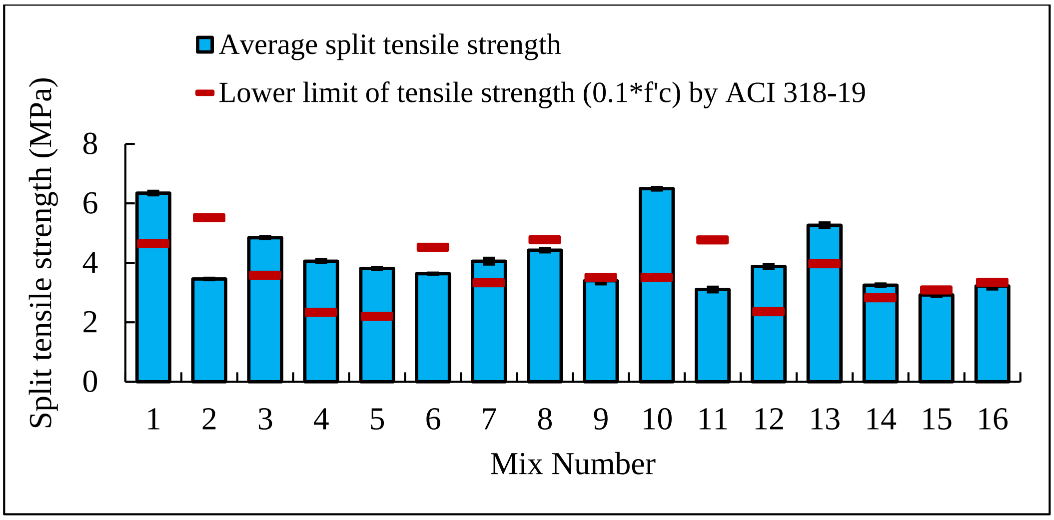

Fig. 4.14: Splitting tensile strength for different mixes.

Conversely, Mix-15 had the lowest tensile strength at 2.92 MPa, potentially limiting its structural use. Additionally, Mix-2, Mix-6, Mix-11, and Mix-15 did not meet the minimum tensile requirement, likely due to their 0.5% jute fibre content, which may not have provided sufficient bridging action to enhance tensile capacity. Increasing the jute content could enhance the fibre bridging effect, improving tensile strength if fibres are well distributed. However, excessive fibre content may compromise workability if not properly managed. Overall, these results highlight the positive effect of natural fibres on tensile strength, but also underscore the need for optimized fibre dosage and proper mixing to achieve desirable structural performance in JFRCCs.

4.7.5 Unit Weight Variations

Unit weight of cementitious composites is a key parameter influencing design considerations for structural members. It influences the dead load of structural elements and reflects the material's internal compactness, which relates to strength and durability. The unit weight of the JFRCCs mixes varied based on composition, shown in Fig. 4.15.

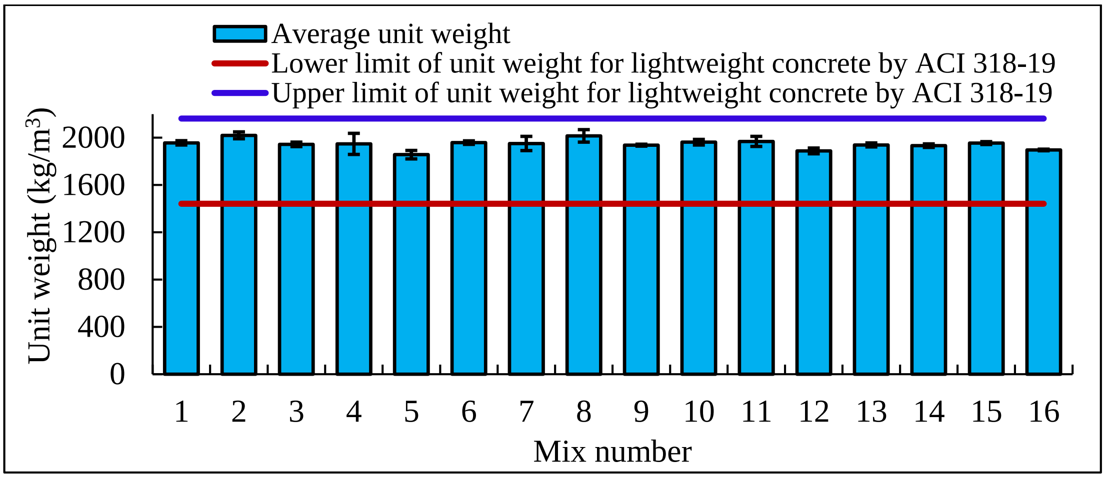

Fig. 4.15: Unit weight variations for different mixes.

Mix-2 had the highest unit weight at 2019.70 kg/m³, indicating a dense and well-compacted matrix suitable for high load-bearing applications like beams and columns. In contrast, Mix-5 showed the lowest unit weight at 1856.93 kg/m³, making it more suitable for lightweight construction where reduced dead load is desirable. It is noteworthy that all mix designs fall within the lightweight concrete category as defined by ACI 318-19, confirming their potential for structural use while offering the advantage of reduced self-weight.

4.7.6 Ultrasonic Pulse Velocity (UPV)

Ultrasonic Pulse Velocity (UPV) testing offers a non-destructive means to evaluate the internal quality and homogeneity of cementitious composites. This has a strong correlation with compressive behaviour and modulus of elasticity of concrete (Espinosa et al., 2023). The distribution of UPV values across different mixes is presented in Fig. 4.16 and the corresponding UPV data as per IS 13311 is provided in Table 4.14.

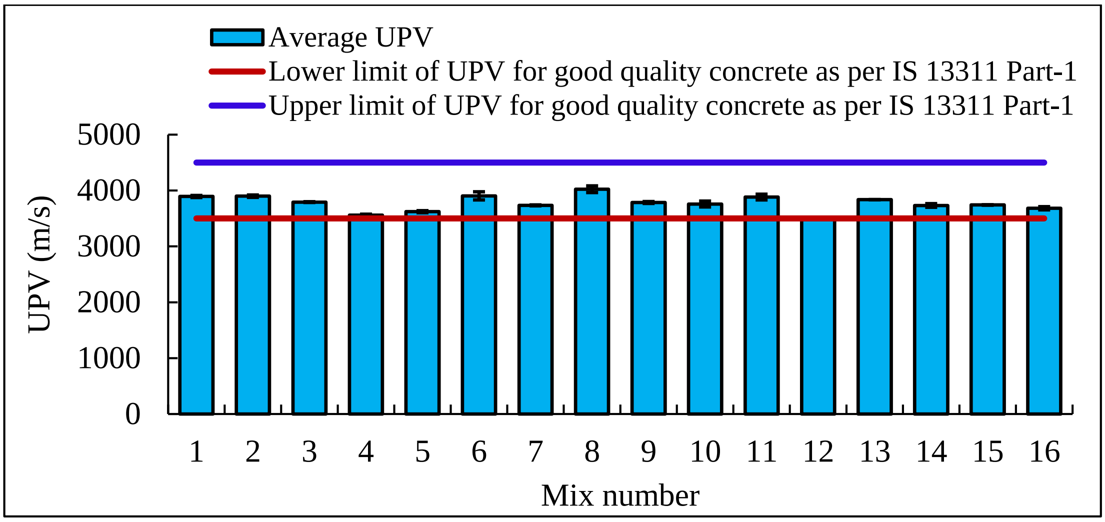

Fig. 4.16: UPV for different mixes.

Table 4.14: Classification of concrete quality ratings based on IS 13311 (Part 1): 1992 (Bureau of Indian Standards, 1992)

Pulse velocity (km/s)	Concrete quality (Ratings)
≥ 4.5	Excellent (E)
3.5 - 4.5	Good (G)
3.0 - 3.5	Medium (M)
Below 3.0	Doubtful (D)

Among the various mixes, Mix-8 showed the highest UPV at 4023 m/s, indicating excellent internal compactness and quality. Conversely, Mix-12 had the lowest UPV at 3506 m/s, suggesting potential micro-defects or porosity. Notably, mixes with 1.0% jute fibre content—including Mix-4, Mix-5, Mix-12, and Mix-16—generally exhibited lower UPV values, likely due to fibre agglomeration or uneven dispersion.

Nevertheless, all mixes fall within the "good quality" category based on UPV results shown in Table 4.14 (Bureau of Indian Standards [BIS], 1992), demonstrating that the JFRCCs maintain acceptable internal consistency and structural soundness even with higher fibre content.

4.7.7 Material Cost

Material cost is a key factor in selecting concrete mixes for budget-sensitive or large-scale construction projects. A detailed cost analysis was performed for each mix, based on local market prices of materials such as cement, fly ash, sand, jute fibre, and superplasticizer. The material cost for different mixes are shown in Fig. 4.17.

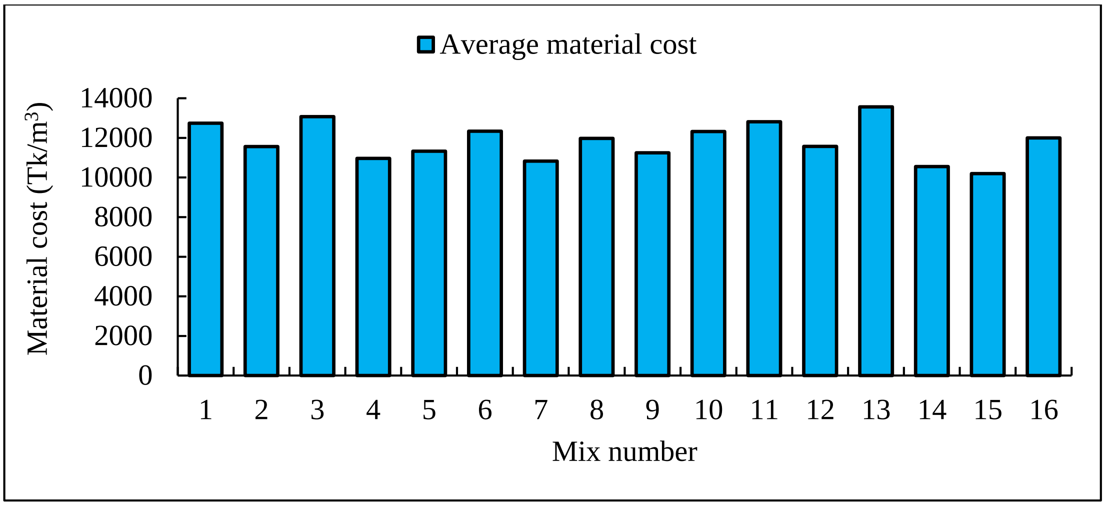

Fig. 4.17: Material cost for different mixes.

Mix-13 had the highest cost at 13,563 BDT/m³, mainly due to its higher binder content and use of performance-enhancing components. However, this cost is justified by its greater mechanical properties, making it suitable for high-strength or critical structural applications. On the other hand, Mix-15 was the most economical, costing 10,198 BDT/m³, yet still meeting the minimum strength requirements for residential use according to ACI 318-19. This mix strikes a good balance between cost and performance, making it ideal for budget-constrained projects. This comparison emphasizes the importance of evaluating both cost-effectiveness and structural performance when selecting JFRCCs mixes for practical applications.

The comprehensive performance evaluation identified several mixes suitable for distinct applications:

- For high strength applications: Mix-2 is recommended, exhibiting the highest compressive strength and favourable strain characteristics, making it ideal for demanding structural roles despite its higher cost.

- For tensile load resistance: Mix-1, with its superior tensile strength, presents the most suitable option for components subjected to tensile stresses.
- For specialized properties: Mix-10's high ultrasonic pulse velocity (UPV) suggests a dense and uniform microstructural integrity, while Mix-8 offers a combination of high unit weight and strength suitable for high-stress applications.
- For economic viability: Mix-15 represents the most balanced choice for general-purpose use, providing adequate mechanical performance at a minimal material cost.

Therefore, this comprehensive analysis underscores the necessity to optimize the mix ratios of the proposed composite to enhance both performance and cost-efficiency in construction and engineering projects.

4.8 Life Cycle Assessment

A Life Cycle Assessment (LCA) was conducted to quantify the environmental impacts inherent to the production of the composites. The analysis was performed for all 16 mix designs, adopting a cradle-to-gate system boundary. This boundary encompassed the life cycle stages of raw material extraction, transportation, and the manufacturing (mixing) process.

The CO_2 emission values for the materials used in preparing JFRCCs are presented in Table 4.15 (Ahmed et al., 2021), which was considered to calculate CO_2 footprint for each different mixes. In order to calculate the CO_2 emission from transportation, cement, sand and fly ash were assumed to be transported from closest local sources in Bangladesh.

Table 4.15: CO_2 emission of different materials (Ahmed et al., 2021).

Material	Cement	Fly ash	Fine aggregate	Water	Admixture[a]
CO_2 emission per ton of material (kg)	959	93	5	1	508

[a]Including liquid content.

Other materials (i.e., water, jute, admixtures) was not considered for calculating CO_2 emission from transportation as these materials emit comparatively less CO_2 emission from transportation. The cement and fly ash were assumed to be sourced from 62 km away from Islamic University of Technology (IUT), while the sand was assumed to be obtained from 280 km away from IUT. Considering the availability of transport, truck was taken as mode of transport for above material and in our country, truck usually consumed 1 litre of diesel fuel to run 6-8 km distance based on loading condition of truck. The combustion of diesel fuel emits 2.69 kg CO_2 from 1 liter of diesel (Mickūnaitis et al., 2007). A comparative analysis of the carbon footprint associated with the sixteen composite formulations is presented in Fig. 4.18, showing emissions from raw material production and cumulative emissions from material sourcing, transport, and mixing processes.

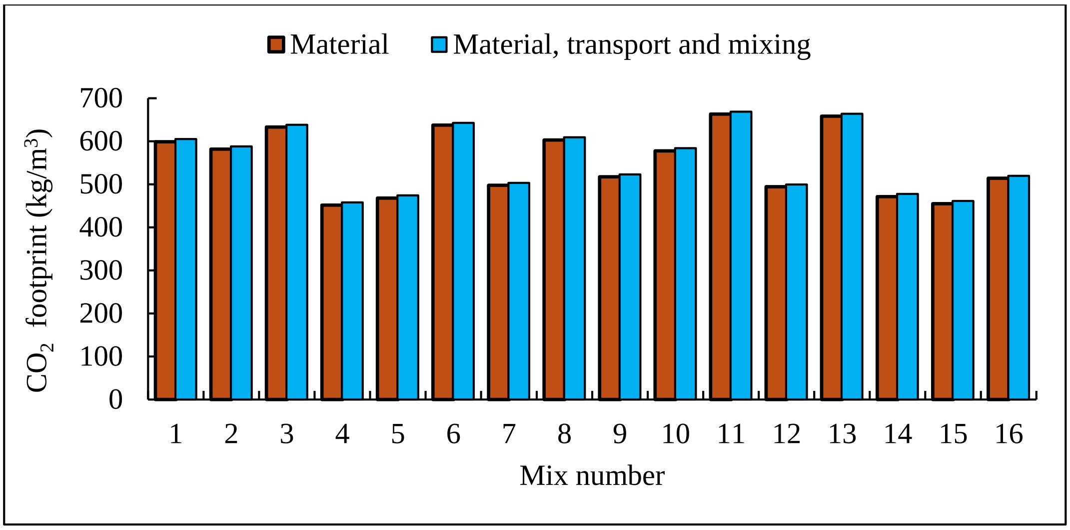

Fig. 4.18: CO_2 footprint of different mixes

Here, CO_2 emission from material varies from 451 kg/m^3 to 663 kg/m^3 for different composites mixes. For normal strength concrete, the range of CO_2 emission varies within 290 kg/m^3 to 320 kg/m^3 where Portland cement used only as binder (Flower & Sanjayan, 2007). Also, CO_2 emission from material, transport and mixing changes from 458 kg/m^3 to 668 kg/m^3 for composites mixes. Another study reported that concrete of varying compressive strength (30 MPa to 50 MPa) emit CO_2 from 246 kg/m^3 to 514 kg/m^3 up to production stage (Kerr et al., 2022). The lowest CO_2 emission was observed for the Mix-4 for its compressive strength 23.31 MPa and the highest CO_2 emission was observed for the Mix-11 for its compressive strength 47.68 MPa. Therefore, it is mentionable that the CO_2 footprint of composites declines with increasing FA/C ratio and S/B ratio.

The CO_2 intensities (*ci*) which represent the CO_2 footprint per unit of compressive strength for various types of composites are shown in Fig. 4.19. This provides a clearer understanding of the environmental impact of these concrete types.

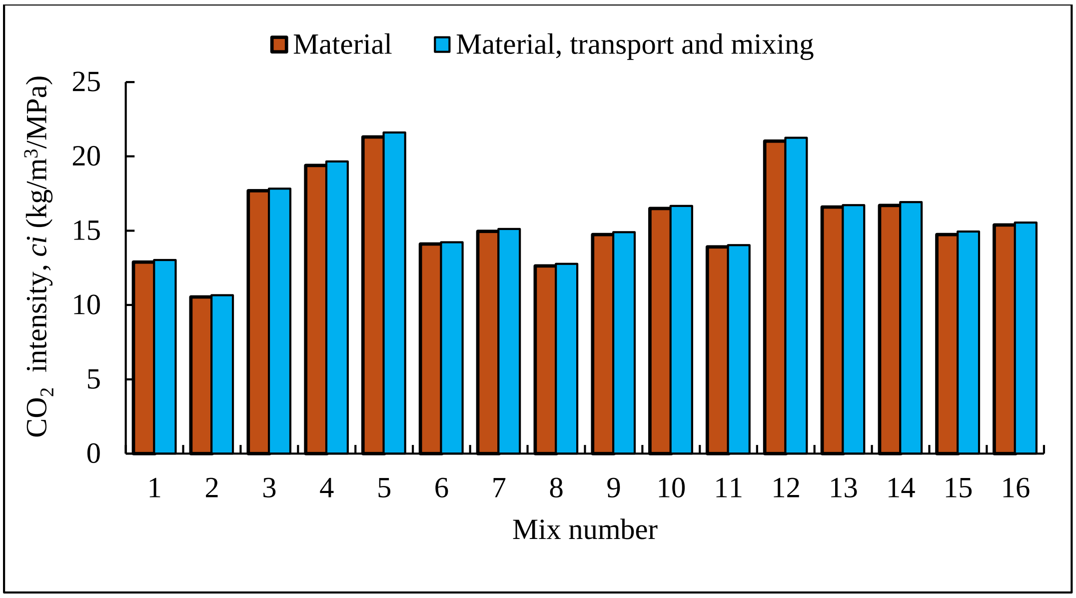

Fig. 4.19: CO_2 intensity of different mixes

The minimum CO_2 intensity i.e. 10.54 kg/m^3/MPa was observed for Mix-2 for its compressive strength 55.19 MPa and maximum CO_2 intensity i.e. 21.31 kg/m^3/MPa was observed for Mix-5 for its compressive strength 21.97 MPa; though, CO_2 intensity of all the mixes shows more than the international future benchmark of *ci*, 5.00 kg/m^3/MPa (Elchalakani et al., 2017), which would be the target for reducing CO_2 emissions by incorporating supplementary cementitious materials (SCMs).

4.9 Microstructural Analysis of Developed JFRCCs

A comprehensive microstructural investigation of the cementitious composites was performed using a TESCAN VEGA3 scanning electron microscope (SEM) to evaluate long-term morphological evolution. Following mechanical testing, fracture surfaces of specimens aged nine months were examined to characterize critical microstructural attributes, as presented in Fig. 4.20 to 4.24. The SEM analysis revealed distinct features governing composite performance, including the morphology of hydration products, interfacial transition zone (ITZ) integrity, pore structure uniformity, spatial distribution of jute fibres, and bonding efficacy at the fibre-matrix interface.

The surface morphology and microstructural characteristics of Mix-2 composites are shown in Fig. 4.20.

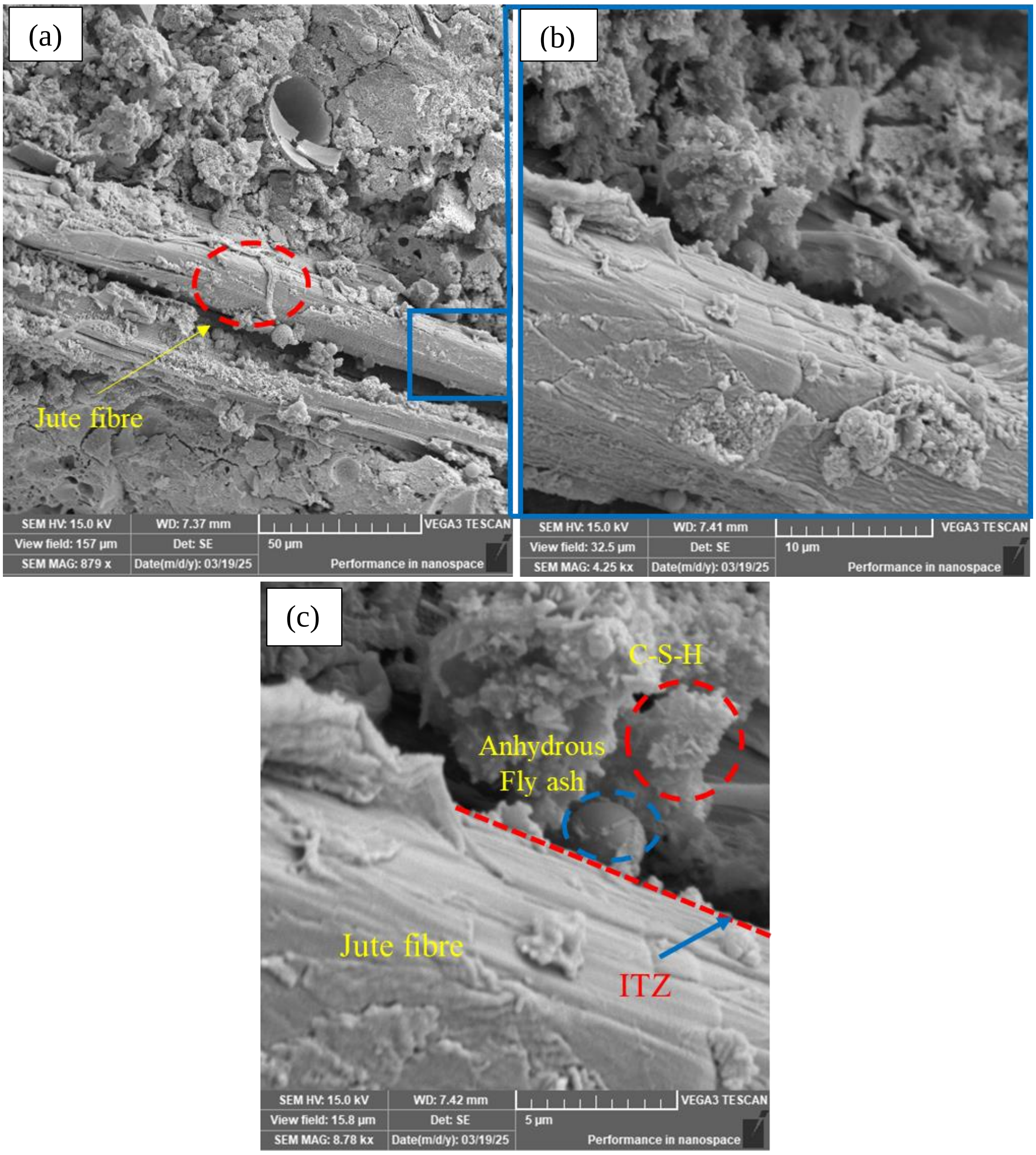

Fig. 4.20: SEM analysis of Mix-2: microstructural features at FA/C = 1.2 with 0.5% jute fibre

The SEM images demonstrate the interfacial transition zone (ITZ) between the jute fibre and cementitious matrix, highlighting the bonding efficiency. The presence of Calcium Silicate Hydrate (C-S-H) gel was observed near the ITZ, indicating hydration and matrix densification. Through the pozzolanic reaction, fly ash reacts with calcium hydroxide to produce additional C-S-H gel, which improves strength and durability. Furthermore, finer fly ash particles fill voids effectively, resulting in a denser and more homogeneous microstructure. The matrix shows a heterogeneous microstructure, with regions of dense hydration products.

The images reveal a partial encapsulation of jute fibre by the cementitious matrix, suggesting a mechanical interlock that enhances fibre adhesion. Voids and weak bonding areas appeared within the ITZ may contribute to fibre pullout, affecting composite strength and ductility. Unreacted anhydrous fly ash particles were visible, signifying incomplete pozzolanic reactions at certain locations. The presence of jute fibre embedded in the matrix suggests potential crack-bridging mechanisms, improving toughness and energy absorption. The combination of fly ash and jute fibres creates a synergistic effect, with the pozzolanic reaction complementing the reinforcing action of the fibres.

Extending the discussion further, the surface morphology and microstructural characteristics of Mix-15 composites are presented in Fig. 4.21. Here, the SEM images reveal the surface morphology and bonding interactions between the jute fibre and the cementitious matrix. A rough interfacial transition zone (ITZ) was observed, which plays a crucial role in the composites mechanical behaviour.

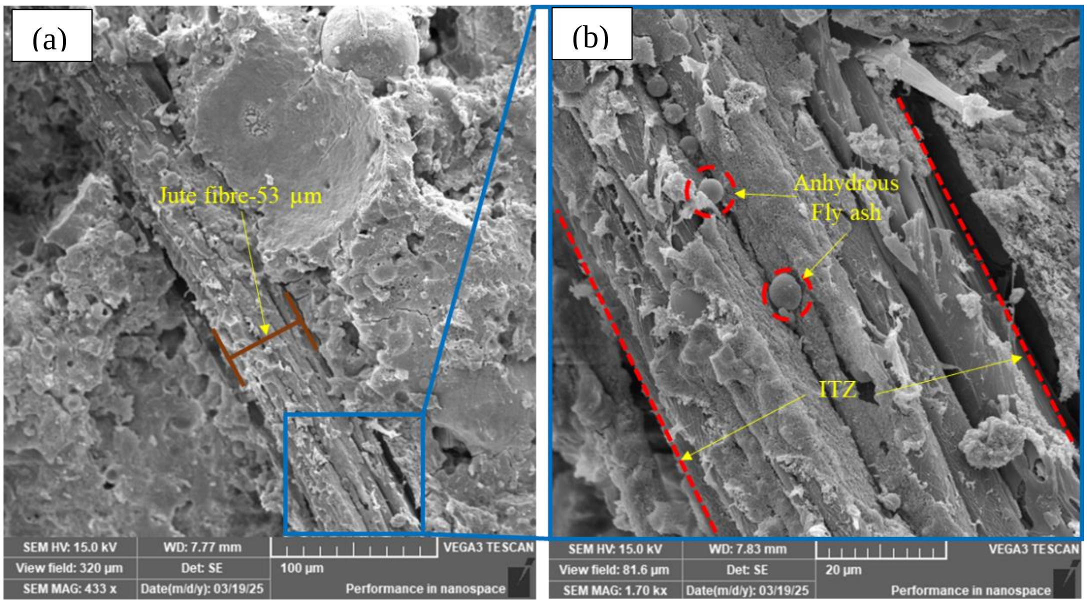

Fig. 4.21: Microstructure of Mix-15: composites at FA/C = 2.0 incorporating 0.5% jute fibre

But, the presence of some micro cracks along the ITZ indicates potential weak zones that could affect composite toughness. Embedded jute fibre within the cementitious matrix showing signs of partial encapsulation. The adhesion between jute fibre and the cementitious matrix is not fully uniform, which might influence the mechanical performance of the composites.

Visible gaps between the fibre and the matrix indicate potential weak bonding at certain locations, which could contribute to fibre pullout during loading. Well-hydrated zones surrounding some fly ash particles suggest secondary C-S-H formation, which improves overall matrix densification and strength. The presence of anhydrous fly ash particles was noticeable in the matrix, indicating incomplete pozzolanic reaction in those areas. The ITZ appears porous compared to the bulk matrix, with a relatively heterogeneous distribution of hydration products.

In continuation of the above findings, the fracture surface of composites with changing jute fibre content are presented in Fig. 4.22. The SEM images show how the fibres are dispersed and bonded within the cementitious matrix. The interfacial transition zone (ITZ) between the jute fibres and the cement matrix plays a critical role in load transfer and the integrity of the composite. Fig. 4.22(a) shows the microstructure of the composite without jute fibre, where visible cracks have formed on the surface. In contrast, composites with jute fibre, as shown in Fig. 4.22(b) (0.5% jute fibre) and Fig. 4.22(c) (1.0% jute fibre), exhibited significantly fewer surface cracks.

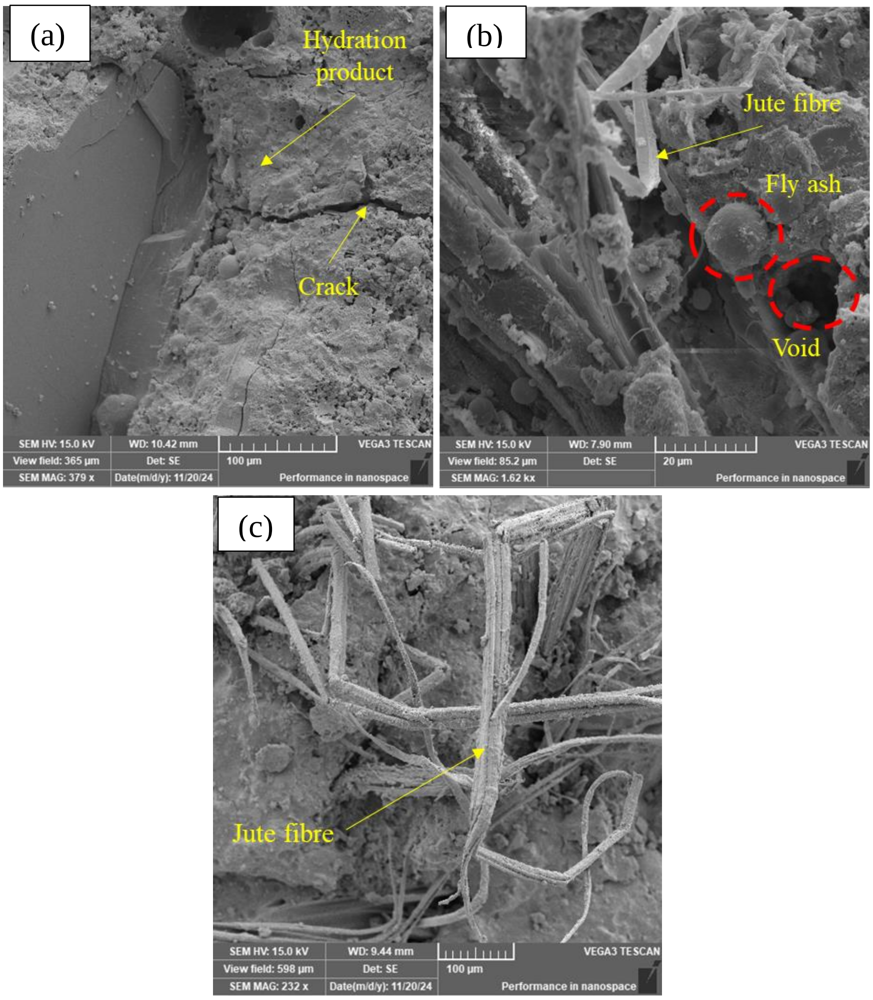

Fig. 4.22: SEM comparison of composites: (a) without fibre, (b) with 0.5% jute fibre, (c) with 1.0% jute fibre

Jute fibres provide enhanced crack resistance through fibre-bridging action. At 0.5% fibre content, the SEM image shows comparatively homogeneous dispersion of fibres within the matrix than 1.0% jute fibre content and strong attachment to the cementitious matrix. This uniform dispersion forms a network that effectively arrests crack propagation. However, at 1.0% jute fibre content, uneven dispersion and inadequate anchoring were observed, leading to bulk defects and stress concentration, ultimately causing failure at lower stress levels.

Above observation is further supported by the SEM image of fracture surface shown in Fig. 4.23, which depicts a 9-month-old composite specimen (FA/C = 1.2, jute content = 1.0%) after undergoing a compressive strength test. Uneven fibre distribution is observed in this SEM image of composite. It is highly likely that at higher fibre contents, jute fibres may tend to clump together, leading to uneven distribution. Poor dispersion can also create voids and gaps within the matrix, which reduce the overall density and compressive strength.

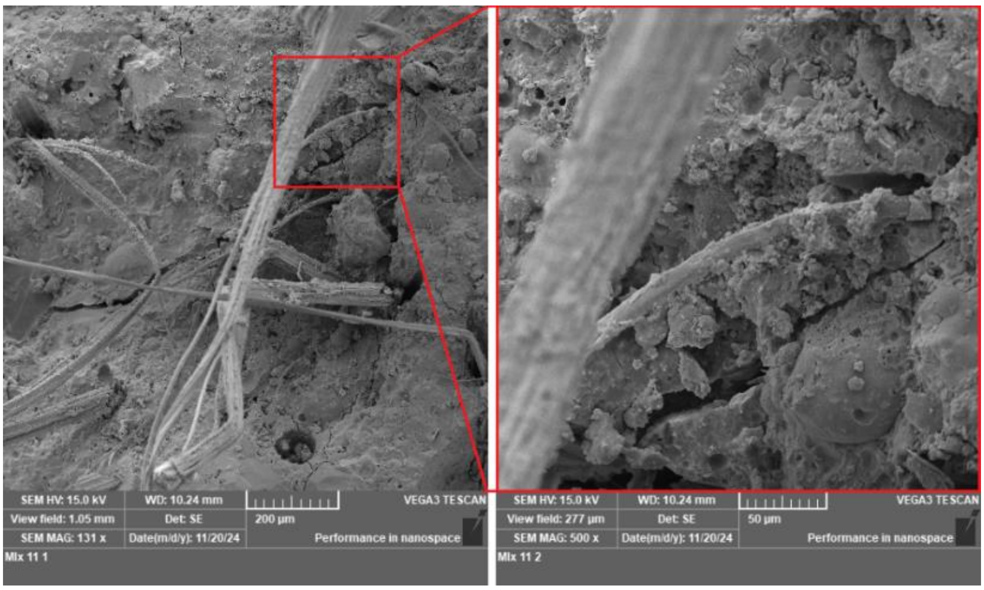

(a)

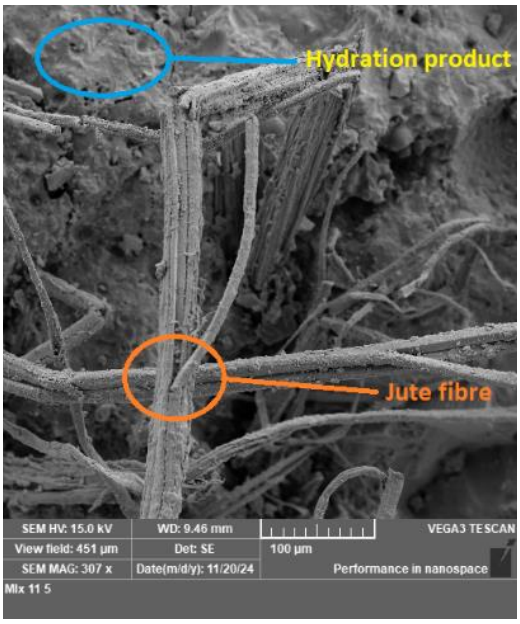

(b)

Fig. 4.23: The microstructure of the composites at FA/C-1.2 and jute content-1.0 % (Mix-10).

Furthermore, the poor bonding between the jute fibres and the cement matrix is evident in the specimen shown in Fig. 4.23(b). This is caused by the high fibre content, which can dilute the cement matrix and reduce the available binding material to hold the composite together. This dilution can lead to several adverse effects, such as poor adhesion between the fibres and the matrix, uneven fibre distribution, and an increase in voids or weak zones within the material. Additionally, the fibres may create stress concentrations or hinder the uniform transfer of loads across the matrix. These factors collectively compromise the structural integrity and reduce the compressive strength of the composite.

Following the earlier analysis, the fracture surface of the composite with a fly ash-to-cement ratio of 2.0 and 1.0% jute content, is presented in Fig. 4.24.

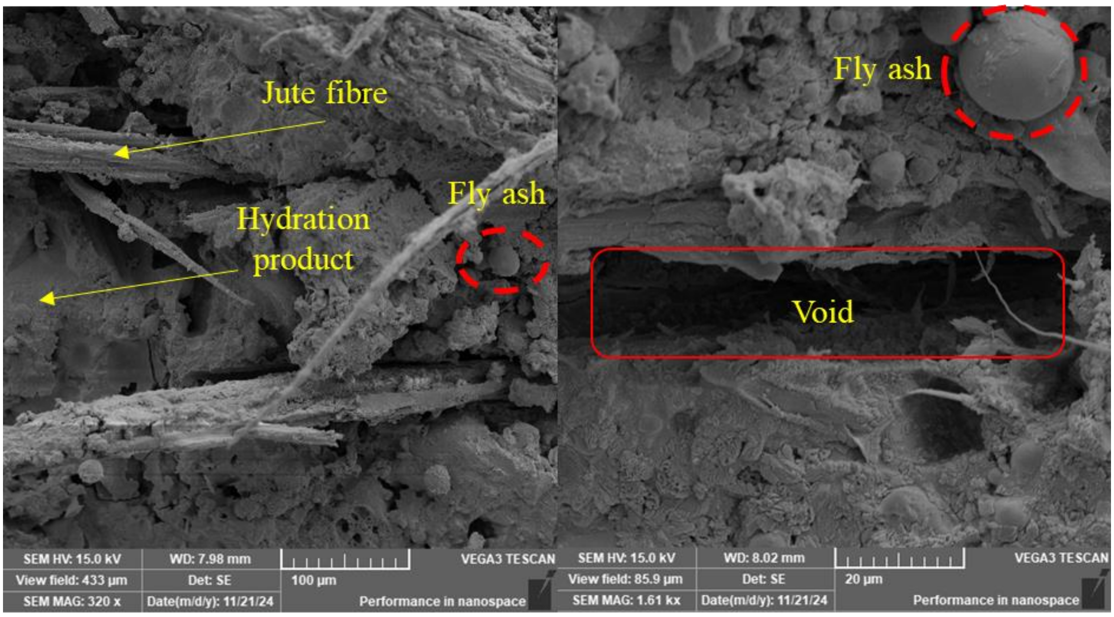

(a) (b)

Fig. 4.24: The microstructure of the composites at FA/C-2.0 and jute content-1.0 % (Mix-4).

An uneven distribution of jute fibres within the matrix is observed in Fig. 4.24(a), potentially leading to localized weaknesses. Also, large voids exist in the matrix as well as unreacted fly ash, shown in Fig. 4.24(b). It is occurred in the matrix as quantity of fly ash and jute fibre content were increased in the composite.

A higher fly ash content slows the hydration process, reducing the formation of calcium silicate hydrate (C-S-H) gel and excess fibres may introduce voids or agglomerations within the matrix, disrupting uniform load transfer and creating stress concentration zones. When both fly ash and jute fibre quantities are increased simultaneously, the negative effects compound. The matrix becomes less cohesive, and the interface between the fibres and the cementitious material is further weakened due to the diluted matrix. This combination results in a highly porous structure with reduced mechanical properties, such as compressive strength and durability, unless the proportions are carefully optimized.

4.10 Summary

Phase I investigation reveals that water-to-binder proportion, fly ash-to-cement proportion, sand-to-binder proportion, and jute fibre length are significant mixing parameters influencing the compressive behaviour of composites. Subsequently, Phase II results identified key mixes with distinct advantages: Mix-2 for high compressive strength, Mix-1 for superior tensile strength, Mix-10 for excellent internal quality, Mix-8 for high-stress applications, and Mix-15 as a cost-effective alternative. These findings highlight the importance of optimizing mix ratios to balance performance and cost-efficiency in construction. In the following chapter, a comprehensive statistical analysis will be presented based on the experimental results obtained in the Phase II investigation to determine the optimum mix ratios of JFRCCs. Based on the optimization, the research was continued in Phase III investigation in the next chapter, which focuses on evaluating the performance of the optimized JFRCCs under various environmental and thermal conditions.

CHAPTER 5: STATISTICAL OPTIMIZATION AND PERFORMANCE EVALUATION OF OPTIMIZED JFRCCs^

5.1 Introduction

This chapter presents a comprehensive statistical analysis of the experimental results obtained in the Phase II investigation to optimize the mix ratios of Jute Fibre-Reinforced Cementitious Composites (JFRCCs). Optimization process includes, determining relationships between response variables by Pearson correlation coefficients, developing and validating regression models for response variables, assessing the effects and interactions of mixing parameters on mechanical responses, and performing multi-objective optimization to identify the optimal mix ratio. Based on the optimized mix design, the research then advanced to the Phase III investigation, which aimed to examine the performance JFRCCs under a variety of environmental and thermal conditions. Specifically, the Phase III investigation includes assessments under various curing methods (water, wet, and natural curing) and elevated temperature exposures (200 °C, 400 °C, 600 °C, and 800 °C). Together, these investigations provide a comprehensive understanding of the materials performance and confirm the suitability of the optimized JFRCCs in diverse structural applications.

---

^ The experimental investigations and corresponding findings presented in this chapter have been partially disseminated through the following publications:

Rahman, M. A., & Kabir, M. I. (2025). Development of a sustainable and cost-optimized cementitious composites incorporating local resources and jute fibre. *Cleaner Materials*, 17, 100322. DOI: https://doi.org/10.1016/j.clema.2025.100322

5.2 Pearson Correlation Coefficient

The Pearson correlation coefficient serves as a statistical tool to ascertain the magnitude and orientation of linear relations between continuous variable pairs. In the context of this study, it was employed to evaluate the degree of linear association among key performance parameters, including compressive strength, strain at peak compressive stress, splitting tensile strength, ultrasonic pulse velocity, and material cost. This analysis aids in identifying interdependencies that may influence the overall behaviour and economic viability of the composites. According to widely accepted interpretation standards, a coefficient ranging from 0.0 to 0.3 signifies a weak positive correlation, values between 0.3 and 0.5 indicate a moderate positive correlation, and coefficients exceeding 0.5 reflect a strong positive correlation. To evaluate the interrelationships among the key performance indicators of the developed JFRCCs, Pearson correlation coefficients were calculated, as shown in Table 5.1.

Table 5.1: Pearson correlation matrix among response variables

Response variables	Compressive strength (MPa)	Peak strain	Splitting tensile strength (MPa)	UPV (m/s)	Material Cost (Tk/m^3)
Compressive strength (MPa)	—	0.33	0.15	0.91	0.49
Peak strain	0.33	—	0.48	0.34	0.29
Splitting tensile strength (MPa)	0.15	0.48	—	0.18	0.56
UPV (m/s)	0.91	0.34	0.18	—	0.44
Material Cost (Tk/m^3)	0.49	0.29	0.56	0.44	—

A strong positive correlation (r = 0.91) was observed between compressive strength and UPV, confirming UPV as a reliable non-destructive indicator of internal compactness and strength, consistent with previous findings (Espinosa et al., 2023; Revilla-Cuesta et al., 2022).

Compressive strength also demonstrated a moderate correlation with material cost (r = 0.49), implying that higher strength mixes often require more costly or denser constituent materials. Splitting tensile strength exhibited the strongest correlation with material cost (r = 0.56), suggesting that improvements in tensile capacity typically come at increased material expenses, possibly due to higher binder or fibre contents. Overall, the correlation analysis highlights valuable relationships between response variables, which can guide the optimization of mix designs. This ensures improved performance efficiency and cost-effectiveness in the application of JFRCCs.

5.3 Determination of Optimal Mix Ratio for JFRCCs

The development of high-performance cementitious composites necessitated systematic optimization of key mixture parameters, including the W/B ratio, FA/C ratio, S/B ratio, and jute fibre content. This optimization was achieved through a comprehensive statistical analysis implemented utilizing Minitab software, following a rigorous three-phase methodology. Initially, regression models were formulated to predict the major response variables, and their validity was assessed to ensure reliable predictive capability. Subsequently, the influence of each mixing parameter on various mechanical properties was examined to evaluate their statistical significance and potential interactions. In the final stage, a multi-objective optimization technique was applied to simultaneously maximise the desirability of multiple performance outcomes, thereby identifying the optimal combination of mixing parameters for the composite formulation.

5.3.1 Development and Adequacy of the Statistical Model

The relationship among the input variables and each response parameter was developed based on full factorial experimental scheme, utilizing the dataset outlined in Table 4.13. For each response variable, a separate regression model was developed to adopt the influence of the mix design parameters. The resulting models are summarized in Table 5.2, which presents the corresponding regression equations along with the coefficient of determination (R^2) and the adjusted coefficient of determination (R^2_{adj}). These statistical indicators were used to evaluate the goodness-of-fit and predictive accuracy of each model, thereby ensuring the robustness and reliability of the developed equations for subsequent analysis and optimization.

Table 5.2: Predictive regression equations and coefficients of determination for JFRCCs response variables

Compressive strength	R^2 (%)	93.35%	R^2_{adj} (%)	88.92%
Compressive strength, MPa = -37.7 + 295×W/B + 3.90×FA/C + 89.4×S/B + 119.8×Jute - 494×W/B×Jute - 57.8×FA/C×S/B				
Strain at peak compressive strength	R^2 (%)	93.47%	R^2_{adj} (%)	75.53%
Strain at peak compressive strength = 0.039 - 0.17×W/B + 0.0066×FA/C - 0.087×S/B - 0.051×Jute + 0.40×W/B×S/B + 0.23×W/B×Jute - 0.015×FA/C×S/B - 0.0079×FA/C×Jute + 0.13×S/B×Jute - 0.56×W/B×S/B×Jute + 0.0167×FA/C×S/B×Jute				
Splitting tensile strength	R^2 (%)	99.06%	R^2_{adj} (%)	96.47%
Splitting tensile strength, MPa = -40.2 + 135.0×W/B - 1.16×FA/C + 125.8×S/B + 51.4×Jute + 20.69×W/B×FA/C - 435×W/B×S/B - 166.0×W/B×Jute - 6.75×FA/C×S/B - 4.33×FA/C×Jute - 112.9×S/B×Jute + 443×W/B×S/B×Jute				
UPV	R^2 (%)	97.93%	R^2_{adj} (%)	94.82%
UPV, m/s = -3905 + 29262×W/B + 4552×FA/C + 20007×S/B + 987×Jute - 17003×W/B×FA/C - 70622×W/B×S/B - 4546×W/B×Jute - 12035×FA/C×S/B + 42578×W/B×FA/C×S/B				

Material cost	R^2 (%)	100.00%	R^2_{adj} (%)	100.00%
Material Cost, Tk/m^3 = 22123.2 - 23281.7×W/B - 3141.66×FA/C - 9368.0×S/B + 1623.55×Jute + 3421.4×W/B×FA/C + 14990.3×W/B×S/B - 791.92×W/B×Jute + 1575.8×FA/C×S/B + 7.91×FA/C×Jute + 229.38×S/B×Jute - 2422.4×W/B×FA/C×S/B				

Legend: R^2=Coefficient of determination, R^2_{adj}=Adjusted coefficient of determination

The coefficient of determination (R^2) serves as an indicator of how well the regression equation represents the observed results. Its value ranges from 0% to 100%, where an R^2 of 100% indicates that the model perfectly explains the variability observed in the response variable, while an R^2 of 0% implies no explanatory capability. Therefore, a higher R^2 value signifies a stronger association between the regression model and the actual observations, indicating greater predictive accuracy. Additionally, the adjusted coefficient of determination (R^2_{adj}) provides a modified version of R^2 that accounts for the number of predictors included in the model. This adjustment offers a more realistic evaluation of the model's explanatory power, particularly when comparing models of varying complexity, as it penalizes the inclusion of irrelevant predictors.

The developed regression models demonstrate strong predictive capability, as evidenced by their high coefficients of determination (R^2) for each response variable: compressive strength (93.35%), strain at peak stress (93.47%), splitting tensile strength (99.06%), ultrasonic pulse velocity (97.93%), and material cost (100%), as detailed in Table 5.2. The adjusted coefficients (R^2_{adj}) maintain comparable values at 88.92%, 75.53%, 96.47%, 94.82%, and 100% respectively. However, a strong correlation between R^2 and R^2_{adj} was observed for all response variables, with the exception of the strain at peak compressive strength, where the discrepancy suggests a potential variability not fully captured by the model. Nonetheless, the overall results indicate that the developed regression models are reliable and can be confidently utilized to forecast the respective responses within the experimental limit of the selected mixing parameters.

5.3.2 Validation of Regression Models with Test Results

The reliability and predictive capability of the developed regression models were thoroughly assessed by comparing the model-generated predictions with the corresponding experimental results. This evaluation is demonstrated in Figs. 5.1 through 5.5, which present comparative plots for key performance indicators such as compressive strength, splitting tensile strength, UPV, strain at peak compressive stress, and material cost. These graphical comparisons provides a clear visual demonstration of the accuracy and consistency of the regression models. Notably, the predicted values for compressive strength exhibited a strong agreement with the experimental observations, as shown in Fig. 5.1, thereby affirming the model's strength in capturing the behaviour of the composite under compression.

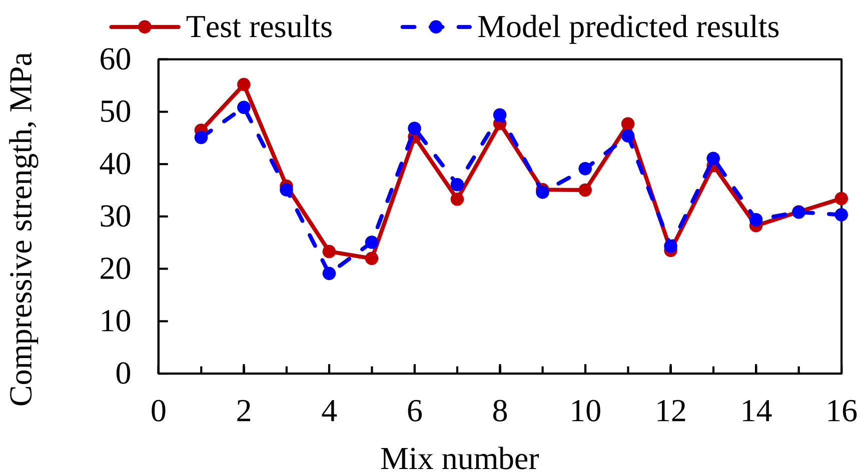

Fig. 5.1: Comparison of experimental and predicted compressive strength from regression Model

As shown in the figure, the maximum residual i.e., the absolute difference between the predicted and actual values was recorded as 4.35 MPa, indicating excellent predictive capability and low deviation within acceptable engineering limits. Similarly, the regression model for splitting tensile strength also demonstrated high consistency, with a maximum deviation of only 0.175 MPa, as shown in Fig. 5.2. This small variation suggests the model is well-calibrated to account for the effects of jute content and other mix parameters on tensile performance.

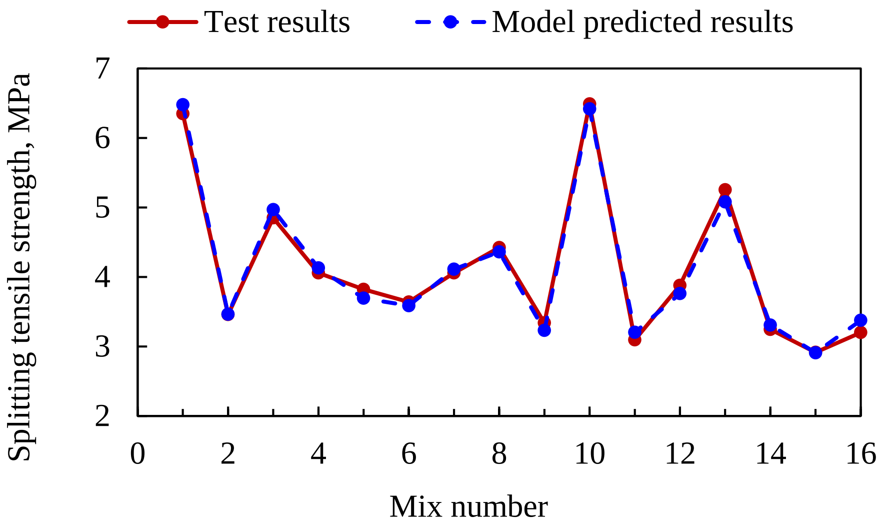

Fig. 5.2: Test vs model predicted results for splitting tensile strength.

For the UPV results, the predicted values closely matched the experimental results, with a highest difference of only 30 m/s, as depicted in Fig. 5.3. This slight variation is negligible considering the overall UPV range of the mixes, reaffirming the models ability to capture the internal compactness and homogeneity of the composites.

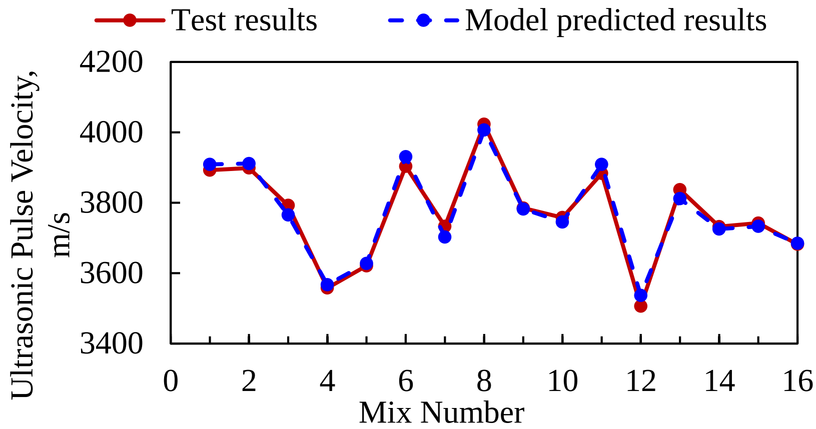

Fig. 5.3: Test vs model predicted results for Ultrasonic Pulse Velocity.

In terms of peak strain (Fig. 5.4), the regression predictions remained very close to the experimental measurements, with a maximum deviation of just 0.00017. Such a small discrepancy indicates that the model is effective in simulating the composites ductility behaviour under load.

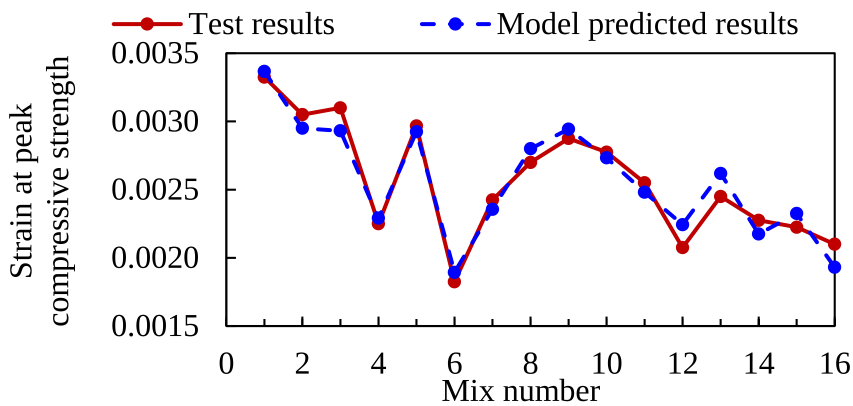

Fig. 5.4: Test vs model predicted results for strain at peak compressive strength

Lastly, the regression model for material cost demonstrated perfect alignment with the actual calculated costs for all mixes, as shown in Fig. 5.5. This exact match is attributed to the direct dependence of cost on known quantities of ingredients and unit prices, making it a deterministic outcome.

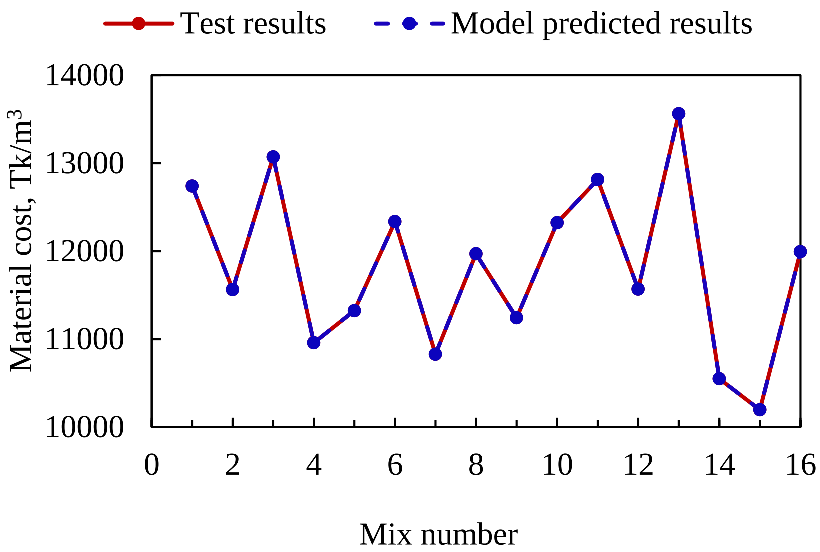

Fig. 5.5: Test vs model predicted results for material cost.

The above evaluation indicates that the developed regression models are capable of predicting the response variables, exhibiting minimal deviation from the experimental data. Therefore, these regression models can be used to determine response variables, while keeping key mixing parameters within specified limits.

5.3.3 Analysis of Variance (ANOVA) of Response Models

An ANOVA was performed at a 95% confidence level to assess the statistical significance of the mixing parameters. Within this framework, parameters demonstrating P-values below the 0.05 threshold were considered statistically important effects on the response variables. This threshold indicates a high level of confidence in the influence of those parameters on the model outcomes. The results derived from ANOVA, which assess the statistical relevance of each factor within the developed models, are presented in Table 5.3. The analysis revealed that the P-values associated with compressive strength, splitting tensile strength, UPV, and material cost were all below the 0.05 threshold, which confirms the statistical significance and adequacy of these models in accordance with the standard P-value hypothesis testing criteria (Rahman and Kabir, 2025).

Table 5.3: ANOVA results for response models

Statistical Parameter	Compressive Strength	Strain at Peak Stress	Splitting Tensile Strength	UPV	Material Cost
Source	Model	Model	Model	Model	Model
DF	6	11	11	9	11
SS_{Adj}	1365.40	0	17.87	274,044	13.68x10^{6}
MS_{Adj}	227.57	0	1.62	30,449	12.4x10^{5}
F-value	21.05	5.21	38.32	31.49	92.7x10^{6}
P-value	0.001	0.062	0.002	0.000	0.000
Significant	Yes	No	Yes	Yes	Yes

Legend: DF=Degrees of freedom, SS_{Adj}=Adjusted Sum of Squares, MS_{Adj}=Adjusted Mean Square, F-value=Randomization test, P-value=Probability value

However, the P-value for the peak strain response model was found to be 0.062, which is greater than the significance level of 0.05. This observation suggests a lack of statistical significance in the model and may not reliably predict the corresponding response variable.

5.3.4 Statistical Significance of Mixing Variables and Their Interactions

The statistical evaluation of individual and interactive effects of each mixing variable is presented in Table 5.4. This statistical analysis help to understand how each factor, alone and with others, affects the performance of JFRCCs.

Table 5.4: Statistical significance and interaction effects of mixing parameters on composite properties

Term		Constant	W/B	FA/C	S/B	Jute	W/B ×Jute	FA/C× S/B	W/B× S/B	FA/C× Jute	S/B× Jute	W/B× FA/C	W/B×S/B ×Jute	FA/C×S/B ×Jute	W/B×FA/C ×S/B
Compressive Strength	T-value	44.30	-1.38	-9.36	-0.38	-4.88	-2.25	-2.81	—	—	—	—	—	—	—
	P-value	0.00	0.20	0.00	0.72	0.00	0.05	0.02	—	—	—	—	—	—	—
Strain at peak compressive strength	T-value	48.31	-1.79	-3.05	2.56	1.32	0.28	-1.99	-0.49	-2.28	1.20	—	-3.97	3.14	—
	P-value	0.00	0.15	0.04	0.06	0.26	0.80	0.12	0.65	0.09	0.30	—	0.02	0.04	—
Splitting tensile strength	T-value	80.24	0.75	-10.98	4.18	11.81	0.83	-5.24	-2.99	-8.41	4.40	2.41	3.23	—	—
	P-value	0.00	0.49	0.00	0.01	0.00	0.45	0.01	0.04	0.00	0.01	0.07	0.03	—	—
UPV	T-value	485.19	-4.53	-13.10	0.82	-8.48	-2.19	-1.68	-0.48	—	—	0.02	—	—	3.29
	P-value	0.00	0.00	0.00	0.44	0.00	0.07	0.14	0.65	—	—	0.98	—	—	0.02
Material cost	T-value	407918	-7227	-25284	-12491	13034	-103	1256	576	27	198	508	—	—	-50
	P-value	0.00	0.00	0.00	0.00	0.00	0.00	0.00	0.00	0.00	0.00	0.00	—	—	0.00

In the case of compressive strength, the fly ash-to-cement ratio (FA/C), jute fibre content, the interaction between water-to-binder ratio (W/B) and jute, as well as the interaction between FA/C and sand-to-binder ratio (S/B), were identified as significant contributors based on their respective P-values; conversely, the individual effects of W/B and S/B were not statistically significant, indicating a limited direct influence on the compressive strength of the developed composites (Rahman and Kabir, 2025).

For strain at peak compressive strength, only the FA/C ratio showed a significant influence. All other parameters and their interactions were statistically insignificant. This suggests that fly ash content plays a critical role in affecting the ductility of the composites, while other parameters have limited standalone effects. As previously discussed in relation to model adequacy, the regression model for strain at peak compressive stress was determined to be statistically insignificant based on hypothesis testing outcomes. Although the model exhibited an R^2 value of 93.47%, the adjusted R^2 was considerably lower at 75.53%, indicating that the model does not sufficiently capture the variability of the dependent variable with respect to the selected independent variables.

Afterwards, the analysis of splitting tensile strength revealed that, while the water-to-binder ratio (W/B) did not show statistical significance, the effects of the fly ash-to-cement ratio (FA/C), sand-to-binder ratio (S/B), and jute fibre content were significant according to their corresponding P-values (Rahman and Kabir, 2025). Additionally, it was found that all interaction terms, except for the interaction among W/B and jute, had a statistically substantial impact on splitting tensile strength. For the ultrasonic pulse velocity (UPV), statistical analysis confirmed that W/B, FA/C, and jute, along with the three-way interaction among W/B, FA/C, and S/B, had significant effects, all with P-values below the 0.05 threshold (Rahman and Kabir, 2025). However, the individual effect of S/B and the remaining interaction terms were not found to be significant for UPV.

Lastly, the evaluation of individual and interaction effects on the material cost response, as summarized in Table 5.4, demonstrated that all principal mixing parameters significantly contributed to the regression model, thereby affirming its adequacy in representing material cost within the scope of the experimental design (Rahman and Kabir, 2025).

5.3.5 Evaluation of Critical Mixing Parameters Influencing JFRCCs

The influence of crucial mixing parameters on the observed responses is graphically represented in Figs. 5.6 through 5.10. These main influence plots demonstrate the relative significance of individual parameter, where steepness of the lines reflects the magnitude of their impact.

The compressive strength was significantly influenced by both the FA/C ratio and jute content, showing a decreasing trend as the values of these parameters increased, as shown in Fig. 5.6.

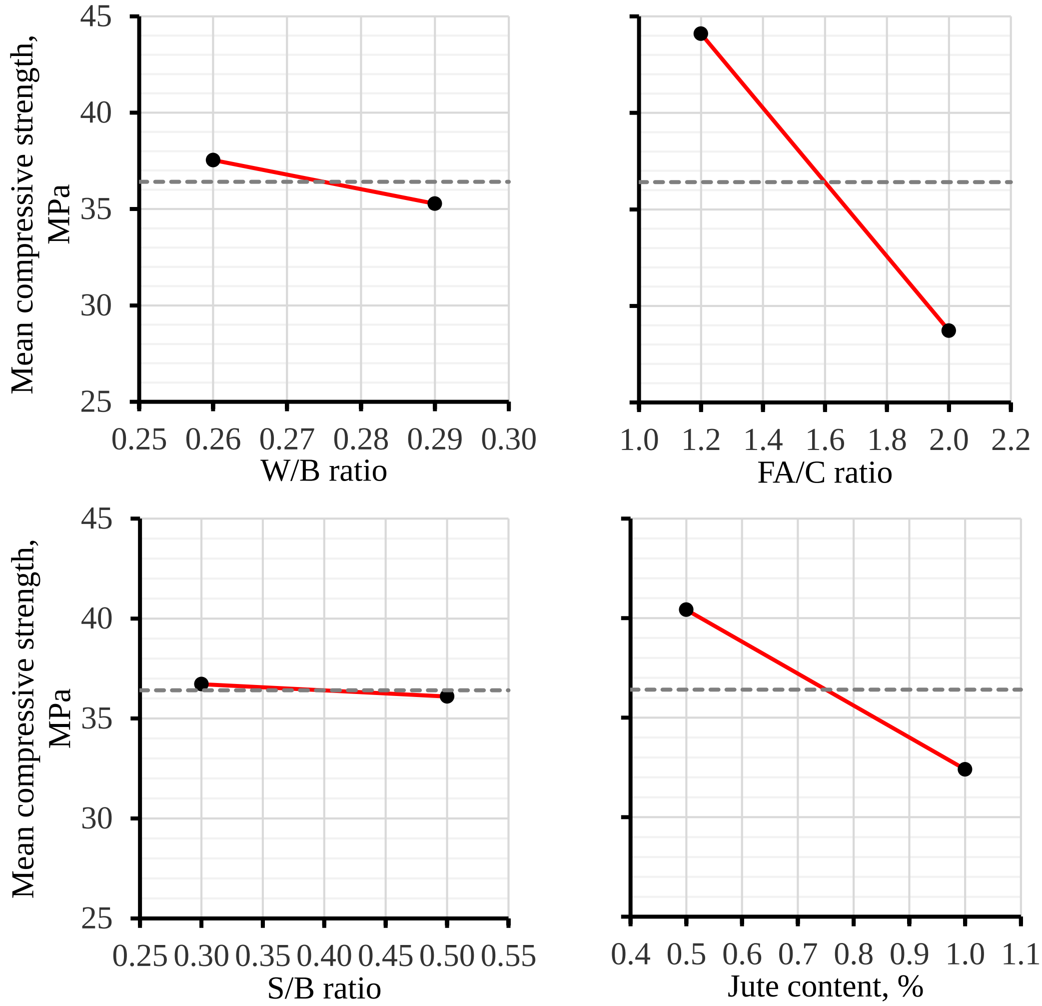

Fig. 5.6: Main effect diagram highlighting influential mixing parameters for compressive strength

It was also reported that the compressive strength of composites decreases with increasing fly ash content (Tian et al., 2015). When comparing with bagasse fibre (3% bagasse fibre) reinforced composites for the same volume of fly ash (FA/C-2.0), the compressive strength of the jute fibre composites shows almost similar results for 0.5% jute fibre (Tian et al., 2015). In another study jute fibre composites exhibited superior compressive strength results than coconut, sugarcane, basalt and sisal fibre when 2.5 % fibre content was applied (Asim et al., 2020).

Among the variables affecting strain at peak compressive stress, the FA/C ratio emerged as the most influential factor, followed by the S/B ratio. As shown in Fig. 5.7, a rise in the FA/C ratio led to a reduction in strain at peak compressive stress, whereas a higher S/B ratio contributed to an increase in this response.

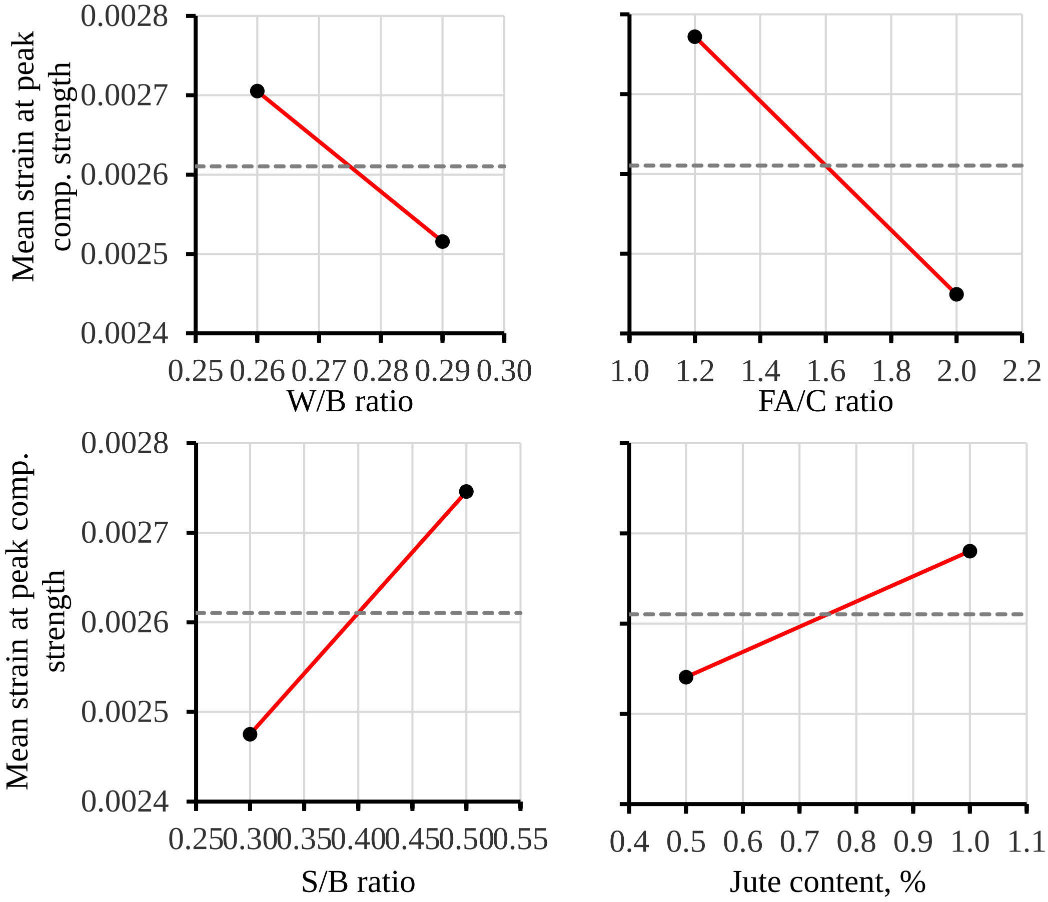

Fig. 5.7: Key effect plots for strain at peak compressive strength.

Both the FA/C ratio and the jute fibre content had a significant impact on the splitting tensile strength, as demonstrated in Fig. 5.8. Explicitly, a lower FA/C ratio led to an improvement in tensile strength, likely due to the higher cement content contributing to enhanced matrix bonding. Additionally, an increase in jute fibre content led to a further enhancement in tensile strength, a phenomenon attributable to the fibres capacity to bridge microcracks and more effectively dissipate stress throughout the composite matrix.

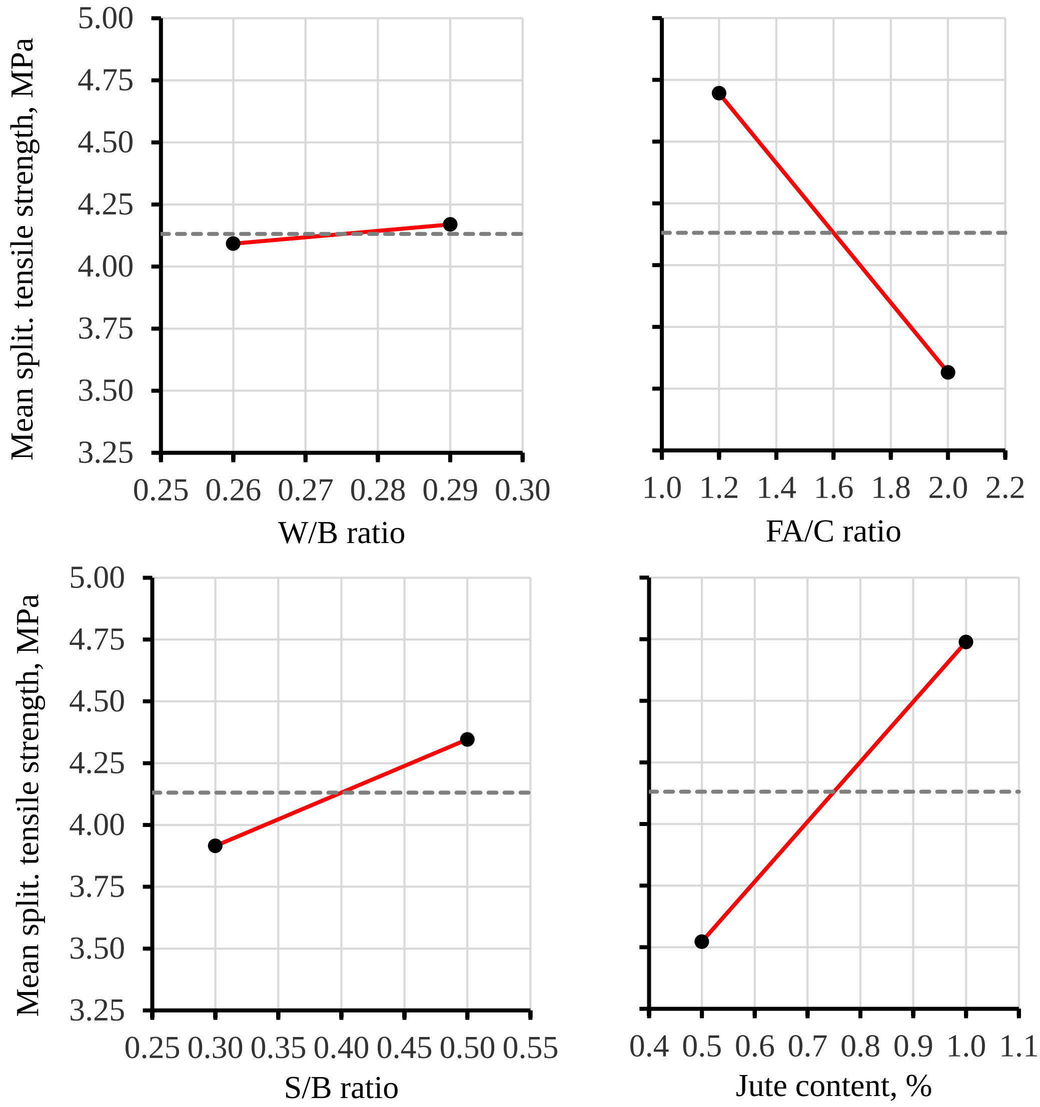

Fig. 5.8: Key effect plots for splitting tensile strength

In the case of UPV, the results also showed greater dependency on the FA/C ratio and jute content, which are presented in Fig. 5.9. A decrease in the FA/C ratio led to higher UPV values, indicating a denser and more uniform matrix structure. However, with increased jute fibre content, a decline in UPV was observed. This reduction may be due to the introduction of voids or imperfect fibre dispersion, which disrupt the continuity of the matrix and hinder the propagation of ultrasonic waves. Additionally, the water-to-binder (W/B) ratio played a notable role, with higher W/B ratios generally reducing UPV, likely due to increased porosity in the matrix.

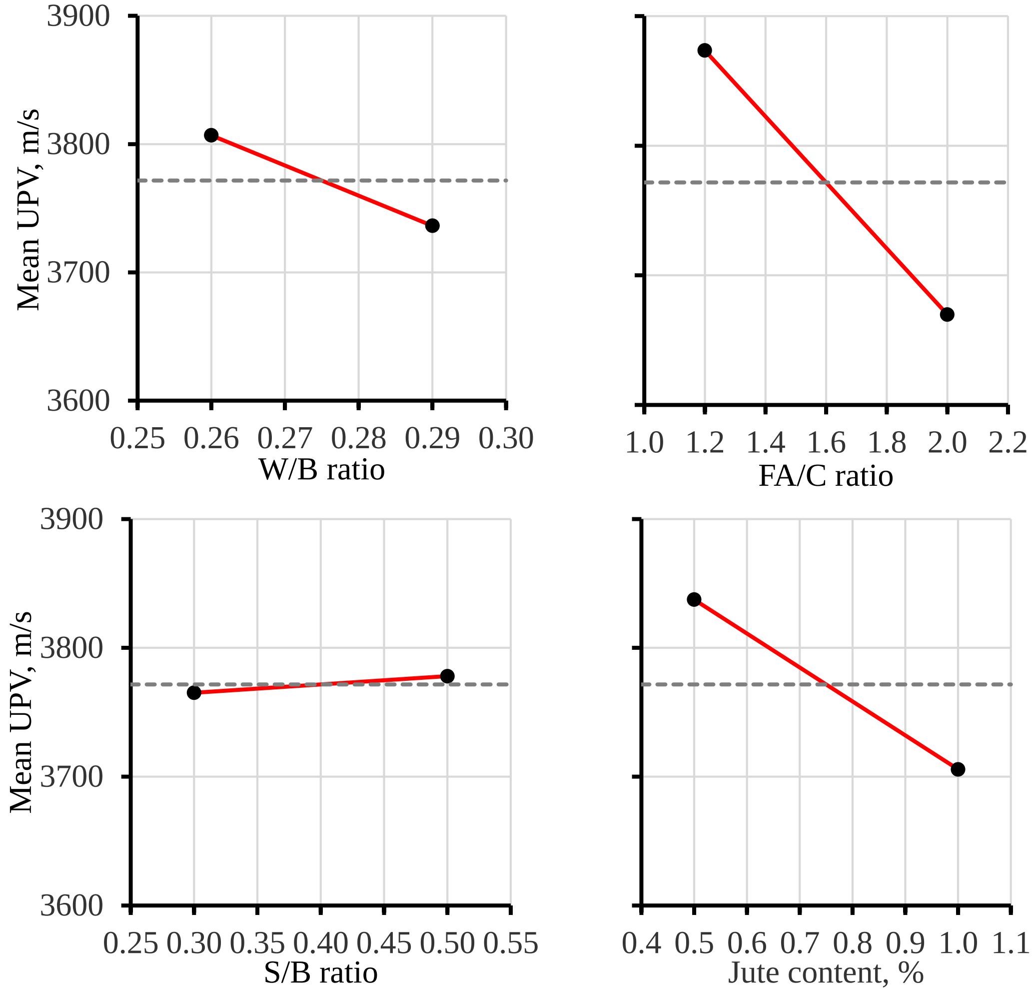

Fig. 5.9: Key effect plots for UPV.

Lastly, key effect plots related to material cost revealed that the FA/C ratio was a major determining factor, as shown in Fig. 5.10. As the FA/C ratio decreased, the proportion of cement increased, leading to higher material costs due to the relatively higher price of cement compared to fly ash. Conversely, increasing the sand-to-binder (S/B) ratio helped to reduce overall cost by minimizing the quantities of both cement and fly ash in the mix design.

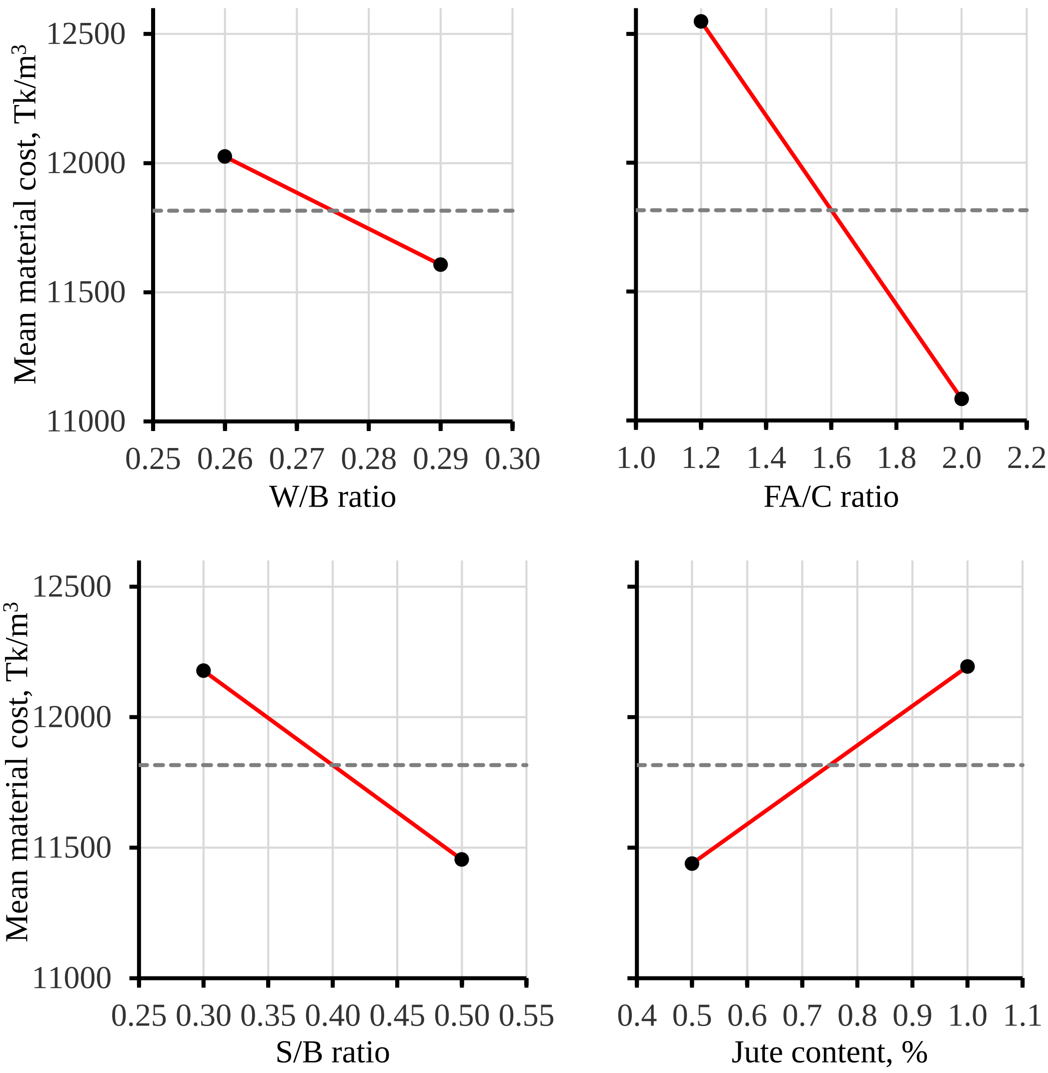

Fig. 5.10: Key effect plots for material cost.

Further insights into the complex relationships between the key mixing parameters and their effects on the performance of cementitious composites are visually represented through the surface and contour plots in Figs. 5.11, 5.12, and 5.13. These plots provide both three-dimensional (3-D) and two-dimensional (2-D) representations, facilitating a more intuitive understanding of how two variables simultaneously influence the response parameters.

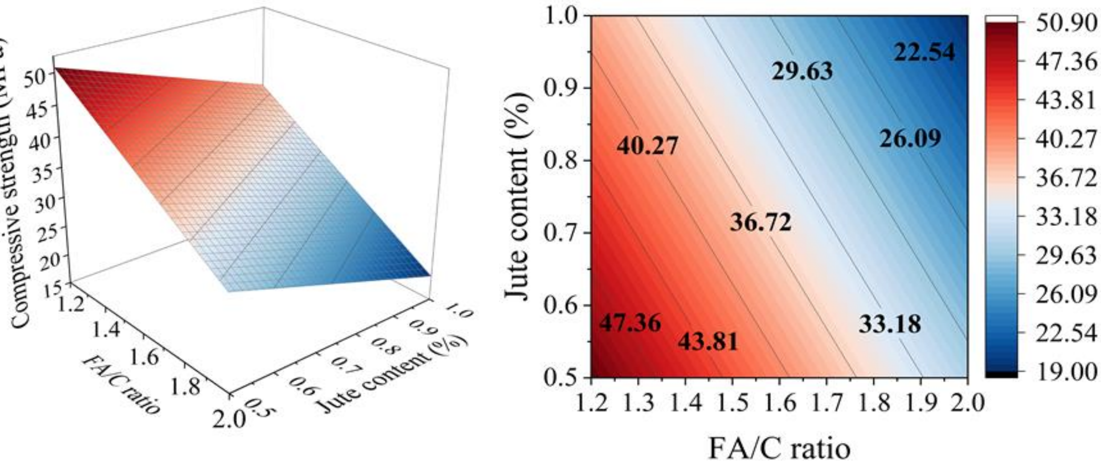

(a) Compressive strength depending on FA/C and jute content

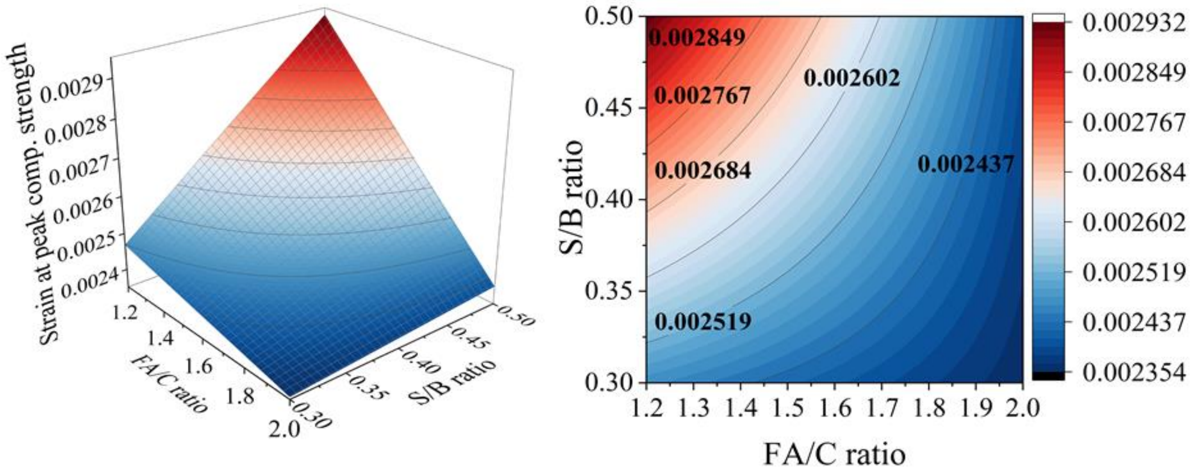

(b) Strain at peak compressive strength depending on FA/C and S/B

Fig. 5.11: Contour and surface plots showing effects of mix parameters on (a) compressive strength, and (b) strain at peak compressive strength.

From these graphical analyses shown in Fig. 5.11(a), it becomes evident that compressive strength shows a declining trend with an increase in both the FA/C ratio and jute content. This finding supports the statistical results, suggesting that excessive substitution of cement with fly ash slows the rate of pozzolanic reactions, thereby limiting strength development. Similarly, higher jute content beyond the optimum threshold may hinder uniform matrix formation due to fibre agglomeration, leading to reduced strength.

For strain at peak compressive stress, the plots presented in Fig. 5.11(b) reveal a positive correlation with the sand-to-binder (S/B) ratio, implying enhanced ductility at higher sand contents. Conversely, strain decreases as the FA/C ratio increases, likely due to the stiffer and less reactive matrix formed with excessive fly ash. Therefore, the combination of low FA/C and high S/B ratios yields more favourable strain values, promoting ductile behaviour.

In continuation of the previous findings, the splitting tensile strength results, shown in Fig. 5.12(a), exhibit a contrasting trend. It increases with higher jute content, attributed to the fibre-bridging effect that resists crack propagation under tensile stress. However, similar to compressive strength, tensile strength is negatively affected by higher FA/C ratios, reaffirming the detrimental impact of excessive fly ash content on early-age strength development.

The ultrasonic pulse velocity exhibited a similar trend to that of compressive strength, decreases with increasing FA/C and jute content, which are demonstrated in Fig. 5.12(b). This indicates a potential reduction in internal compactness and homogeneity, possibly due to poor fibre dispersion and delayed hydration caused by excess fly ash.

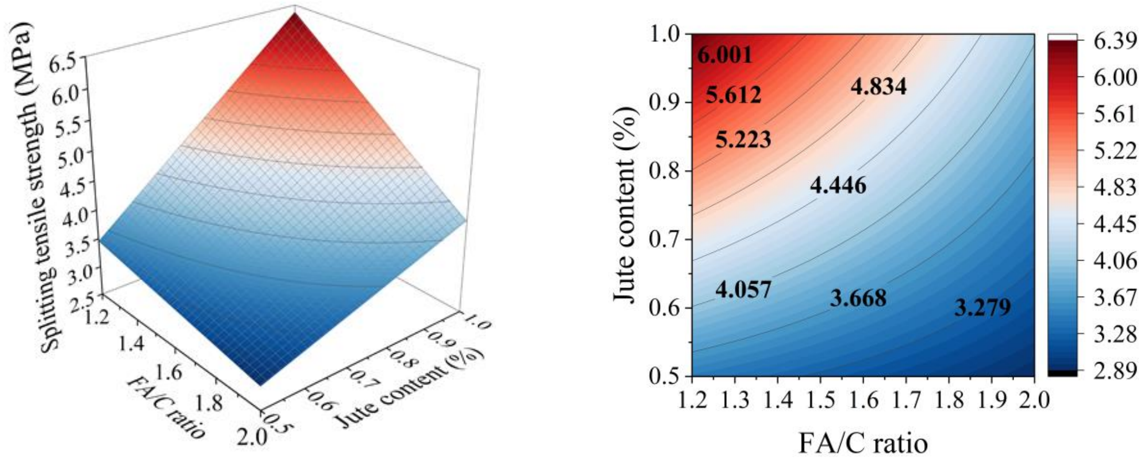

(a) Splitting tensile strength depending on FA/C and jute content

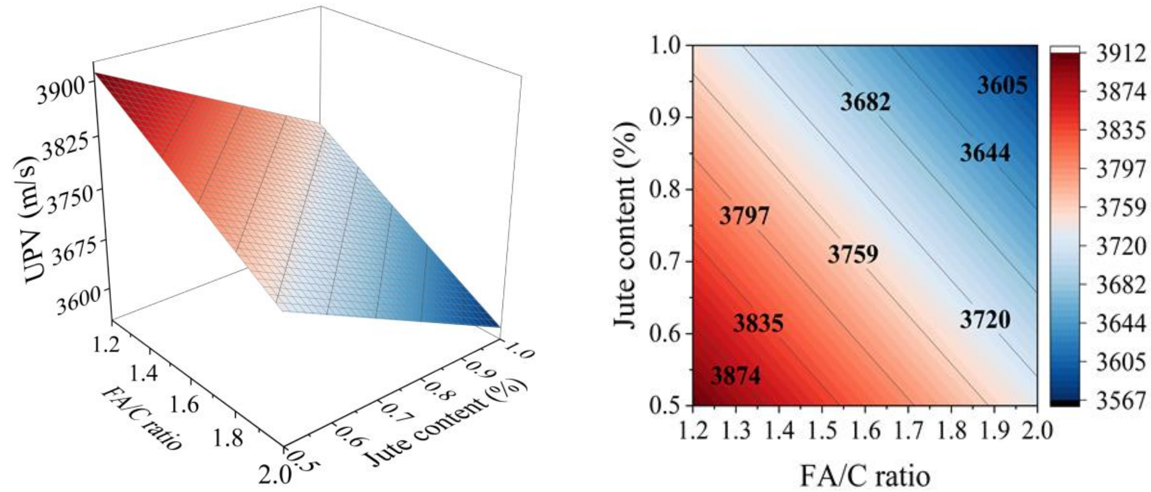

(b) UPV depending on FA/C and jute content

Fig. 5.12: Surface and contour plots- influence of FA/C and jute content on (a) splitting tensile strength, and (b) UPV

In terms of material cost, a noticeable reduction was observed in Fig. 5.13 with an increase in the FA/C ratio, due to the lower unit price of fly ash in comparison to cement. However, incorporating higher amounts of jute fibres raises the overall cost due to the additional processing and material expenses associated with natural fibre integration. Furthermore, a higher S/B ratio also contributes to cost savings by reducing the total amount of binder material (cement and fly ash), thereby making the mix more economical.

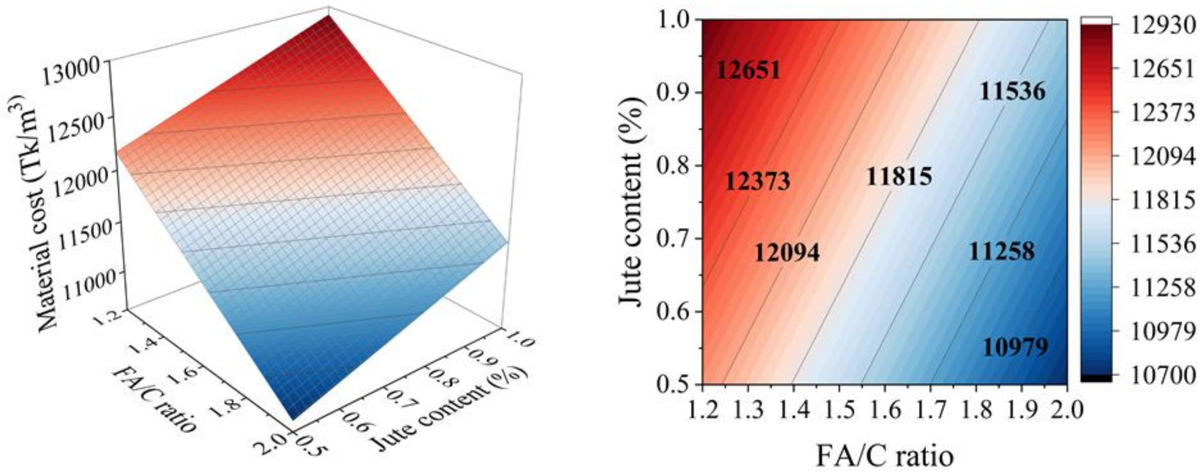

Fig. 5.13: Surface and contour plots depicting material cost variation with FA/C and jute content

In conclusion, these surface and contour plots reinforce the importance of selecting optimal ranges for mixing parameters to achieve a balance between mechanical performance and cost-effectiveness. The ability to visualize interactions between variables not only validates statistical trends but also aids in practical mix design decisions for sustainable and high-performance JFRCCs.

5.3.6 Optimization of Developed JFRCCs Using Multi-objective Desirability Function

The desirability function is a widely used statistical tool to optimize multiple response variables simultaneously (Khan et al., 2016; Montgomery, 2013; Asadzadeh & Khoshbayan, 2018; Sangwann & Sihag, 2019; Sharma et al., 2021). It transforms each response variable into a scale-free value, called desirability, which ranges from 0 to 1.

A desirability value of 0 indicates a completely undesirable response, while a value of 1 represents the ideal or most desirable response (Montgomery, 2013). In this study, multi-objective optimization was conducted using Minitab software, where the overall desirability (*D*) was computed as the geometric mean of the individual desirability values. This composite measure provides an overall assessment of how effectively the selected responses align with the predefined target criteria. The optimization process started by converting each response variable, denoted as y, into an individual desirability function d_i, where d_i ranges between 0 and 1; if an individual response meets the target value, the desirability is $d_i = 1$; if the response falls outside the acceptable range, the desirability is $d_i = 0$ (Montgomery, 2013). The design variables are then selected to maximize the overall desirability *D*, defined as:

$$D = (d_1,\ d_2,\ d_3\ \dots\dots\ d_m\,)^{\,1/m} \qquad (5.1)$$

Where, m denotes the number of responses. When the target T for response y is a maximum value, the desirability function is expressed as:

$$d = \begin{cases} 0 & y < L \\ \left(\frac{y-L}{T-L}\right)^r & L \leq y \leq T \\ 1 & y > T \end{cases} \qquad (5.2)$$

Where, L is lower limit of response; r represents a weightage factor determined by the targeted response region, and the individual desirability function is influenced by this factor. When the target for the response (y) is a minimum value, the desirability function is expressed as:

$$d = \begin{cases} 1 & y < T \\ \left(\frac{U-y}{U-T}\right)^{r} & T \leq y \leq U \\ 0 & y > U \end{cases} \tag{5.3}$$

Where, U is upper limit of response. When the target response is situated between a lower and an upper bound, with the objective of achieving maximal closeness to the target, the desirability function is mathematically defined as:

$$d = \begin{cases} 0 & y < L \\ \left(\frac{y-L}{T-L}\right)^{r1} & L \leq y \leq T \\ \left(\frac{U-y}{U-T}\right)^{r2} & T \leq y \leq U \\ 0 & y > U \end{cases} \tag{5.4}$$

A schematic representation of the optimization process employing the multi-objective desirability function approach is shown in Fig. 5.14. This optimization framework was developed to identify the most suitable mix design for the proposed JFRCCs by simultaneously considering multiple performance criteria. The optimization process incorporated five key performance criteria: manufacturing cost, compressive strength, splitting tensile strength, strain at peak compressive stress, and ultrasonic pulse velocity (UPV). Specific optimization targets were established for each performance parameter, with manufacturing cost targeted for minimization, compressive strength and splitting tensile strength set to threshold values of 35 MPa and 4.0 MPa respectively, while strain capacity and UPV were designated for maximization.

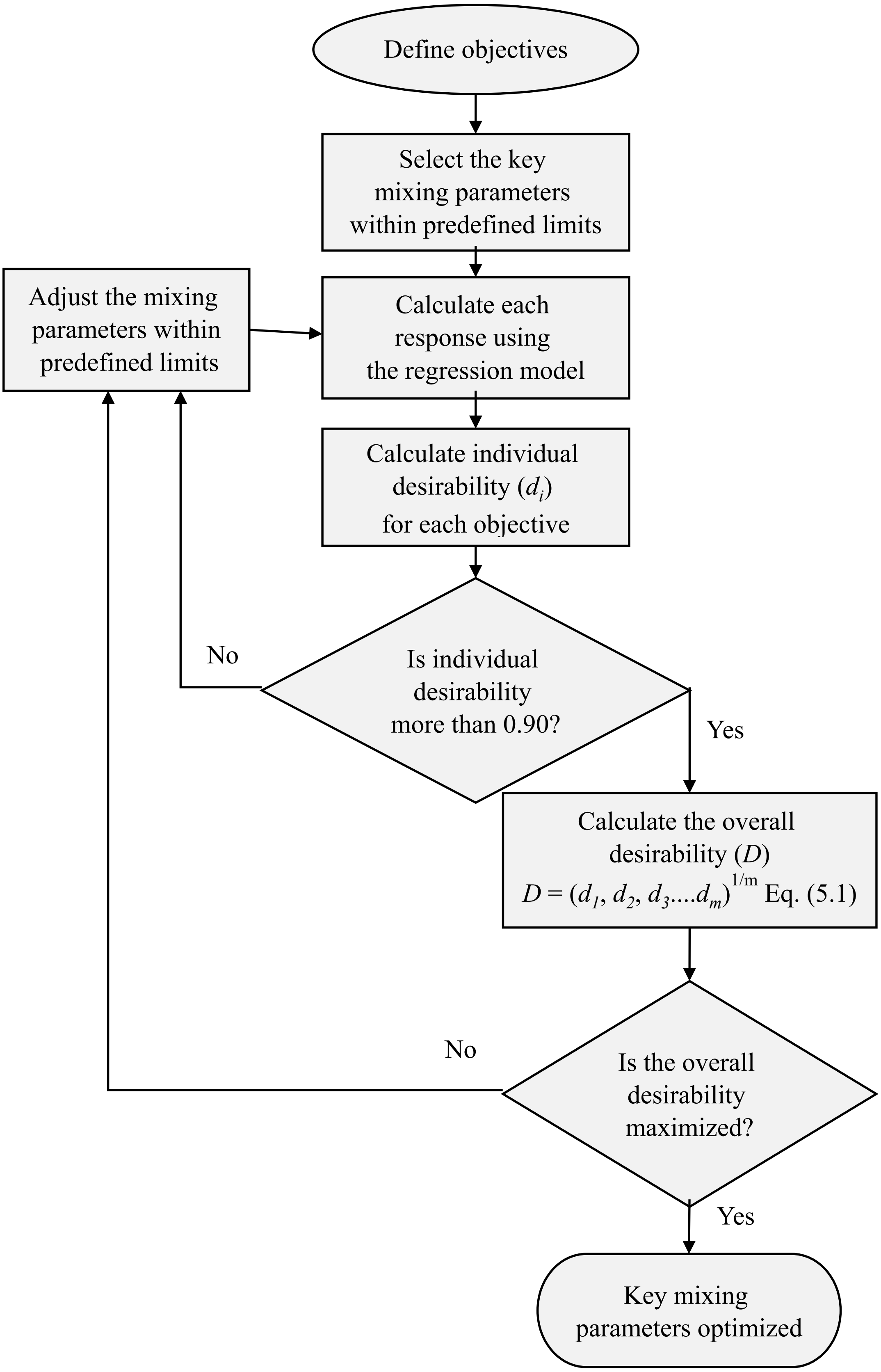

Fig. 5.14: Workflow for multi-objective optimization using desirability functions

The research identified multiple solutions for optimization, with desirability scores ranging from 0.953 to 0.961, are shown in Table 5.5. These solutions meet above-mentioned targets for the responses. Furthermore, it is noteworthy that each of the solutions closely approximated the target responses, and the levels of key mixing parameters varied within the predefined range, depending on their individual effects. This indicates a well-optimized process, demonstrating stable performance despite minor adjustments.

Table 5.5: Desirability scores for various mix design scenarios

Solutions	W/B	FA/C	S/B	Jute %	Cost, Tk/m^3	UPV, m/s	$f_{st}{}^{a}$, MPa	ϵ (peak)^{b}	$f'_c{}^{c}$, MPa	Composite Desirability, D
1	0.26	1.68	0.50	0.63	11320	3819	4.01	0.0026	35.04	0.961
2	0.26	1.69	0.50	0.64	11321	3813	4.00	0.0026	34.81	0.960
3	0.26	1.66	0.50	0.61	11323	3828	4.00	0.0026	35.52	0.960
4	0.26	1.64	0.50	0.64	11400	3827	4.10	0.0027	35.76	0.957
5	0.26	1.64	0.50	0.64	11400	3827	4.10	0.0027	35.76	0.957
6	0.26	1.64	0.50	0.59	11336	3841	4.00	0.0026	36.28	0.957
7	0.26	1.67	0.50	0.70	11454	3805	4.20	0.0027	34.66	0.956
8	0.26	1.62	0.50	0.58	11347	3850	4.00	0.0026	36.82	0.955
9	0.26	1.62	0.50	0.58	11349	3851	4.00	0.0026	36.90	0.955
10	0.29	1.91	0.30	0.50	10999	3752	4.00	0.0024	34.61	0.953

[a]Splitting tensile strength, [b]Strain at peak compressive strength, [c]Compressive strength

Nevertheless, the first solution was ultimately selected as the optimal mix, based on its ability to meet the targeted performance responses. Fig. 5.15 demonstrates the optimal levels of the primary mixing parameters, highlighted in red, along with their influence on the various response variables of the developed composites. For each key mixing parameter, the figure presents the low, current, and high values, enabling a comprehensive understanding of their individual and combined effects on the mechanical and economic performance of the cementitious composites.

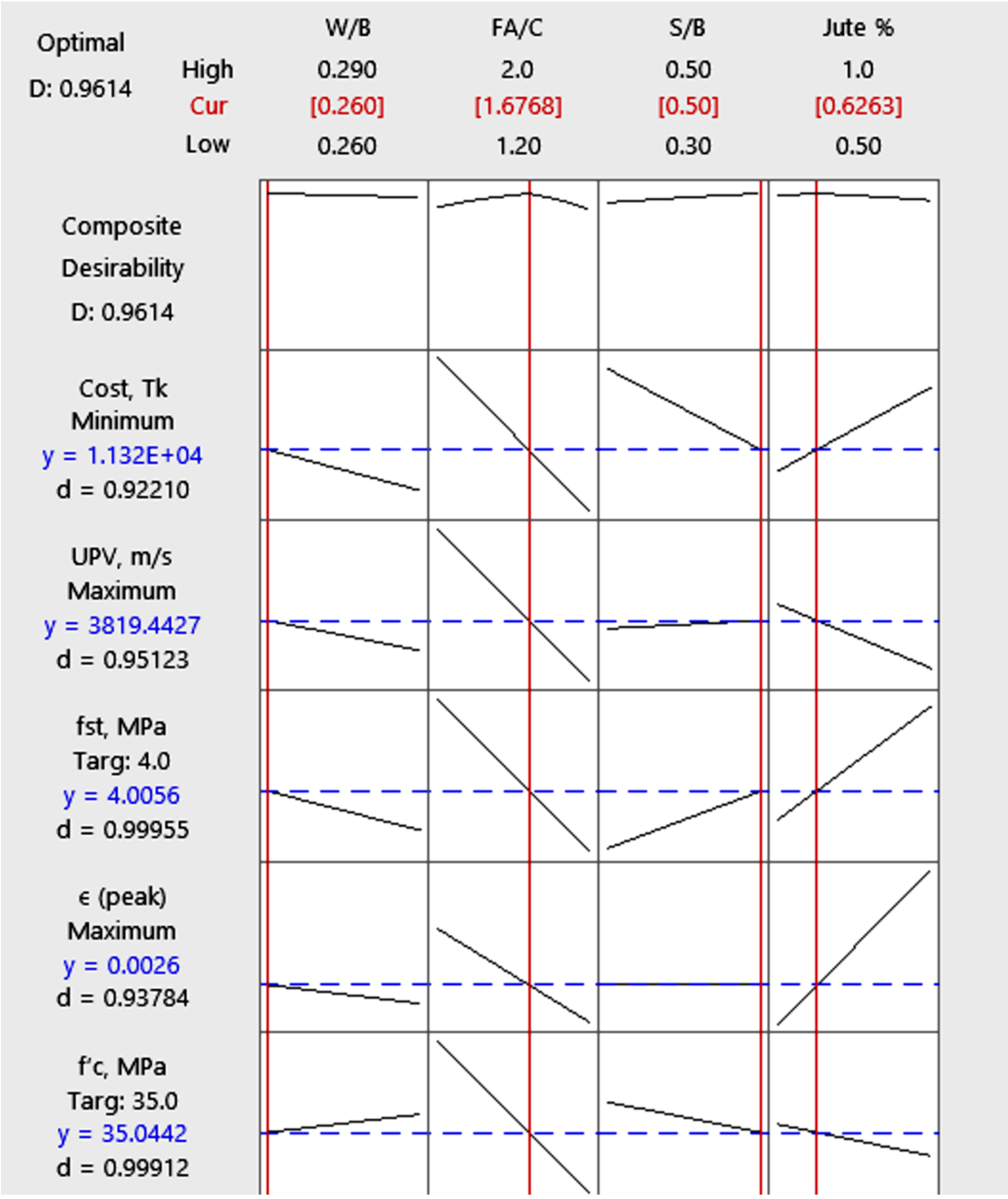

Legend:

f_{st} = Splitting tensile strength, ϵ (peak) = Strain at peak compressive strength, f'_c = Compressive strength

Fig. 5.15: Desirability analysis for response optimization

In terms of cost-effectiveness, the optimized mix design demonstrated exceptional cost-efficiency with a material cost of 11,320 Tk/m^3, achieving a desirability score of 0.9221. For Ultrasonic Pulse Velocity (UPV), the optimal value reached 3819.44 m/s, associated with a desirability of 0.9512, which indicates a high level of internal uniformity and structural integrity. The splitting tensile strength (f_{st}) reached an optimal level of 4.0056 MPa, achieving a desirability score of 0.9995, demonstrating the mix's considerable resistance to tensile stresses. The strain at peak compressive stress (ε) was found to be optimal at 0.0026, with a desirability of 0.9378, reflecting adequate ductility and deformation capacity under compressive loading. Furthermore, the compressive strength (f'_c) was optimized at 35.0442 MPa, with a desirability of 0.99912, demonstrating excellent load-bearing capability. Collectively, the composite's exceptional performance across all measured parameters was confirmed by the high overall desirability index (D = 0.9614), suggesting that the mix design is well-optimized and effectively satisfies the targeted performance criteria across mechanical and economic considerations.

The analysis of the influence of individual mixing parameters provided several notable observations. The W/B ratio exhibited a marginal increase in overall desirability when adjusted from 0.26 to 0.29, suggesting that a slightly higher W/B ratio may enhance the overall performance of the mix. The FA/C ratio demonstrated a more noticeable effect, with the optimum desirability observed at approximately 1.68, indicating its critical role in achieving the target mechanical properties. Similarly, the S/B ratio achieved peak desirability at a value of 0.50, underscoring its substantial influence on the composite's performance. Furthermore, the optimal jute fibre content was identified as 0.63%, emphasizing its contribution to the composite's tensile strength and durability, and highlighting its importance in achieving the desired balance of properties within the mix.

In conclusion, the optimized combination of the selected parameters leads to a balanced mix design capable of achieving the desired performance criteria effectively. This comprehensive evaluation highlights the significance of adjustments in individual mixing ratios to enhance both the mechanical properties and cost-effectiveness of the proposed JFRCCs. The findings confirm that careful proportioning not only ensures structural integrity and economic feasibility but also supports the suitability of the developed composites for a wide range of construction applications. Following the identification of the optimized mix ratio (W/B-0.26, FA/C-1.68, S/B-0.5, and jute fibre content of 0.63%), the research was advanced to Phase III investigation. The subsequent Phase III investigation focused on the preparation of JFRCCs utilizing this established optimal mix ratio and rigorously evaluating their performance under a variety of environmental and thermal conditions.

5.4 Phase III Experimental Procedure

In the Phase III experimental investigation, JFRCCs were prepared using the optimized mix proportions established in the second phase. The optimized mixture proportions, aimed at achieving a target compressive strength of 35 MPa and other performance indicators, were determined to be a water-to-binder ratio of 0.26, a fly ash-to-cement ratio of 1.68, a sand-to-binder ratio of 0.5, and a jute fibre content of 0.63% by weight. The primary objective of this phase was to systematically evaluate the mechanical performance of the developed JFRCCs under diverse testing conditions, including both ambient and elevated temperatures.

Three different curing methods were implemented at ambient temperature to assess their influence on the mechanical properties and durability of JFRCCs. These methods included natural curing, wet curing, and water curing. The objective of employing these distinct curing techniques was to investigate their impact on the hydration process and overall performance of JFRCCs, providing insights into the most effective curing approach for enhancing material properties. Additionally, thermal exposure evaluations at varying temperatures aimed to determine the composites thermal stability and residual compressive strength, providing insights into materials potential for fire-resistant construction applications. However, the following subsection describes the mix design procedure used to prepare JFRCCs for the Phase III investigation.

5.4.1 Mix Design- Phase III Experiment

Mix design of the Phase III experiments was determined using the optimized mix ratio from statistical analysis of Phase II investigation. The material quantities for 1.0 m³ of each cementitious composite mix are detailed in Table 5.6.

Table 5.6: Mix design of cementitious composites for phase III experiment

Mix No.	Water to Binder ratio	Fly Ash to Cement ratio	Sand to Binder ratio	Jute fibre content (% of total volume)	Water, Kg/m^3	Fly Ash, Kg/m^3	Sand, Kg/m^3	Jute fibre, Kg/m^3	Cement, Kg/m^3
1	0.26	1.68	0.5	0.63	292.1	704.3	561.8	12.6	419.2

In alignment with the phase II investigation, 10 mm jute fibres were utilized in the preparation of JFRCCs. Finally, prepared specimens were tested for compressive strength and flexural strength at 28 days of casting. The detailed experimental programme can be found in the following sections.

5.4.2 Phase III Experimental Programme

The experimental program conducted during the phase III investigation are outlined in Table 5.7. For cylindrical specimens, investigations included compressive strength under varying temperature and curing conditions, while beam specimens were tested for flexural strength across all three curing conditions. The detailed procedures for the various curing methods are described in Chapter 3. Additionally, the thermal performance of optimized JFRCCs was tested by exposing cylindrical samples to 200 °C, 400 °C, 600 °C, and 800 °C in a controlled furnace environment for two hours. Following thermal exposure, both compressive strength and weight loss measurements were determined.

Table 5.7: Phase III experimental programme (based on optimum mix ratio)

Testing Conditions		Cylinder (100 mm x 200 mm)	Beam (300 mm x 75 mm x 75 mm)	Test
Ambient temperature	Natural Curing	3	3	**Cylinder-** Compressive strength **Beam-** Flexural Behaviour
	Wet Curing	3	3	
	Water Curing	12	12	
Elevated temperature	200 °C	3	-	**Cylinder-** Compressive strength, loss of weight
	400 °C	3	-	
	600 °C	3	-	
	800 °C	3	-	
Total Specimens =		30	18	

Overall, this phase III experiment was performed to understand the mechanical performance and durability of JFRCCs under diverse environmental and thermal conditions, thereby providing insights into their suitability for practical applications. The detailed procedures for achieving and maintaining the temperature conditions are provided in a subsequent section.

5.4.3 Elevated Temperature Conditioning of Specimens

In the elevated temperature testing phase, specimens designated for thermal exposure were first weighed and then placed inside as electric furnace, as depicted in Fig. 5.16. Only cylinder specimens were tested in elevated temperature testing condition where target temperatures were set at 200 °C, 400 °C, 600 °C, and 800 °C. The heating procedure involved a controlled rate of 2°C per minute until reaching the specified peak temperature, which was then maintained for an additional two hours to ensure uniform thermal exposure. These parameters align with established methodologies for isothermal heating in existing literature (Rawat et al., 2021; Rawat et al., 2024).

(a) (b)

Fig. 5.16: Specimen kept inside an electric furnace

After the heating phase, specimens were allowed to cool naturally within the furnace for 24 hours. Subsequently, they were re-weighed to assess mass loss and then subjected to mechanical testing under compression to evaluate their residual performance. In the following sections, effects of curing conditions and elevated temperatures on the performance of JFRCCs are discussed.

5.5 Effect of Different Curing Conditions

5.5.1 Compressive Behaviour

The compressive strength of JFRCCs under three different curing conditions, including water curing, natural curing, and wet curing are presented in Fig. 5.17. The JFRCCs subjected to water curing exhibited a compressive strength of 40.98 MPa. This indicates that continuous submersion in water provided optimal conditions for hydration and strength development in the composite.

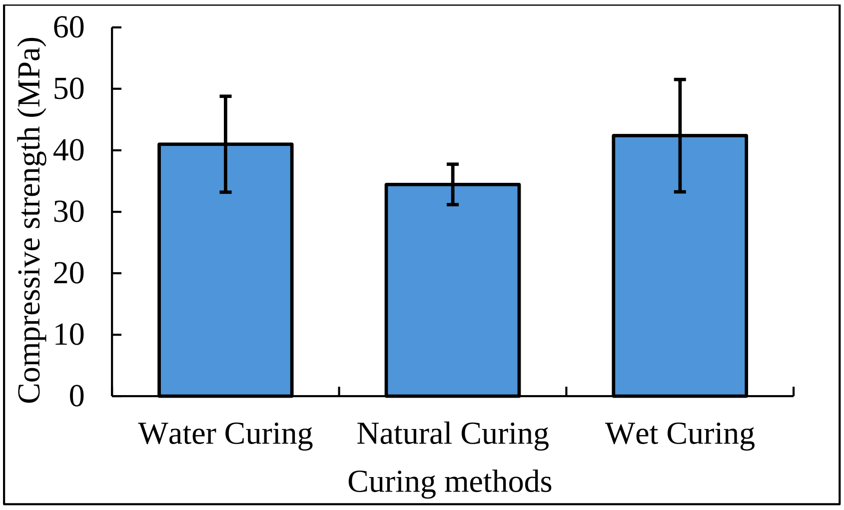

Fig. 5.17: Compressive strength of JFRCCs under different curing conditions.

Conversely, the JFRCCs subjected to natural curing demonstrated a lower compressive strength of 34.33 MPa than water curing condition, likely due to insufficient moisture retention, which may have led to incomplete hydration of cementitious materials. But, the JFRCCs subjected to wet curing showed a compressive strength of 42.38 MPa. This value is comparable to that of water curing, indicating that maintaining a consistently moist environment, even without full submersion, can achieve similar strength development. Comparing with other studies, almost the same compressive strength was observed for wet curing and water curing conditions at 14, 28, and 60 days of the curing period (Ibrahim et al., 2013). However, in another study, the application of wet curing showed slightly better compressive strength than water curing conditions for both plain and blended cement concretes (Al-Gahtani, 2010). Also, Zhang et al. (2024) reported that compressive strength exhibited superior results up to 28 days of wet curing compared to water curing, though this trend reversed at 90 days.

Above results indicate that both water curing and wet curing are effective methods for achieving high compressive strength in JFRCCs with high fly ash content and low water-to-binder ratio. Natural curing, on the other hand, resulted in reduction in strength, highlighting the importance of adequate moisture availability for proper hydration and strength development in these composites. This is particularly relevant given the high fly ash content, which requires prolonged moist curing for optimal pozzolanic reactions.

Additionally, the compressive strength of cementitious composites was determined under various conditions such as treated jute fibre, untreated jute fibre, without jute fibre, and treated jute fibre without admixture, are shown in Fig. 5.18. Here, the optimized mix ratios were used for this investigation unless otherwise mentioned above and specimens were cured under water curing condition.

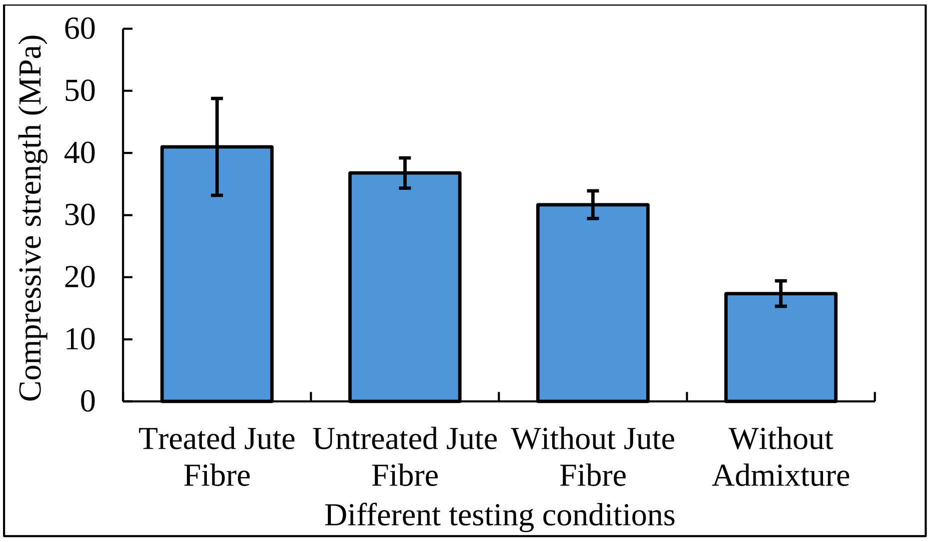

Fig. 5.18: Compressive strength of cementitious composites under different conditions: treated jute fibre, untreated jute fibre, without jute fibre, and treated jute fibre without admixture.

Notably, the composites with treated jute fibres exhibited the highest compressive strength of 40.98 MPa. This suggests that the treatment process enhanced the fibre-matrix interface, leading to improved stress transfer and higher strength. This improvement can be attributed to better fibre-matrix adhesion resulting from the removal of natural impurities and surface modifications that enhance bonding with the cementitious matrix. On the contrary, the composites with untreated jute fibres showed a compressive strength of 36.78 MPa. This result is lower than that of the treated jute fibre composites, indicating that the treatment process positively influenced the strength development. On the other hand, the composite without jute fibre exhibits lower strength compared to those with jute fibres. This suggests that jute fibres contribute to crack-bridging mechanisms, improving the load-bearing capacity of the composite. Moreover, the composites with treated jute fibre but without admixture exhibited the lowest compressive strength of 17.36 MPa, indicating that the polycarboxylate-based superplasticizer significantly improves the workability and hydration efficiency of the matrix. The absence of an admixture likely led to poor particle dispersion and reduced compaction, negatively affecting strength development. However, flexural characteristics of JFRCCs under various curing conditions are discussed in next section.

5.5.2 Flexural Behaviour and Deformation Characteristics

Flexural strength known as bending strength or modulus of rupture, is a material property that describes its ability to resist deformation under bending or flexural load. The flexural strength of JFRCCs subjected to three different curing conditions like natural curing, wet curing, and water curing, are presented in Fig. 5.19.

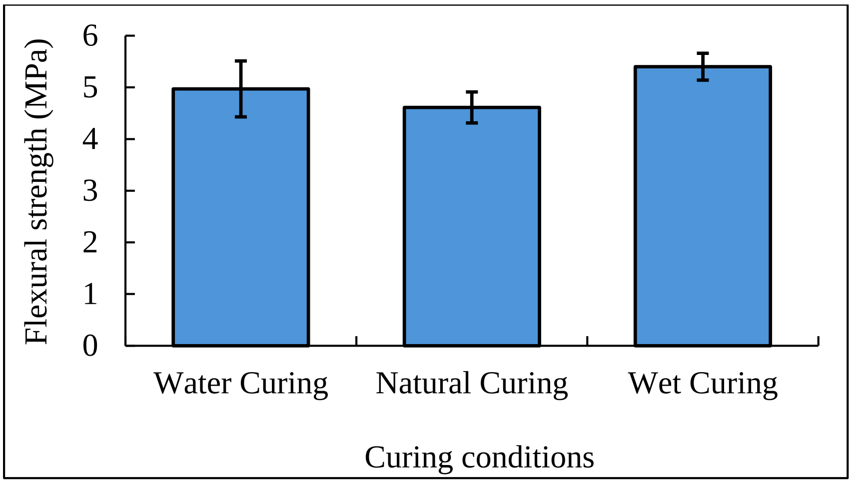

Fig. 5.19: Flexural strength of JFRCCs under different curing conditions.

As shown in the figure, the results indicate that wet curing exhibited the highest flexural strength, followed closely by water curing, while natural curing resulted the lowest flexural strength. This trend suggests that moisture availability during curing influences the development of flexural strength. Here, the improved performance in wet and water curing can be attributed to better hydration of the cementitious matrix, leading to enhanced bonding between the jute fibres and the cement matrix. In contrast, the slightly lower flexural strength observed under natural curing suggests that the hydration reactions were likely hindered by moisture limitations, particularly for the fly ash component. The high fly ash content in JFRCCs highlights the importance of providing sufficient moisture for pozzolanic reactions.

Furthermore, the flexural strength versus deformation behaviour of JFRCCs beam specimens, tested under third-point loading, is presented in Fig. 5.20. All the specimens in this testing were water-cured and prepared using the previously optimized mix design, which included W/B of 0.26, FA/C of 1.68, S/B of 0.5, and a jute content of 0.63% by weight.

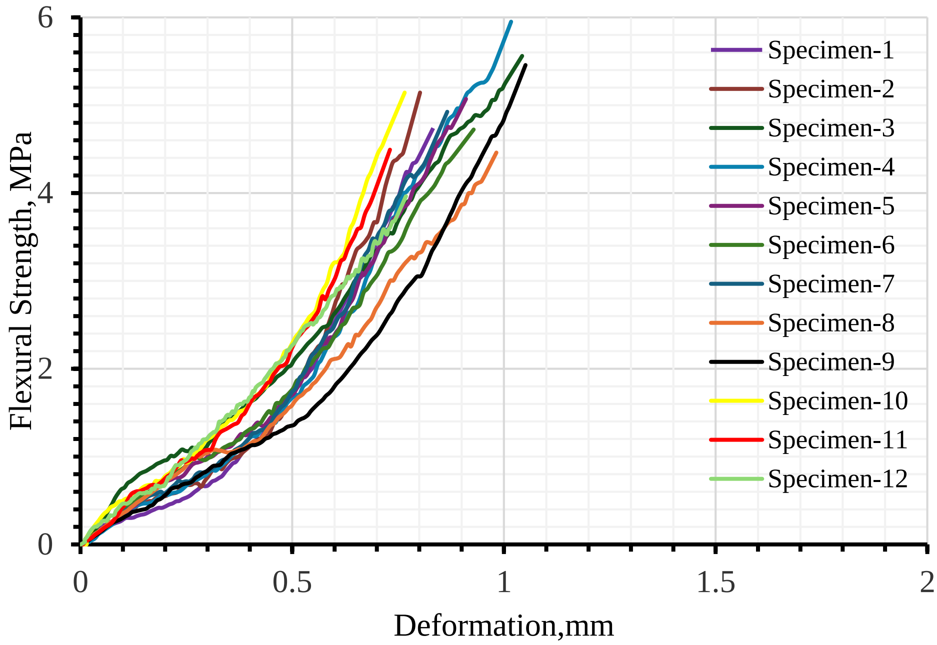

Fig. 5.20: Flexural strength versus deformation behaviour of JFRCCs.

As shown in the figure, the flexural strength of the specimens ranged from 3.96 MPa to 5.95 MPa, while the corresponding deformation at failure varied from 0.731 mm to 1.043 mm. It is observed from the curves that the specimens generally exhibited linear elastic behaviour followed by a relatively abrupt failure upon reaching peak load. Moreover, Fig. 5.21 also shows that the failure mode observed was predominantly brittle, with a sudden drop in load-carrying capacity after reaching the maximum flexural strength. This sudden failure suggests that the jute fibres did not effectively bridge developing cracks or contribute to post-cracking toughness. This behaviour indicates a lack of significant post-peak ductility, which was a targeted characteristic for the JFRCCs due to the inclusion of jute fibres. Despite the presence of jute fibres, the desired ductile behaviour was not achieved at the fibre content of 0.63%. This suggests that the relatively low fibre content might not have been sufficient to effectively bridge cracks and provide significant post-peak energy absorption.

(a) (b)

Fig. 5.21: Failure pattern of beam specimen tested under third-point loading.

In summary, the results highlight the importance of fibre content in achieving ductility in JFRCCs. The brittle failure mode observed in this investigation suggests that a higher jute fibre content might be necessary to induce significant post-cracking deformation and improve the composites toughness. Therefore, the observed brittle failure underscores the need for further optimization of the composites mix design and fibre content to achieve the desired ductile performance.

5.6 Effect of Elevated Temperature

Effect of elevated temperature on the optimized JFRCCs was investigated by exposing cylindrical specimens to temperatures of 200 °C, 400 °C, 600 °C, and 800 °C under controlled furnace conditions for two hours. Following the thermal exposure, key parameters including surface appearance, weight loss, and residual compressive strength were assessed to understand the effects of temperature on the physical and mechanical behaviour of the composites, are discussed in following sections.

5.6.1 Surface Appearance

The surface appearance of JFRCCs exposed to elevated temperatures exhibits distinct changes, reflecting thermal degradation. Fig. 5.22 shows the surface texture of specimens subjected to different temperature levels. At ambient temperature, the composites maintains its standard colour. Upon exposure to temperatures around 200 °C, the surface begins to lighten. Composite experienced noticeable surface roughness at moderate temperatures (200-400 °C) shown in Fig. 5.22(b) and Fig. 5.22(c). The loss of physically bound water leads to matrix shrinkage, promoting micro crack development. Additionally, some fibre degradation occur, contributing to localized void formation.

(a) Ambient (b) 200 °C (c) 400 °C (d) 600 °C (e) 800 °C

Fig. 5.22: Surface texture of JFRCCs exposed to elevated temperatures

At approximately 600 °C, a yellowish tint start to develop, and beyond this point, the material exhibit a whitish appearance. These colour shifts are indicative of chemical changes within the matrix, such as the dehydration of calcium hydroxide and the decomposition of calcium carbonate. At higher temperatures (600 °C and above), severe surface deterioration is observed which are visible in Fig. 5.22(e) and Fig. 5.22(f). Thermal decomposition of hydrated cement phases and the combustion of fibres lead to further structural weakening. Additionally, discoloration and surface roughness intensify, indicating progressive thermal degradation.

Overall, the surface texture analysis suggests that elevated temperatures significantly impact the integrity of JFRCCs, with structural deterioration becoming prominent beyond 400 °C. These observations underscore the importance of understanding the thermal behaviour of JFRCCs, especially in applications where fire resistance and structural integrity at high temperatures are critical considerations.

5.6.2 Weight Loss

In general, the weight loss of cementitious composites increases with rising temperature, primarily influenced by the composition of the matrix. At the initial stages of heating, weight reduction occurs mainly due to the evaporation of free, absorbed, and chemically bound water. As the temperature further increases, the decomposition of calcium silicate hydrate (C–S–H) and other hydration products contributes significantly to the overall weight loss (Sanchayan & Foster, 2016). Fig. 5.23 demonstrates the weight loss of composites subjected to temperatures ranging from 200 °C to 800 °C, relative to their initial weight before heating. As presented in the figure, the weight loss in all composites increased with increasing temperature, indicative of thermal degradation processes. Specifically, the JFRCCs exhibited a progressive weight loss with increasing temperature, reaching approximately 17.03% at 800 °C. This weight loss could be attributed to several factors, including, e.g., moisture loss, degradation of jute fibres (including hemicellulose, cellulose, and lignin), dehydration of cement hydrates (calcium silicate hydrates).

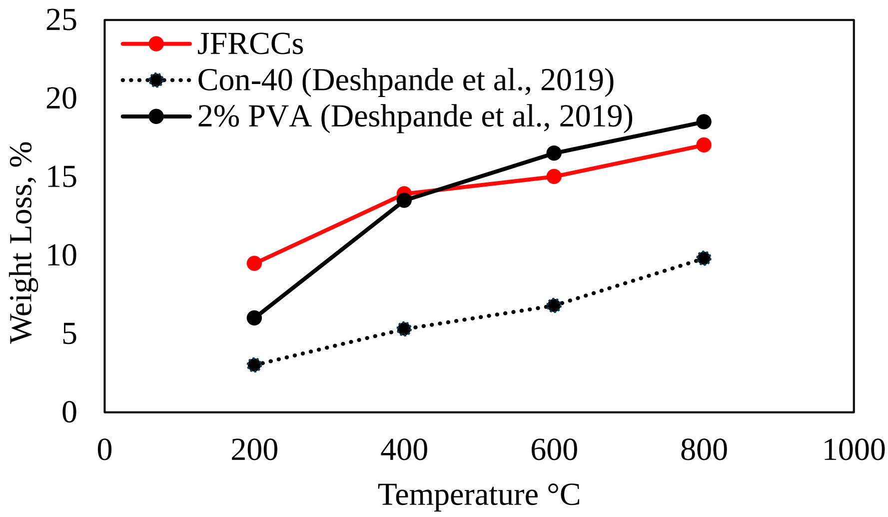

Fig. 5.23: Weight loss in JFRCCs at elevated temperature

Previously, Deshpande et al. (2019) examined the weight loss of Con-40 (conventional concrete with a compressive strength of 40 MPa) and 2% PVA cementitious composites, which exhibited almost the same compressive strength comparable to the optimized JFRCCs in this investigation. The Con-40 concrete showed a lower weight loss compared to the JFRCCs across the entire temperature range. At 800 °C, the weight loss for Con-40 was approximately 9.80%. Reduced weight loss in Con-40 indicates a lower presence of chemically bound water, likely attributed to the absence of fibres, which are prone to thermal decomposition. In contrast, the 2% PVA composite demonstrated a weight loss trend similar to the JFRCCs, but with a slightly higher overall weight loss. At 800 °C, the weight loss for 2% PVA composite was approximately 18.50% which is more that JFRCCs but at 200 °C, 2% PVA composite experienced lower weight loss than JFRCCs. Overall, the weight loss data indicate that JFRCCs experience significant thermal degradation at elevated temperatures. While the inclusion of jute fibres enhances composite performance under ambient conditions, their susceptibility to decomposition at high temperatures must be carefully considered in applications involving thermal exposure.

5.6.3 Compressive Strength at Elevated Temperature

The variation in residual compressive strength of JFRCCs with temperature are demonstrated in Fig. 5.24. The control specimens, tested at ambient temperature, exhibited a compressive strength of approximately 40.98 MPa.

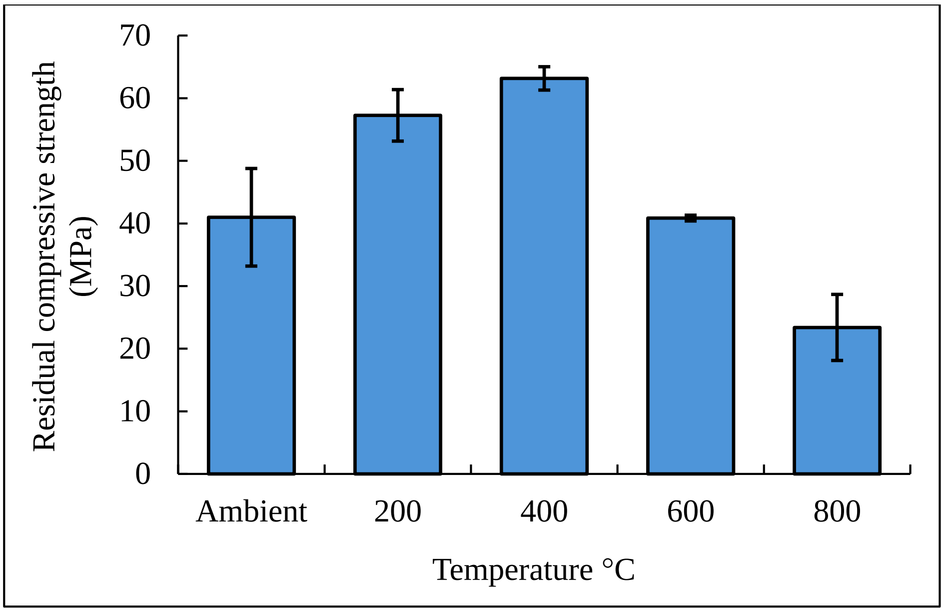

Fig. 5.24: Residual compressive strength of JFRCCs at elevated temperatures

Upon exposure to elevated temperatures, the compressive strength of the JFRCCs showed a complex trend. Specifically, an initial increase in compressive strength was observed at 200 °C and 400 °C, reaching a maximum of 63.17 MPa at 400 °C. This increase could be attributed to improved hydration due to heat and densification of the cementitious matrix. However, beyond 400 °C, a significant decrease in compressive strength was observed. This type of behaviour is consistent with findings from previous studies, which reported similar strength development up to 400 °C followed by a decline when the FA/C ratio was maintained within the range of 1.5 to 2.33 (Rashad, 2015; Mo et al., 2018).

At 600 °C, the strength decreased to 40.86 MPa, and further declined to 23.39 MPa at 800 °C. This reduction in strength at higher temperatures is likely due to thermal degradation of the jute fibres, dehydration of the cement hydrates and, changes in the microstructure of the composite. Overall, these findings suggest that while JFRCCs demonstrate improved compressive strength at moderate temperatures (up to 400 °C), their performance deteriorates considerably at higher temperatures. Therefore, the thermal sensitivity of both the jute fibres and the cementitious matrix must be carefully considered in designing JFRCCs for applications where exposure to elevated temperatures is expected.

Furthermore, the normalized residual compressive strength of JFRCCs compared to conventional concrete (Con-40) over a temperature range of 200 °C to 800 °C is presented in Fig. 5.25.

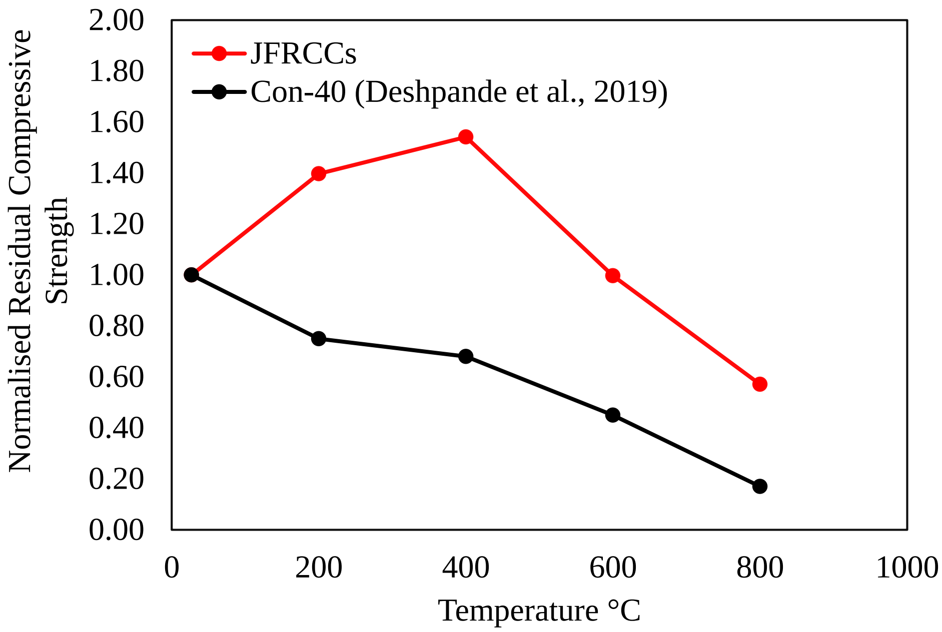

Fig. 5.25: Normalised residual compressive strength at elevated temperatures

The normalization was done with respect to the compressive strength at ambient temperature for each material, allowing for a direct comparison of their high-temperature performance. As shown in the figure, JFRCCs exhibit an initial increase in normalized residual compressive strength, reaching its peak, 1.54 at 400 °C, before gradually declining at higher temperatures. In contrast, Con-40 shows a continuous decrease in strength as the temperature rises. The superior performance of JFRCCs at elevated temperatures can be attributed to the synergistic effect of fly ash and jute fibres, which enhance fire resistance and microstructural stability. The presence of fly ash may also contribute to additional pozzolanic reactions and improved thermal stability, delaying strength degradation. Notably, a more significant reduction in compressive strength is observed in Con-40 compared to JFRCCs, with Con-40 retaining only approximately 17% of its ambient compressive strength at 800 °C. In contrast, JFRCCs demonstrate superior thermal resistance, preserving around 57% of their initial compressive strength at the same temperature. Overall, at all temperature levels, JFRCCs outperforms Con-40 in retaining its strength, demonstrating enhanced thermal resistance. To further understand the surface morphology due to thermal and curing conditions, the next section presents a detailed microstructural investigation of JFRCCs under these varying conditions.

5.7 Microstructural Analysis of Composites under Different Environmental Conditions

Microstructural analysis of JFRCCs was conducted under varying thermal and curing conditions to understand the internal structural behaviour of composites. Specimens were subjected to elevated temperatures of 200 °C, 400 °C, 600 °C, and 800 °C to assess the effects of heat exposure, while others were cured under different conditions such as water curing, natural curing, and wet curing to evaluate hydration development and fibre–matrix interactions. Scanning Electron Microscopy (SEM) was used to investigate morphological changes, the condition of jute fibres, the bonding at the fibre–matrix interface, and porosity levels. This SEM analysis helps to explain how both thermal exposure and curing methods influence the microstructure, which in turn affects the mechanical performance and durability of the composites.

5.7.1 Temperature Conditions

The SEM images of JFRCCs specimens exposed to 200 °C are shown in Fig. 5.26. The image shows intact jute fibres with no significant signs of degradation, which aligns with the expected thermal stability at 200 °C. The surrounding cementitious matrix exhibits noticeable porosity, likely resulting from the initial water-to-binder (W/B) ratio and further enhanced by the evaporation of free and loosely bound water at this temperature. This image also clearly shows several fly ash spherical particles and some of these spheres appear to be embedded within the cementitious matrix.

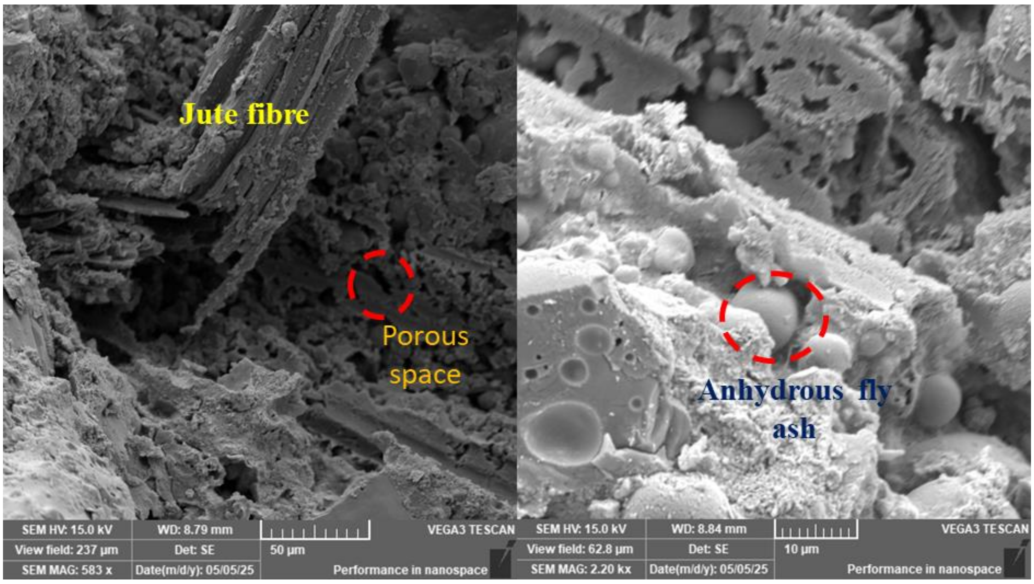

Fig. 5.26: Microstructure of JFRCCs after exposure to 200 °C

However, there is no evidence of severe thermal degradation such as burning of fibres or extensive cracking of the matrix, which aligns with the relatively moderate temperature of 200 °C (Rawat et al., 2024).

When the composite was exposed to 400 °C, notable microstructural changes were observed, are presented in Fig. 5.27. The fibre shows clear signs of thermal degradation and noticeable gaps have formed at the fibre-matrix interface, indicating a loss of bond and dimensional changes in the fibre. Fibrils in the fibre also started to separate, indicating a breakdown of the fibres internal structure and the materials binding the fibrils together. The observed degradation of the fibres and their interface with the matrix implies a substantial reduction in the reinforcing capability of the jute. Therefore, the fibres are less able to bridge cracks or transfer stress effectively.

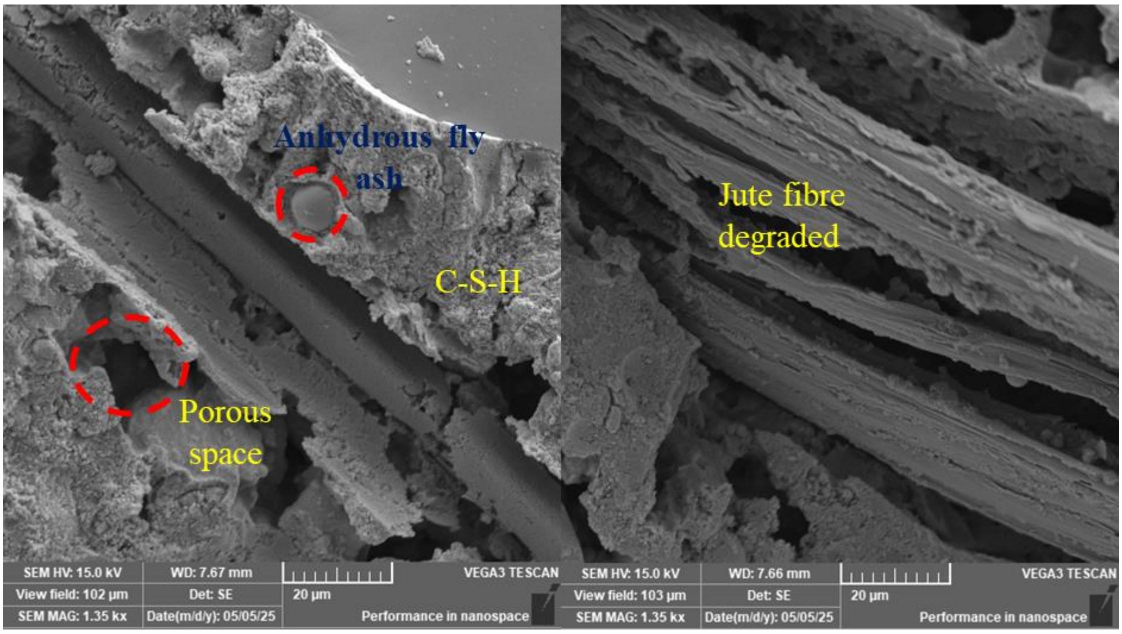

Fig. 5.27: Microstructure of JFRCCs after exposure to 400 °C

Nevertheless, the high compressive strength (63.17 MPa) observed at 400 °C. At this temperature like 400 °C, any unhydrated cement particles (e.g., from fly ash or cement) may undergo additional hydration due to thermal activation in the presence of residual moisture. This can lead to formation of more C-S-H gel, which enhances the matrix density and mechanical interlocking, thereby increasing strength. Moreover, SEM image of composites exposed to 400 °C demonstrate the densification of the cementitious matrix.

The surface morphology of the cementitious composites after exposure to 600 °C is presented in Fig. 5.28. At this elevated temperature, significant degradation of the jute fibres is evident, primarily due to thermal burnout. The cementitious matrix exhibits extensive decomposition, resulting from dehydration of hydration products due to exposure at high temperature. Pronounced porosity is observed throughout the matrix, indicating substantial microstructural damage. Additionally, noticeable debonding is present at the fine sand–matrix interface, which is likely intensified by differential thermal expansion and shrinkage caused by both dehydration and material decomposition. Overall, the microstructural features reflect a severe loss of cohesion and structural integrity in the composite.

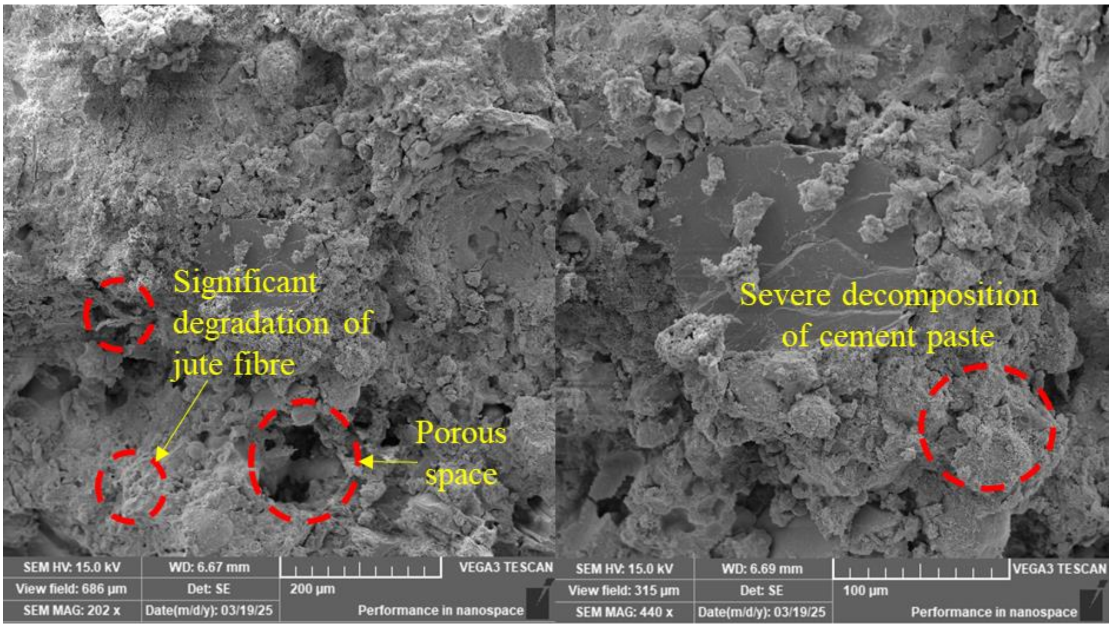

Fig. 5.28: Microstructure of JFRCCs after exposure to 600 °C

The effects of thermal exposure become more profound at 800 °C, as evident in Fig. 5.29.

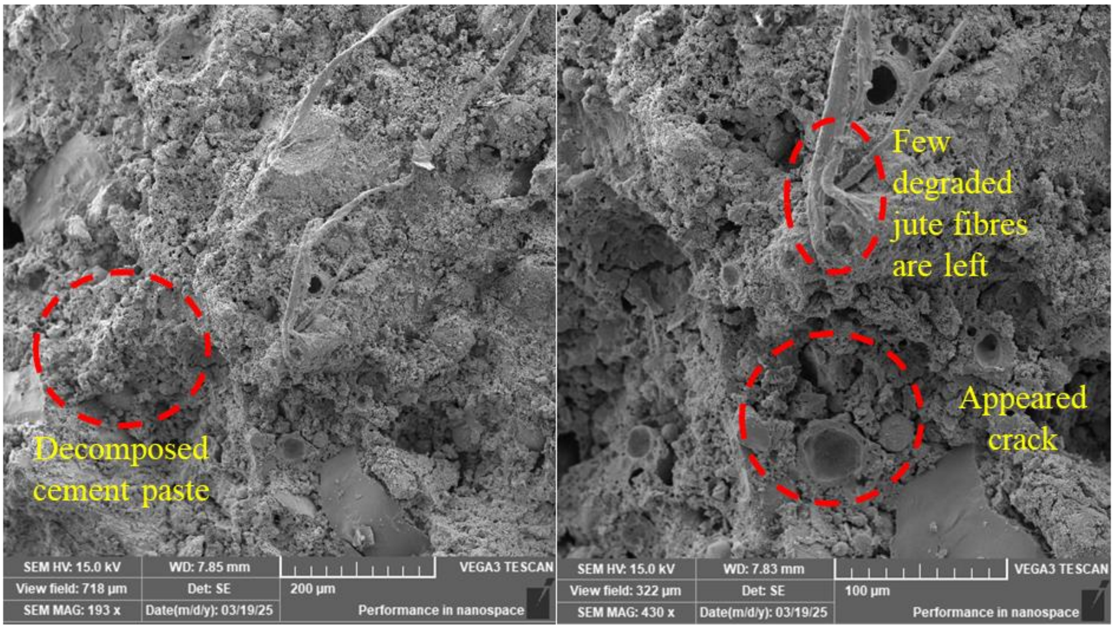

Fig. 5.29: Microstructure of JFRCCs after exposure to 800 °C

As shown in the figure, the matrix appears significantly deteriorated, showing signs of microcracking, and loss of cohesiveness. This suggests thermal-induced dehydration and breakdown of calcium silicate hydrate (C–S–H) and other hydration products at elevated temperatures. The compressive strength results also indicate the breakdown of hydration products, as evidenced above by the retention of only 57% of the original strength after exposure to 800 °C. On the other hand, most of the jute fibre are burnout but few jute fibres are left which show signs of decomposition. This degradation of jute fibres at high temperature adversely affects the composites ability to carry tensile or flexural loads. Additionally, numerous fine cracks are visible on the matrix surface. These are attributed to differential thermal expansion and contraction during heating and subsequent cooling, which induces internal stresses and structural damage.

5.7.2 Curing Conditions

The surface morphology and microstructural details of cementitious composites were analysed under different curing conditions such as natural curing, water curing, and wet curing. The SEM image of JFRCCs subjected to natural curing conditions are shown in Fig. 5.30. This image shows a cementitious matrix with significant porosity. Apart from this, the interface between jute fibre and the surrounding cementitious matrix in the immediate vicinity seems to show a gap or poor adhesion, indicating a potentially weak interfacial transition zone (ITZ). This weak ITZ is likely due to insufficient hydration products, leading to debonding. The overall texture of the hydrated paste appears less dense, indicating a lower degree of cement and fly ash hydration.

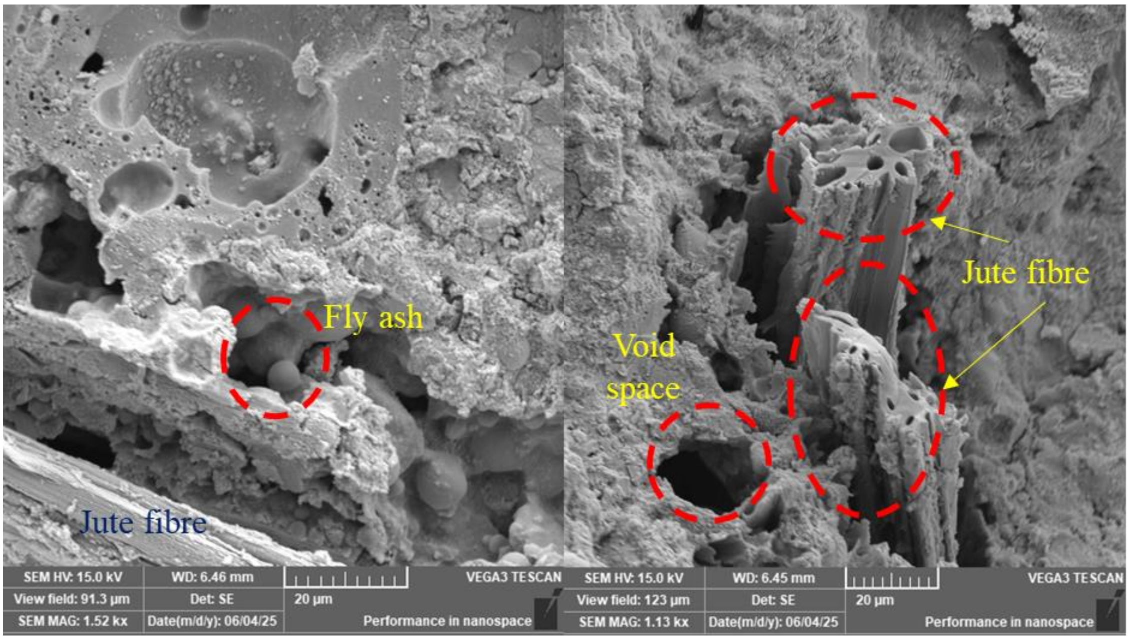

Fig. 5.30: Microstructure of JFRCCs under natural curing conditions

For water curing and wet curing conditions, the microstructure of composites shows comparatively well hydrated cementitious matrix than natural curing conditions, as shown in Fig. 5.31.

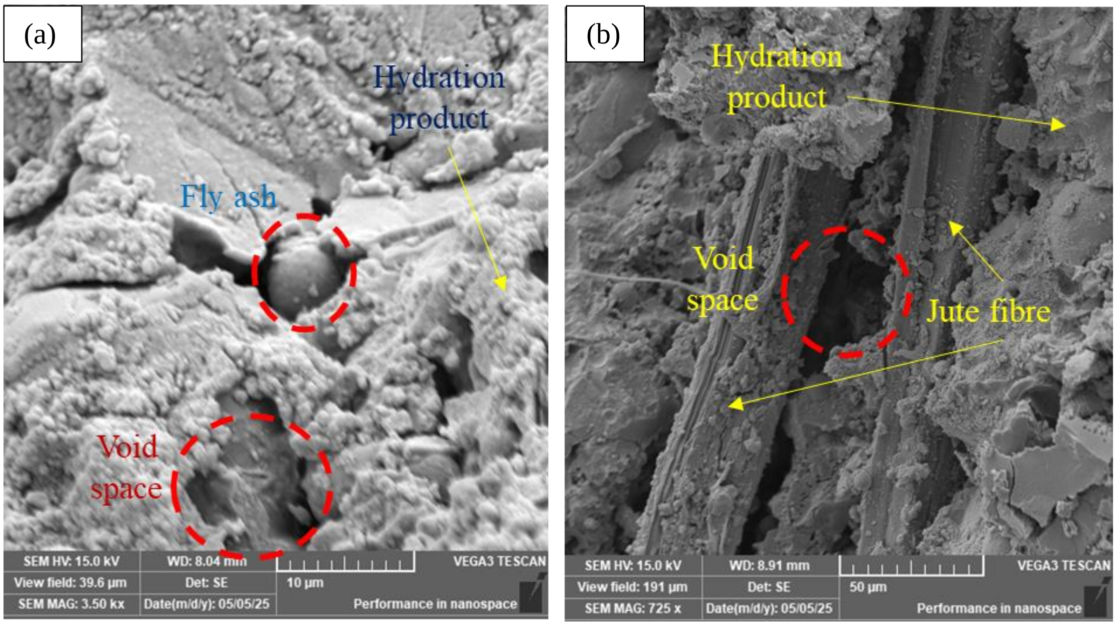

Fig. 5.31: Microstructure of JFRCCs under (a) water curing condition, (b) wet curing condition

The SEM image of composites cured under water immersion reveals a homogeneous microstructure and the hydration appears uniform throughout the matrix, indicating that moisture was evenly available. This contrasts with specimens cured in natural condition, where partial hydration or uneven product distribution is often seen. On the other side, the matrix cured in wet conditions appears relatively compact with visible hydration products, though not as densely packed as in water-cured specimens. This indicates that the wet-curing method provided sufficient moisture retention to support continued hydration, though at a slightly slower rate than complete immersion in water. However, the jute fibre–matrix interface appears partially bonded in several regions under wet curing conditions. Some fibres are visibly embedded in the matrix, indicating moderate fibre-matrix adhesion, while a few areas show minor gaps or loose contact, suggesting an incomplete interfacial transition zone (ITZ) likely caused by non-uniform moisture exposure during curing. Nevertheless, composites cured in wet conditions show fewer voids than those cured naturally. This suggests that the use of wet burlap and polythene helped to maintain a moist environment, preventing rapid moisture loss and promoting more stable hydration. Overall, the wet-curing condition provided a balanced environment, contributing to an improved microstructure compared to natural curing, though not as superior as water curing.

5.8 Summary

Using full factorial statistical analysis, the developed regression models accurately and reliably predicted compressive strength, splitting tensile strength, UPV, and material cost, though the model for peak strain was comparatively less significant. Subsequently, the optimal mix proportions, determined to achieve a target compressive strength of 35 MPa among other objectives, were identified as a water-to-binder ratio of 0.26, a fly ash-to-cement ratio of 1.68, a sand-to-binder ratio of 0.5, and a jute fibre content of 0.63% by weight. Following the identification of the optimized mix ratio, the Phase III investigation on optimized JFRCCs revealed that both water curing and wet curing methods led to higher compressive strength compared to natural curing, indicating the critical role of adequate moisture in enhancing hydration and overall performance. Furthermore, during the flexural behaviour assessment, the predominantly brittle failure mode highlighted the necessity for further optimization of the composite mix design and fibre content in order to achieve the desired ductility.

In terms of thermal performance, the JFRCCs exhibited superior resistance to elevated temperatures when compared to conventional concrete, demonstrating their potential in application involving thermal exposure.

CHAPTER 6: CONCLUSIONS AND RECOMMENDATIONS

6.1 Introduction

This chapter presents a concise summary of the study's key findings based on the discussions in Chapter 4 and Chapter 5. It also offers recommendations for optimizing the performance of JFRCCs and highlights potential directions for future research to further develop their structural and durability properties for sustainable construction applications.

6.2 Conclusions

This researches emphasized on the development of eco-friendly and cost effective construction material by using locally available materials. The findings from this research make a significant contribution to the advancement of sustainable construction materials by integrating eco-friendly and locally sourced materials to develop JFRCCs, offering an environmentally responsible alternative to conventional concrete. This study would promote green materials in construction, paving the way for further optimization and broader application of natural fibre-reinforced composites. Based on the results discussed in this study, following conclusions were made as listed here:

i. Preliminary or Phase I investigation revealed that incorporating 10 mm jute fibres in cementations composites yielded superior compressive strength compared to composites containing 20 mm fibres. This finding suggests an influence of fibre length on the mechanical properties of JFRCCs.

ii. Phase I investigation further exhibited that using a high proportion of fly ash as a cement replacement not only enhanced mechanical performance but also contributed to the development of sustainable cementitious composites.

iii. Developed JFRCCs during Phase II investigations exceeded the minimum compressive strength requirement specified by ACI 318-19. Mix-2 demonstrates exceptional compressive strength and favourable strain behaviour, making it suitable for high-strength applications, though at a higher cost. Mix-10's elevated UPV indicates superior internal quality, while Mix-1 offers strong tensile resistance, making it ideal where tensile performance is critical.

iv. During Phase II investigations, Mix-10 exhibited the highest tensile strength (6.49 MPa), demonstrating strong crack resistance and suitability for tensile load–bearing applications, while Mix-15 recorded the lowest (2.92 MPa), limiting its structural applicability. Furthermore, Mix-2, Mix-6, Mix-11, and Mix-15 failed to meet the minimum tensile requirement, likely due to insufficient fibre bridging at the 0.5% jute fibre content.

v. Mix-1 exhibited the highest peak strain at 0.0033, while Mix-6 recorded the lowest at 0.0018. Notably, the majority of the mixes, except Mix-6, Mix-12, and Mix-16, exceeded the upper limit of 0.0022, demonstrating that the integration of jute fibres and supplementary cementitious materials enhanced ductility.

vi. Life cycle assessment shown that CO_2 emissions ranged from 458 to 668 kg/m^3 for material, transport & mixing, where Mix-2 achieving the lowest CO_2 intensity and Mix-5 the highest. All mixes exceeded the international future benchmark of 5.00 kg/m^3/MPa (Elchalakani et al., 2017), emphasizing the necessity of reducing CO_2 emissions by integrating supplementary cementitious materials (SCMs).

vii. SEM analysis highlighted the critical role of both jute fibre content and FA/C ratio in influencing the microstructure and mechanical performance of JFRCCs. A balanced jute content is essential, as lower concentrations promote homogeneous dispersion and effective crack control, while higher concentrations can lead to detrimental agglomeration and weakened performance. Similarly, optimizing the FA/C ratio is crucial, as excessive fly ash can hinder cement hydration and limit the formation of strength-enhancing calcium silicate hydrate gel. These findings emphasize the importance of careful mix design optimization to achieve the desired microstructural characteristics and maximize the mechanical properties of JFRCCs.

viii. ANOVA analysis demonstrated that regression models for predicting compressive strength (R^2_{adj} = 88.92%), splitting tensile strength (R^2_{adj} = 96.47%), UPV (R^2_{adj} = 94.82%), and material cost (R^2_{adj} = 100%) are statistically significant, though the model for strain at peak compressive strength (R^2_{adj} = 75.53%) showed less significance.

ix. Key insights from the individual parameter assessments revealed that adjustments in the fly ash-to-cement ratio (FA/C) and sand-to-binder ratio (S/B) significantly influenced the mechanical properties and cost-efficiency of the composites.

x. This study successfully developed a cost-effective, optimized JFRCCs utilizing locally sourced materials and industrial by-products. By employing a full factorial design of experiments and subsequent statistical analyses through multi-objective desirability function, the optimal mix ratio of W/B = 0.26, FA/C = 1.68, S/B = 0.50, and jute content = 0.63% was identified. This mix achieved compressive and splitting tensile strengths of 35 MPa and 4 MPa, respectively, while also maximizing strain at peak compressive strength and ultrasonic pulse velocity (UPV) and minimizing cost. The desirability score of 0.9614 for the optimal mix ratio underscores the efficiency and practicality of the proposed composite material.

xi. The optimal mix ratio not only met but exceeded the minimum standards for residential concrete as per ACI 318-19, confirming the feasibility of using JFRCCs in real-world applications.

xii. The findings indicate that curing conditions play a crucial role in the strength development of JFRCCs. Water and wet curing demonstrated higher compressive and flexural strength than natural curing, likely due to improved hydration of the cementitious matrix. This enhanced hydration facilitates stronger fibre-matrix bonding, contributing to the overall improved performance of the composite.

xiii. Treated jute fibre-reinforced composites exhibited superior compressive strength than untreated fibre, confirming that fibre treatment enhances the fibre-matrix interface and stress transfer. Also, composites without jute fibre showed even lower strength than composites with jute fibre, emphasizing the role of jute fibres in crack-bridging and enhancing load-bearing capacity.

xiv. While JFRCCs exhibited a higher weight loss (approximately 17.03%) at 800 °C compared to conventional concrete of similar compressive strength, they demonstrated superior residual strength retention at elevated temperatures. Notably, JFRCCs retained 57% of their initial compressive strength after exposure to 800 °C for two hours, significantly higher than the 17% retained by conventional concrete. Moreover, JFRCCs displayed an initial increase in normalized residual compressive strength, peaking at 1.54 at 400 °C, before gradually decreasing at higher temperatures. This contrasts with the continuous strength reduction observed in conventional concrete with increasing temperature. These findings highlight the potential of JFRCCs for applications requiring enhanced fire resistance and structural integrity at elevated temperatures.

xv. Flexural testing of JFRCCs beams under third-point loading exhibited brittle failure with a sudden loss of load-carrying capacity after peak flexural strength, indicating insufficient crack bridging and post-cracking toughness at a fibre content of 0.63%. This suggests the need for higher fibre content to enhance ductility of JFRCCs.

xvi. SEM analysis revealed that both curing conditions and elevated temperatures significantly influence the microstructure of JFRCCs. Water and wet curing promoted a denser matrix with improved fibre-matrix bonding, contributing to enhanced mechanical properties. In contrast, natural curing resulted in a relatively porous structure due to inadequate hydration. Upon exposure to elevated temperatures, SEM images showed progressive matrix degradation, fibre decomposition, and microcracking, particularly beyond 400 °C.

6.3 Recommendations for Future Work

Drawing from the conclusions derived from this study, a series of recommendations are presented for both future scholarly inquiry and practical utilization:

i. This investigation focused on the short-term performance of JFRCCs. Further research is necessary to evaluate the long-term behaviour of this composites under various environmental conditions, including their durability, creep, and shrinkage characteristics over extended periods.

ii. Global warming potential analysis of developed JFRCCs suggested that reducing CO_2 intensity of JFRCCs would be the future scope of investigation by incorporating various supplementary cementitious materials (SCMs), such as ground granulated blast-furnace slag, metakaolin, and silica fume.

iii. The potential for using alternative binders (geopolymers, alkali-activated materials) in combination with jute fibres and fly ash should be explored, as these may further enhance the sustainability and durability of the cementitious composites.

iv. While the incorporation of jute fibres was expected to enhance the ductility of JFRCCs, the observed brittle failure in beam specimens indicates the need for further refinement of the mix design. Specifically, increasing the jute fibre content is recommended to promote post-cracking deformation and improve the overall toughness of the composite. Future investigations should focus on determining the optimal fibre content that balances strength, ductility, and economic considerations. This may involve exploring the effects of higher fibre contents on flexural behaviour, including crack bridging, energy absorption, and post-crack performance. The investigations of full stress-strain relationship under compression could provide a valuable insight in this regard.

v. Hybrid composites combining jute with other fibres could improve mechanical properties, while life-cycle assessments (LCAs) would evaluate environmental and economic benefits. These efforts will further optimize and expand the application of JFRCCs in sustainable construction.

References

Aamr-Daya, E., Langlet, T., Benazzouk, A., & Quéneudec, M. (2008). Feasibility study of lightweight cement composite containing flax by-product particles: Physico-mechanical properties. *Cement and Concrete Composites*, 30(10), 957-963.

Abdalla, J. A., Hawileh, R. A., Bahurudeen, A., Jyothsna, G., Sofi, A., Shanmugam, V., & Thomas, B. S. (2023). A comprehensive review on the use of natural fibers in cement/geopolymer concrete: A step towards sustainability. *Case Studies in Construction Materials*, 19, e02244.

ACI Committee 318. (2019). Building Code Requirements for Structural Concrete (ACI 318-19). American Concrete Institute.

Aggarwal, L. K. (1995). Bagasse-reinforced cement composites. *Cement and Concrete Composites*, 17(2), 107-112.

Agopyan, V., & John, V. M. (1992). Durability evaluation of vegetable fibre reinforced materials: sisal and coir vegetable fibres as well as those obtained from disintegrated newsprint found to be the most suitable fibres for building purposes. *Building research and information*, 20(4), 233-235.

Ahmad, S., & Alghamdi, S. A. (2014). A statistical approach to optimizing concrete mixture design. *The Scientific World Journal*, 2014(1), 561539.

Ahmad, J., Aslam, F., Martínez-García, R., de Prado-Gil, J., Abbas, N., & Hechmi EI Ouni, M. (2021). Mechanical performance of concrete reinforced with polypropylene fibers (PPFs). *Journal of Engineered Fibers and Fabrics*, 16, 15589250211060399.

Ahmed, T., Elchalakani, M., Karrech, A., Dong, M., Mohamed Ali, M. S., & Yang, H. (2021). ECO-UHPC with high-volume class-F fly ash: new insight into mechanical and durability properties. *Journal of Materials in Civil Engineering*, 33(7), 04021174.

Akhtar, T., Ali, B., Kahla, N. B., Kurda, R., Rizwan, M., Javed, M. M., & Raza, A. (2022). Experimental investigation of eco-friendly high strength fiber-reinforced concrete developed with combined incorporation of tyre-steel fiber and fly ash. *Construction and Building Materials*, 314, 125626.

Alberti, M. G., Enfedaque, A., & Gálvez, J. C. (2017). Fibre reinforced concrete with a combination of polyolefin and steel-hooked fibres. *Composite Structures*, 171, 317-325.

Ali, M. S., Khan, I. A., & Hossain, M. I. (2008). Chemical analysis of ordinary Portland cement of Bangladesh. *Chemical Engineering Research Bulletin*, 12, 7-10.

Ali, B., Raza, S. S., Kurda, R., & Alyousef, R. (2021). Synergistic effects of fly ash and hooked steel fibers on strength and durability properties of high strength recycled aggregate concrete. *Resources, Conservation and Recycling*, 168, 105444.

Al-Gahtani, A. S. (2010). Effect of curing methods on the properties of plain and blended cement concretes. *Construction and Building Materials*, 24(3), 308-314.

Al-Oraimi, S. K., & Seibi, A. C. (1995). Mechanical characterisation and impact behaviour of concrete reinforced with natural fibres. *Composite Structures*, 32(1-4), 165-171.

Anandamurthy, A., Guna, V., Ilangovan, M., & Reddy, N. (2017). A review of fibrous reinforcements of concrete. *Journal of Reinforced Plastics and Composites*, 36(7), 519-552.

Antony, J. (2023). Design of experiments for engineers and scientists. Elsevier.

Arivalagan, S. (2012). Earthquake-Resistant Performance of Polypropylene Fiber Reinforced Concrete Beam. *Journal of Engineering & Technology*, 2(1), 63-63.

Arsène, M. A., Okwo, A., Bilba, K., Soboyejo, A. B. O., & Soboyejo, W. O. (2007). Chemically and thermally treated vegetable fibers for reinforcement of cement-based composites. *Materials and manufacturing processes*, 22(2), 214-227.

Arsene, M.A., Bilba, K., Savastano, H.Jr., & Ghavami, K. (2013). Treatment of non-wood plant fibres used as reinforcement in composites materials. *Materials research*, 16, 903-923.

Asadzadeh, S., & Khoshbayan, S. (2018). Multi-objective optimization of influential factors on production process of foamed concrete using Box-Behnken approach. *Construction and Building Materials*, 170, 101-110.

Asim, M., Uddin, G. M., Jamshaid, H., Raza, A., Hussain, U., Satti, A. N., Hayat, N., & Arafat, S. M. (2020). Comparative experimental investigation of natural fibers reinforced light weight concrete as thermally efficient building materials. *Journal of Building Engineering*, 31, 101411.

ASTM C39 (2018). Standard Test Method for Compressive Strength of Cylindrical Concrete Specimens, ASTM International, West Conshohocken, PA.

ASTM C78 (2018). Standard Test Method for Flexural Strength of Concrete (Using Simple Beam with Third-Point Loading), ASTM International, West Conshohocken, PA.

ASTM C192 (2007). Standard Practice for Making and Curing Concrete Test Specimens in the Laboratory, ASTM International, West Conshohocken, PA.

ASTM C496 (2004). Method for Splitting Tensile Strength of Cylindrical Concrete Specimens, ASTM International, West Conshohocken, PA.

ASTM C597 (2016). Standard Test Method for Pulse Velocity Through Concrete, ASTM International, West Conshohocken, PA.

Aziz, M. A., Paramasivam, P., & Lee, S. L. (1981). Prospects for natural fibre reinforced concretes in construction. *International Journal of Cement Composites and Lightweight Concrete*, 3(2), 123-132.

Balea, A., Fuente, E., Monte, M. C., Blanco, A., & Negro, C. (2021). Recycled fibers for sustainable hybrid fiber cement based material: A review. *Materials*, 14(9), 2408.

Bantie, E. N. Y. E. W. (2010). A study of flexural and compressive strengths of jute fibre-reinforced concrete. Addis Ababa University, Addis Ababa, Ethiopia.

Bentz, D. P. (2006). Influence of water-to-cement ratio on hydration kinetics: Simple models based on spatial considerations. *Cement and concrete research*, 36(2), 238-244.

Bergström, S. G., & Gram, H. E. (1984). Durability of alkali-sensitive fibres in concrete. *International journal of cement composites and lightweight concrete*, 6(2), 75-80.

Berhane, Z. (1994). Performance of natural fibre reinforced mortar roofing tiles. *Materials and Structures*, 27, 347-352.

Bessell, T. J., & Mutuli, S. M. (1982). The interfacial bond strength of sisal—cement composites using a tensile test. *Journal of Materials Science Letters*, 1(6), 244-246.

Bhat, K. M. U. D., & Khan, M. Z. (2018). Effect of Steel Fibre Reinforcement on Early Strength of Concrete. *Int. J. Trend Sci. Res*. Dev, 2, 198-225.

Bheel, N., Tafsirojjaman, T., Liu, Y., Awoyera, P., Kumar, A., & Keerio, M. A. (2021). Experimental study on engineering properties of cement concrete reinforced with nylon and jute fibers. *Buildings*, 11(10), 454.

Blankenhorn, P. R., Blankenhorn, B. D., Silsbee, M. R., & DiCola, M. (2001). Effects of fiber surface treatments on mechanical properties of wood fiber–cement composites. *Cement and Concrete Research*, 31(7), 1049-1055.

Bledzki, A. K., & Gassan, J. (1999). Composites reinforced with cellulose based fibres. *Progress in polymer science*, 24(2), 221-274.

Brandon, C. J., Hohlfelder, R. L., & Oleson, J. P. (2008). The concrete construction of the Roman harbours of Baiae and Portus Iulius, Italy: The ROMACONS 2006 field season. *International Journal of Nautical Archaeology*, 37(2), 374-379.

Brandt, A. M. (2008). Fibre reinforced cement-based (FRC) composites after over 40 years of development in building and civil engineering. *Composite structures*, 86(1-3), 3-9.

Bureau of Indian Standards. (1992). Methods of non-destructive testing of concrete, IS 13311, Part-1: Ultrasonic pulse velocity. Bureau of Indian Standards.

C.E.B.-FIP. (1991). C.E.B.-FIP model code 1990. In Bulletin d'Information (No. 203, Chap. 2).

Campbell, M. D., & Coutts, R. S. P. (1980). Wood fibre-reinforced cement composites. *Journal of materials science*, 15, 1962-1970.

Cantero, B., del Bosque, I. S., Matías, A., & Medina, C. (2018). Statistically significant effects of mixed recycled aggregate on the physical-mechanical properties of structural concretes. *Construction and Building Materials*, 185, 93-101.

Cantero, B., Sáez del Bosque, I. F., Matías, A., Sánchez de Rojas, M. I., & Medina, C. (2019). Inclusion of construction and demolition waste as a coarse aggregate and a cement addition in structural concrete design. *Archives of Civil and Mechanical Engineering*, 19, 1338-1352.

Cantero, B., Bravo, M., De Brito, J., del Bosque, I. S., & Medina, C. (2020). Mechanical behaviour of structural concrete with ground recycled concrete cement and mixed recycled aggregate. *Journal of Cleaner Production*, 275, 122913.

Chen, P. W., & Chung, D. D. L. (1993). Concrete reinforced with up to 0.2 vol% of short carbon fibres. *Composites*, 24(1), 33-52.

Claramunt, J., Ardanuy, M., García-Hortal, J. A., & Tolêdo Filho, R. D. (2011). The hornification of vegetable fibers to improve the durability of cement mortar composites. *Cement and Concrete Composites*, 33(5), 586-595.

Colette, D. A., Martial, A. K. D., Joseph, A. Y., Benjamin, Y. K., & Patrick, D. A. (2023). Optimization of the compressive strength of used tire/cement phase composite concretes using a full factorial design. *Construction and Building Materials*, 404, 133252.

Cook, D. J., Pama, R. P., & Weerasingle, H. L. S. D. (1978). Coir fibre reinforced cement as a low cost roofing material. *Building and Environment*, 13(3), 193-198.

Coutts, R. S. P., & Campbell, M. D. (1979). Coupling agents in wood fibre-reinforced cement composites. *Composites*, 10(4), 228-232.

Coutts, R. S. P., & Kightly, P. (1982). Microstructure of autoclaved refined wood-fibre cement mortars. *Journal of Materials Science*, 17, 1801-1806.

Coutts, R.S.P., & Ridikas, V. (1982a). Refined wood fibre-cement products. *Australian Pulp and Paper Industry Techical Industry Technical Association,* 35, 395-400.

Coutts, R. S. P. (1983). Flax fibres as a reinforcement in cement mortars. *International Journal of Cement Composites and Lightweight Concrete*, 5(4), 257-262.

Coutts, R. S. P. (1984). Autoclaved beaten wood fibre-reinforced cement composites. *Composites*, 15(2), 139-143.

Coutts, R. S., & Kightly, P. (1984). Bonding in wood fibre-cement composites. *Journal of materials science*, 19, 3355-3359.

Coutts, R. S. P., & Warden, P. G. (1987). Air-cured abaca reinforced cement composites. *International Journal of Cement Composites and Lightweight Concrete*, 9(2), 69-73.

Coutts, R. S. P. (1987). Fibre-matrix interface in air-cured wood-pulp fibre-cement composites. *Journal of materials science letters*, 6(2), 140-142.

Coutts, R. S. P., & Warden, P. G. (1990). Effect of compaction on the properties of air-cured wood fibre reinforced cement. *Cement and concrete composites*, 12(3), 151-156.

Coutts, R. S. P. (1990). Banana fibres as reinforcement for building products. *Journal of Materials Science Letters*, 9(10), 1235-1236.

Coutts, R. S. P., & Warden, P. G. (1992). Sisal pulp reinforced cement mortar. *Cement and Concrete Composites*, 14(1), 17-21.

Coutts, R. S. P. (2005). A review of Australian research into natural fibre cement composites. *Cement and Concrete Composites*, 27(5), 518-526.

Davies, G. W., Campbell, M. D., & Coutts, R. S. P. (1981). A SEM study of wood fibre reinforced cement composites.

de Andrade Silva, F., Toledo Filho, R. D., de Almeida Melo Filho, J., & Fairbairn, E. D. M. R. (2010). Physical and mechanical properties of durable sisal fiber–cement composites. *Construction and building materials*, 24(5), 777-785.

Deb, S., Mitra, N., Majumder, S. B., & Maitra, S. (2018). Improvement in tensile and flexural ductility with the addition of different types of polypropylene fibers in cementitious composites. *Construction and Building Materials*, 180, 405-411.

Deb, S., Mitra, N., Maitra, S., & Basu Majumdar, S. (2020). Comparison of mechanical performance and life cycle cost of natural and synthetic fiber-reinforced cementitious composites. *Journal of Materials in Civil Engineering*, 32(6), 04020150.

Deshpande, A. A., Kumar, D., & Ranade, R. (2019). Influence of high temperatures on the residual mechanical properties of a hybrid fiber-reinforced strain-hardening cementitious composite. *Construction and Building Materials*, 208, 283-295.

Elchalakani, M., Basarir, H., & Karrech, A. (2017). Green concrete with high-volume fly ash and slag with recycled aggregate and recycled water to build future sustainable cities. *Journal of Materials in Civil Engineering*, 29(2), 04016219.

Espinosa, A. B., Revilla-Cuesta, V., Skaf, M., Faleschini, F., & Ortega-López, V. (2023). Utility of ultrasonic pulse velocity for estimating the overall mechanical behavior of recycled aggregate self-compacting concrete. *Applied Sciences*, 13(2), 874.

Eurocode. (1991). Design of concrete structures (Eurocode No. 2).

Farias, L. D. N., Lima, P. R. L., & Filho, R. D. T. (2024). Short Jute Fiber Reinforced Cement Mortar for Out-of-Plane Strengthening of Masonry Prisms. *Sustainability*, 16(13), 5675.

Fauzan., Kurniawan, R., Lovina, C., Fitrah, O. N., & Basenda, P. T. (2019). The effects of steel fiber waste tyre on properties of high strength fly ash concrete. *In MATEC Web of Conferences* (Vol. 276, p. 01008). EDP Sciences.

Flower, D. J., & Sanjayan, J. G. (2007). Green house gas emissions due to concrete manufacture. *The international Journal of life cycle assessment*, 12, 282-288.

Gassan, J., & Bledzki, A. K. (1999). Correlation between structure and properties of cellulose-based fibers and their effects on composite properties. *In Fifth International Conference on Woodfiber-Plastic Composites* (pp. 147-52).

Gupta, S. D., Aftab, M. S., Zakaria, H. M., & Karmakar, C. (2020). Scope of improving mechanical characteristics of concrete using natural fiber as a reinforcing material. *Malaysian Journal of Civil Engineering*, 32(2).

Hamada, H. M., Al-Attar, A., Shi, J., Yahaya, F., Al Jawahery, M. S., & Yousif, S. T. (2023). Optimization of sustainable concrete characteristics incorporating palm oil clinker and nano-palm oil fuel ash using response surface methodology. *Powder Technology*, 413, 118054.

Haq, E., Saifullah, A., Habib, A., Azim, A. Y. M. A., Alimuzzaman, S., Dhakal, H. N., & Sarker, F. (2024). Improved mechanical properties of environmentally friendly jute fibre reinforced metal laminate sandwich composite through enhanced interface. *Heliyon*, 10(2).

Hossain, M. A., Datta, S. D., Akid, A. S. M., Sobuz, M. H. R., & Islam, M. S. (2023). Exploring the synergistic effect of fly ash and jute fiber on the fresh, mechanical and non-destructive characteristics of sustainable concrete. *Heliyon*, 9(11).

Huda, S. B., & Alam, M. S. (2014). Mechanical behavior of three generations of 100% repeated recycled coarse aggregate concrete. *Construction and building materials*, 65, 574-582.

Ibrahim, M., Shameem, M., Al-Mehthel, M., & Maslehuddin, M. (2013). Effect of curing methods on strength and durability of concrete under hot weather conditions. *Cement and Concrete Composites*, 41, 60-69.

Ilg, P., Hoehne, C., & Guenther, E. (2016). High-performance materials in infrastructure: a review of applied life cycle costing and its drivers–the case of fiber-reinforced composites. *Journal of Cleaner Production*, 112, 926-945.

Islam, M. M., & Islam, M. S. (2014). Utilisation of natural resources for sustainable development: Role of Bangladeshi Fly ash. *Journal of Civil Engineering (IEB)*, 42(1), 137-152.

Islam, M. S., & Ahmed, S. J. (2018). Influence of jute fiber on concrete properties. *Construction and Building Materials*, 189, 768-776.

Islam, M. M., & Ali, M. S. (2018). Industrial research advances of jute in Bangladesh. *International Journal of Agricultural and Biosystems Engineering*, 3(1), 1-9.

Jo, B. W., Chakraborty, S., & Kim, H. (2016). Efficacy of alkali-treated jute as fibre reinforcement in enhancing the mechanical properties of cement mortar. *Materials and Structures*, 49, 1093-1104.

Joaquim, A. P., Tonoli, G. H. D., Santos, S. F. D., & Savastano Junior, H. (2009). Sisal organosolv pulp as reinforcement for cement based composites. *Materials Research*, 12, 305-314.

John, V. M., Cincotto, M. A., Sjöström, C., Agopyan, V., & Oliveira, C. T. D. A. (2005). Durability of slag mortar reinforced with coconut fibre. *Cement and Concrete Composites*, 27(5), 565-574.

John, M. J., & Anandjiwala, R. D. (2008). Recent developments in chemical modification and characterization of natural fiber-reinforced composites. *Polymer composites*, 29(2), 187-207.

Jr Savastano, H., Turner, A., Mercer, C., & Soboyejo, W. O. (2006). Mechanical behavior of cement-based materials reinforced with sisal fibers. *Journal of Materials Science*, 41, 6938-6948.

Karim, M. E., Alam, M. J., & Hoque, M. S. (2017). Effect of salinity of water in lime-fly ash treated sand. *International Journal of Geo-Engineering*, 8(1), 15.

Kerr, J., Rayburg, S., Neave, M., & Rodwell, J. (2022). Comparative analysis of the global warming potential (GWP) of structural stone, concrete and steel construction materials. *Sustainability*, 14(15), 9019.

Khan, M. A. A., Saha, M. S., Sultana, S., Ahmed, A. N., & Das, R. C. (2013). Coal Fly ash of Barapukuria thermal power plant, Bangladesh: Physico chemical properties assessment and utilization. *International Journal of scientific & engineering research*, 4(11), 1456-1460.

Khan, A., Do, J., & Kim, D. (2016). Cost effective optimal mix proportioning of high strength self compacting concrete using response surface methodology. *Computers and Concrete*, 17(5), 629-638.

Kriker, A., Bali, A., Debicki, G., Bouziane, M., & Chabannet, M. (2008). Durability of date palm fibres and their use as reinforcement in hot dry climates. *Cement and Concrete Composites*, 30(7), 639-648.

Kubissa, W., Jaskulski, R., & Reiterman, P. (2017). Ecological concrete based on blast-furnace cement with incorporated coarse recycled concrete aggregate and fly ash addition. *Journal of renewable materials*, 5(1), 53-61.

Kulkarni, A. G., Satyanarayana, K. G., Rohatgi, P. K., & Vijayan, K. (1983). Mechanical properties of banana fibres (Musa sepientum). *Journal of materials science*, 18, 2290-2296.

Kumar, A., Yadav, O., & Kumar, A. (2023). Effect of Fiber Reinforcement on the Tensile Strength and Ductility of Fly Ash Based Composites. *Web of Synergy: International Interdisciplinary Research Journal*, 2(6), 137-143.

Kursuncu, B., Gencel, O., Bayraktar, O. Y., Shi, J., Nematzadeh, M., & Kaplan, G. (2022). Optimization of foam concrete characteristics using response surface methodology and artificial neural networks. *Construction and Building Materials*, 337, 127575.

Le Troëdec, M., Peyratout, C. S., Smith, A., & Chotard, T. (2009). Influence of various chemical treatments on the interactions between hemp fibres and a lime matrix. *Journal of the European Ceramic Society*, 29(10), 1861-1868.

Le Troëdec, M., Dalmay, P., Patapy, C., Peyratout, C., Smith, A., & Chotard, T. (2011). Mechanical properties of hemp-lime reinforced mortars: Influence of the chemical treatment of fibers. *Journal of Composite Materials*, 45(22), 2347-2357.

Li, X., Tabil, L. G., & Panigrahi, S. (2007). Chemical treatments of natural fiber for use in natural fiber-reinforced composites: a review. *Journal of Polymers and the Environment*, 15, 25-33.

Li, H. D., Zhang, Q. M., Feng, G., Mei, L., Wang, Y., & Long, W. J. (2020). Multi-scale improved damping of high-volume fly ash cementitious composite: combined effects of polyvinyl alcohol fiber and graphene oxide. *Construction and Building Materials*, 260, 119901.

Liu, B., Zhang, L. Z., Liu, Q. X., & Ji, T. (2013). Study on behaviors of jute fiber reinforced cement based materials. *Applied mechanics and materials*, 253, 508-511.

Luo, X., Sun, W., & Chan, S. Y. N. (2001). Steel fiber reinforced high-performance concrete: a study on the mechanical properties and resistance against impact. *Materials and Structures*, 34, 144-149.

Mansur, M. A., & Aziz, M. A. (1982). A study of jute fibre reinforced cement composites. *International Journal of Cement Composites and Lightweight Concrete*, 4(2), 75-82.

Mansur, A. A. A., Hossain, A., Anisha, A., Tahmid, A., & Chowdhury, S. R. (2022). PERFORMANCE OF JUTE FIBER REINFORCED CONCRETE IN THE CONTEXT OF BANGLADESH. *Malaysian Journal of Civil Engineering*, 34(3), 25-35.

Marikunte, S., Aldea, C., & Shah, S. P. (1997). Durability of glass fiber reinforced cement composites:: Effect of silica fume and metakaolin. *Advanced Cement Based Materials*, 5(3-4), 100-108.

McCarthy, M. J., & Dhir, R. K. (2005). Development of high volume fly ash cements for use in concrete construction. *Fuel*, 84(11), 1423-1432.

Mehta, P. K. (2004). High-performance, high-volume fly ash concrete for sustainable development. *In Proceedings of the international workshop on sustainable development and concrete technology* (pp. 3-14). Ames, IA, USA: Iowa State University.

Merta, I., Serjun, V. Z., Pranjić, A. M., Šajna, A., Štefančič, M., Poletanović, B., Ameri, F., & Mladenović, A. (2025). Investigating the synergistic impact of freeze-thaw cycles and deicing salts on the properties of cementitious composites incorporating natural fibers and fly ash. *Cleaner Engineering and Technology*, 24, 100853.

Mickūnaitis, V., Pikūnas, A., & Mackoit, I. (2007). Reducing fuel consumption and CO2 emission in motor cars. *Transport*, 22(3), 160-163.

Mo, K. H., Loh, Z. P., Tan, C. G., Alengaram, U. J., & Yap, S. P. (2018). Behaviour of fibre-reinforced cementitious composite containing high-volume fly ash at elevated temperatures. *Sādhanā*, 43(11), 177.

Montgomery, D. C. (2013). Design and analysis of experiments, Eighth edition. Hoboken, NJ: John Wiley & Sons, Inc.

Moropoulou, A., Bakolas, A., & Anagnostopoulou, S. (2005). Composite materials in ancient structures. *Cement and concrete composites*, 27(2), 295-300.

Nehdi, M., Duquette, J., & El Damatty, A. (2003). Performance of rice husk ash produced using a new technology as a mineral admixture in concrete. *Cement and concrete research*, 33(8), 1203-1210.

Norme Tecniche. (1992). Norme tecniche per l’esecuzione delle opere in cemento armato normale e precompresso e per le strutture metalliche, D.M. 14-2-1992. Suppl. G.U. Repubblica Italiana (No. 65).

Oleson, J. P., Brandon, C., Cramer, S. M., Cucitore, R., Gotti, E., & Hohlfelder, R. L. (2004). The ROMACONS Project: A contribution to the historical and engineering analysis of hydraulic concrete in Roman maritime structures. *International Journal of Nautical Archaeology*, 33(2), 199-229.

Olorunnisola, A. O. (2008). Effects of pre-treatment of rattan (Laccosperma secundiflorum) on the hydration of Portland cement and the development of a new compatibility index. *Cement and Concrete Composites*, 30(1), 37-43.

Onuaguluchi, O., & Banthia, N. (2016). Plant-based natural fibre reinforced cement composites: A review. *Cement and Concrete Composites*, 68, 96-108.

Pacheco-Torgal, F., & Jalali, S. (2011). Cementitious building materials reinforced with vegetable fibres: A review. *Construction and building materials*, 25(2), 575-581.

Pappu, A., & Thakur, V. K. (2017). Towards sustainable micro and nano composites from fly ash and natural fibers for multifunctional applications. *Vacuum*, 146, 375-385.

Rahman, M. A., & Kabir, M. I. (2025). Development of a sustainable and cost-optimized cementitious composites incorporating local resources and jute fibre. *Cleaner Materials*, 17, 100322.

Rainey, T. J. (2009). A study into the permeability and compressibility properties of Australian bagasse pulp. *A Dissertation of Queensland University of Technology*.

Ram, K., Serdar, M., Londono-Zuluaga, D., & Scrivener, K. (2023). Does carbon footprint reduction impair mechanical properties and service life of concrete?. *Materials and structures*, 56(1), 6.

Ramakrishna, G., & Sundararajan, T. (2005). Impact strength of a few natural fibre reinforced cement mortar slabs: a comparative study. *Cement and concrete composites*, 27(5), 547-553.

Ramakrishna, G., & Sundararajan, T. (2005a). Studies on the durability of natural fibres and the effect of corroded fibres on the strength of mortar. *Cement and concrete composites*, 27(5), 575-582.

Ramaswamy, H. S., Ahuja, B. M., & Krishnamoorthy, S. (1983). Behaviour of concrete reinforced with jute, coir and bamboo fibres. *International Journal of Cement Composites and Lightweight Concrete*, 5(1), 3-13.

Rashad, A. M. (2015). An exploratory study on high-volume fly ash concrete incorporating silica fume subjected to thermal loads. *Journal of Cleaner Production*, 87, 735-744.

Rawat, S., Lee, C. K., & Zhang, Y. X. (2021). Performance of fibre-reinforced cementitious composites at elevated temperatures: A review. *Construction and Building Materials*, 292, 123382.

Rawat, S., Saliba, P., Estephan, P. C., Ahmad, F., & Zhang, Y. (2024). Mechanical performance of hybrid fibre reinforced magnesium oxychloride cement-based composites at ambient and elevated temperature. *Buildings*, 14(1), 270.

Reddy, N., & Yang, Y. (2005). Biofibers from agricultural byproducts for industrial applications. *TRENDS in Biotechnology*, 23(1), 22-27.

Revilla-Cuesta, V., Shi, J. Y., Skaf, M., Ortega-López, V., & Manso, J. M. (2022). Non-destructive density-corrected estimation of the elastic modulus of slag-cement self-compacting concrete containing recycled aggregate. *Developments in the Built Environment*, 12, 100097.

Revilla-Cuesta, V., Skaf, M., Ortega-López, V., & Manso, J. M. (2023). Multi-parametric flowability classification of self-compacting concrete containing sustainable raw materials: An approach to real applications. *Journal of Building Engineering*, 63, 105524.

Rudnov, V., Belyakov, V., & Moskovsky, S. (2016). Properties and design characteristics of the fiber concrete. *Procedia Engineering*, 150, 1536-1540.

Sadrmanesh, V., & Chen, Y. (2019). Bast fibres: structure, processing, properties, and applications. *International Materials Reviews*, 64(7), 381-406.

Sakai, E., Miyahara, S., Ohsawa, S., Lee, S. H., & Daimon, M. (2005). Hydration of fly ash cement. *Cement and Concrete Research*, 35(6), 1135-1140.

Sanchayan, S., & Foster, S. J. (2016). High temperature behaviour of hybrid steel–PVA fibre reinforced reactive powder concrete. *Materials and Structures*, 49, 769-782.

Sangwan, K. S., & Sihag, N. (2019). Multi-objective optimization for energy efficient machining with high productivity and quality for a turning process. *Procedia CIRP*, 80, 67-72.

Sapkal, A. R., Jadhav, A. V., & Nagendra, M. V. (2021). Experimental study of high strength concrete of M90 grade using unprocessed fly ash and silica fume. *International Journal of Engineering Applied Sciences and Technology*, 6(5), 172–174.

Savastano Jr, H., & Agopyan, V. (1999). Transition zone studies of vegetable fibre-cement paste composites. *Cement and concrete composites*, 21(1), 49-57.

Savastano, H.Jr., Agopyan, V., Nolasco, A.M., & Pimentel, L. (1999a). Plant fibre reinforced cement components for roofing. *Construction and Building Materials*, 13, 433-438.

Savastano Jr, H., Warden, P. G., & Coutts, R. S. P. (2000). Brazilian waste fibres as reinforcement for cement-based composites. *Cement and Concrete Composites*, 22(5), 379-384.

Savastano Jr, H., Warden, P. G., & Coutts, R. S. P. (2001). Ground iron blast furnace slag as a matrix for cellulose-cement materials. *Cement and concrete composites*, 23(4-5), 389-397.

Savastano Jr, H., Warden, P. G., & Coutts, R. S. P. (2003). Mechanically pulped sisal as reinforcement in cementitious matrices. *Cement and Concrete Composites*, 25(3), 311-319.

Savastano Jr, H., Warden, P. G., & Coutts, R. S. (2004). Evaluation of pulps from natural fibrous material for use as reinforcement in cement product. *Materials and Manufacturing Processes*, 19(5), 963-978.

Sawsen, C., Fouzia, K., Mohamed, B., & Moussa, G. (2014). Optimizing the formulation of flax fiber-reinforced cement composites. *Construction and building Materials*, 54, 659-664.

Shaikh, F. U., Nishiwaki, T., & Kwon, S. (2018). Effect of fly ash on tensile properties of ultra-high performance fiber reinforced cementitious composites (UHP-FRCC). *Journal of Sustainable Cement-Based Materials*, 7(6), 357-371.

Sharma, V. K., Rana, M., Singh, T., Singh, A. K., & Chattopadhyay, K. (2021). Multi-response optimization of process parameters using Desirability Function Analysis during machining of EN31 steel under different machining environments. *Materials Today: Proceedings*, 44, 3121-3126.

Shen, W., Cao, L., Li, Q., Zhang, W., Wang, G., & Li, C. (2015). Quantifying CO2 emissions from China's cement industry. *Renewable and Sustainable Energy Reviews*, 50, 1004-1012.

Singh, N. B., Singh, V. D., & Rai, S. (2000). Hydration of bagasse ash-blended Portland cement. *Cement and Concrete Research*, 30(9), 1485-1488.

Siraj-UD-Doulah, M. D., Hassan, M. Z., & Sukanta, M. R. I. (2020). Forecasting the production of jute based on time series models in Bangladesh. *Int. J. Stat. App. Math.*, 5(1), 32-38.

Sjostrom, E. (1981). Wood Chemistry: Fundamentals and Applications. Academic Press, London.

Souza, P. S. L., & Dal Molin, D. C. (2005). Viability of using calcined clays, from industrial by-products, as pozzolans of high reactivity. *Cement and Concrete Research*, 35(10), 1993-1998.

Sultana, S., Ahsan, S., Tanvir, S., Haque, N., Alam, F., & Yellishetty, M. (2021). Coal fly ash utilisation and environmental impact. *In Clean Coal Technologies:*

Beneficiation, Utilization, Transport Phenomena and Prospective (pp. 381-402). Cham: Springer International Publishing.

Swamy, R. N. (1990). Vegetable fibre reinforced cement composites–a false dream or a potential reality?. *In Vegetable Plants and their Fibres as Building Materials: Proceedings of the Second International RILEM Symposium* (Vol. 7, p. 1). Routledge, London, UK. DOI.

Tam, V. W., Soomro, M., & Evangelista, A. C. J. (2018). A review of recycled aggregate in concrete applications (2000–2017). *Construction and Building materials*, 172, 272-292.

Tamim, M. M., Dhar, A., & Hossain, M. S. (2013). Fly ash in Bangladesh-an overview. *International Journal of Scientific & Engineering Research*, 4(4), 809-812.

Tian, H. (2015). Mechanical Behaviour of High Volume Fly Ash Cementitious Composites Reinforced with Hybrid Natural and Steel Fibres (Doctoral dissertation, UNSW Sydney).

Tian, H., Zhang, Y. X., Ye, L., & Yang, C. (2015). Mechanical behaviours of green hybrid fibre-reinforced cementitious composites. *Construction and Building Materials*, 95, 152-163.

Tian, H., Zhang, Y. X., Yang, C., & Ding, Y. (2016). Recent advances in experimental studies of the mechanical behaviour of natural fibre-reinforced cementitious composites. *Structural Concrete*, 17(4), 564-575.

Tipraj, P. E., Prabhanjan, N., Krishna, A. S., & Prasad, M. G. (2018). Experimental study on strength of concrete by partial replacement of cement by nano silica and fly ash. *Int J Civ Eng Technol*, 9, 1763-1771.

Tonoli, G. H. D., Joaquim, A. P., Arsène, M. A., Bilba, K., & Savastano Jr, H. (2007). Performance and durability of cement based composites reinforced with refined sisal pulp. *Materials and Manufacturing Processes*, 22(2), 149-156.

Tonoli, G. H. D., Savastano Jr, H., Fuente, E., Negro, C., Blanco, A., & Lahr, F. R. (2010). Eucalyptus pulp fibres as alternative reinforcement to engineered cement-based composites. *Industrial crops and products*, 31(2), 225-232.

Tonoli, G. H. D., de Souza Almeida, A. E. F., Pereira-da-Silva, M. A., Bassa, A., Oyakawa, D., & Savastano, H. Jr. (2010a). Surface properties of eucalyptus pulp fibres as reinforcement of cement-based composites. *Holzforschung*, 64, 595-601.

Tonoli, G. H. D., Belgacem, M. N., Bras, J., Pereira-da-Silva, M. A., Rocco Lahr, F. A., & Savastano, H. (2012). Impact of bleaching pine fibre on the fibre/cement interface. *Journal of Materials Science*, 47, 4167-4177.

Tonoli, G. H. D., Mendes, R. F., Siqueira, G., Bras, J., Belgacem, M. N., & Savastano Jr, H. (2013). Isocyanate-treated cellulose pulp and its effect on the alkali resistance and performance of fiber cement composites. *Holzforschung*, 67(8), 853-861.

Valadez-Gonzalez, A., Cervantes-Uc, J. M., Olayo, R., & Herrera-Franco, P. J. (1999). Effect of fiber surface treatment on the fiber–matrix bond strength of natural fiber reinforced composites. *Composites Part B: Engineering*, 30(3), 309-320.

Van Damme, H. (2018). Concrete material science: Past, present, and future innovations. *Cement and Concrete Research*, 112, 5-24.

Wei, J., & Meyer, C. (2014). Improving degradation resistance of sisal fiber in concrete through fiber surface treatment. *Applied Surface Science*, 289, 511-523.

Yang, E. H., Yang, Y., & Li, V. C. (2007). Use of high volumes of fly ash to improve ECC mechanical properties and material greenness. *ACI materials journal*, 104(6), 620.

Yaseen, N., Sahar, U., Bahrami, A., Saleem, M. M., Iqbal, M. A., & Siddique, I. (2023). Synergistic impacts of fly ash and sugarcane bagasse ash on performance of polyvinyl alcohol fiber-reinforced engineered cementitious composites. *Results in Materials*, 20, 100490.

Zakaria, M., Ahmed, M., Hoque, M. M., & Hannan, A. (2015). Effect of jute yarn on the mechanical behavior of concrete composites. *SpringerPlus*, 4, 1-8.

Zakaria, M., Ahmed, M., Hoque, M. M., & Islam, S. (2016). Scope of using jute fiber for the reinforcement of concrete material. *Textiles and Clothing Sustainability*, 2, 1-10.

Zakaria, M., Ahmed, M., Hoque, M., & Shaid, A. (2018). A comparative study of the mechanical properties of jute fiber and yarn reinforced concrete composites. *Journal of Natural Fibers*, 676.

Zhang, K., Wu, W., Fan, J., & Yuan, C. (2024). The Influence and Mechanism of Curing Methods and Curing Age on the Mechanical Properties of Yellow River Sand Engineered Cementitious Composites. *Materials*, 17(17), 4307.

Zhu, W. H., Tobias, B. C., Coutts, R. S. P., & Langfors, G. (1994). Air-cured banana-fibre-reinforced cement composites. *Cement and concrete composites*, 16(1), 3-8.

Živica, V. (2009). Effects of the very low water/cement ratio. *Construction and building materials*, 23(12), 3579-3582.